University of Texas at Arlington

MavMatrix

2018

LiFePO4 BATTERIES: IMPACT OF HIGHLY PARALLEL PACKS ON LOAD DISTRIBUTION AND CYCLE LIFE

Caroline Storm Westenhover

LiFePO$_4$ BATTERIES: IMPACT OF HIGHLY PARALLEL PACKS ON

LOAD DISTRIBUTION AND CYCLE LIFE

by

CAROLINE S. S. WESTENHOVER

Presented to the Faculty of the Graduate School of

The University of Texas at Arlington in Partial Fulfillment

of the Requirements

for the Degree of

DOCTOR OF PHILOSOPHY

THE UNIVERSITY OF TEXAS AT ARLINGTON

August 2018

Acknowledgements

Abstract

LiFePO$_4$ BATTERIES: IMPACT OF HIGHLY PARALLEL PACKS ON

LOAD DISTRIBUTION AND CYCLE LIFE

Caroline S. S. Westenhover, PhD

The University of Texas at Arlington, 2018

Supervising Professor: David Alan Wetz

The United States Navy is considering Li-ion batteries for use as a primary power source for future naval shipboard pulsed-power applications. To supply sufficient power to a load, electrochemical cells are connected in series and parallel to create a higher voltage and higher capacity battery. The simplest way of connecting multiple cells in parallel is to tie all positive terminals together, all negative terminals together, and then electrically treat the array of cells as a single cell within the larger battery. In this configuration, a single battery management system (BMS) can be used to manage N parallel cells but there is no monitoring of each 'cell' comprising the parallel array allowing for current imbalances to occur among the N cells. The varying ESRs of the parallel cells can create uneven current sharing, which is compounded by different resistances among the tabs used to connect the cells and subtle manufacturing differences. Current imbalance could negatively impact individual cell lifetimes as well as the array's safety. The magnitude of this effect in highly paralleled arrays has not been thoroughly studied in the past but must be better understood before batteries are operated at high current rates using this manner of construction. The intent of the work being performed and documented here was to collect current data from

parallel arrays of cells using a novel construction and diagnostic techniques. The study performed measured the current imbalance present in 1S/5P and 1S/30P arrays, respectively, under two different high-rate pulsed discharge profiles. The data has been analyzed to study any current imbalances that occur and the impact it has on battery performance and longevity. A novel testbed with independent cell diagnostics has been developed so that each cell has self-contained voltage, current and temperature measurements. Six unique test series were performed and those are discussed in detail here. This dissertation covers the methodology behind the research, the test bed, the results collected, and some implications learned from the analysis performed.

Contents

List of Illustrations

List of Tables

Chapter 1: Introduction and Hypothesis

Preface and Hypothesis

As modern society moves to more advance technology to renewably supply energy for various energy needs this move brings with it a change in the electrical needs of the load profiles. Several of these loads require that the power sources provide power in a pulsed fashion. Pulsed loads are loads that discharge over the course of hundreds of milliseconds up to a few seconds. Pulse power systems generally operate on the principle that there is a primary supply and an intermediate supply. The primary supply is high-energy but low-power, given the pulse power load. The intermediate supply is the reverse: high-power but low-energy, usually comprised of capacitors, inductors or spark-gaps. The intermediate is charged by the primary over an extended period ranging from minutes to hundreds of milliseconds, depending on the intermediate power supply used. Then the intermediate supplies the pulse load.

There are single-stage and dual-stage intermediate supplies. In dual stage supplies, the first stage is a balance of power and energy, while the second is high-energy only. The dual-stage arrangement decreased the demand for the primary supply while still providing sufficient energy to the pulse load. Generally, these two-step intermediate systems are batteries and capacitors/inductors. The strength of LFP and LTO is that they are both balanced between the power density and energy density, making them optimal for standalone intermediate supplies. However, they are not as power-dense as caps. Larger banks of cells stacked in series to achieve the necessary potential and parallel for current must be built to meet power levels like those reached by capacitor banks.

In the two basic configurations, manufacturers and end users assume that the cells evenly share current. There is reason to believe that even current sharing is not what

happens under normal operation. Uneven current sharing can come from small manufacturing dissimilarities, such as differences in initial ESR. In a case where the cells are identical at the beginning, differences in temperature due to a location within the pack or pack circuitry can lead to long-term disparities. Thousand-plus cell packs have begun to be widely used in commercial applications (e.g., EVs and grid ties) to solve some of the future energy needs and to reduce the use of nonrenewable resources. Even current sharing among cells in most commercial applications is a safe assumption as the cells are not operated near their limits.

The step that commercial cell manufacturers take toward mitigating uneven aging is to build the cells into modules first and then use the modules to assemble the pack. This pack design allows the producers to balance the modules using a BMS without having to monitor every cell [1]. This module-based assembly has been presumed to be enough for the minor imbalances that could occur. A simple BMS combined with the relatively low power requirements for these applications allows them to mitigate problems using simple cell balancing, which makes the possible current imbalances of little import to many commercial users. The low discharge along with the pack control means that companies would not profit from investigating the current supplied by each cell because it has a small lifecycle increase at the power levels used in commercial applications. Moreover, the pack assembly makes individual cell monitoring costly, which outweighs the small lifecycle gains.

For high-power applications, the current imbalances can lead to safety and life-cycle issues. The higher the ESR of a cell, the more energy is dissipated through waste heat. The heat loss is especially costly because, along with the energy loss, it accelerates the aging of the cell while also requiring a way to dispose of the waste heat. For shipboard applications, a reduction in life cycle can be costly because the ship must go into dry dock

to replace an onboard battery. Therefore, it is critical that the battery fit into the standard two-year maintained schedule. Furthermore, the high loads the batteries supply onboard increases the likelihood of early failure due to critical thermal stress. Relative to other Li-ion cells, LFP cells have fewer safety issues because their chemistry leads to lower O_2 production [2]. However, the relative safety of the LFP chemistry does not eliminate all safety concerns, as there is still a known failure mode via oxidation on the copper current collector. Oversizing the battery back will increase the life cycle, lower the waste heat and decrease the possibility of safety issues can. However, oversizing is not an option for transportation/mobile platforms, as size and weight are critical resources.

The battery packs used in ocean going vessels are significantly larger than those used in any demanding application (e.g., non-grid tie). In battery pack assemblies, an individual cell often begins to decline before the rest of the pack due to intrinsic differences. These cells can then act as a catalyst for the degradation of the rest of the pack. If the operator identifies these cells and replaces with cells with similar electromechanical characteristics, this action could extend the pack's cycle life. Identifying failing cells remains more of an art than a science, and there is not yet a sufficiently reliable way to know the state-of-health (SoH) of an individual cell. Additionally, cells are difficult to replace in a manner that that significantly increases the life cycle of the whole pack. Even if it were possible, the enormity of the battery banks deployed would make this a drain on personnel time and would require additional logistical consideration when installing the bank. Not only are cells compactly configured, demanding significant work to change out a single cell, but the vast disparity between old cells and replaced cells can increase the circulating current and result in limited net gains in pack longevity [3]. Therefore, the early decline or failure of one cell is a strong indication of a shortened life cycle for the whole pack. The economic

loss caused by pack failure rises in correlation to the size of the battery pack. For the vehicular applications, this comprises a significant financial investment.

Alternately, investments could be made into developing a comprehensive control system for the whole pack. A control system could effectively reduce the likelihood of failure by balancing the pack and detecting noticeable differences before there is a single point of failure. Having a capable control system requires taking measurements from every cell or running real-time calculations in such a way as to obtain every possible measurement. A successful control system would require extensive hardware or software investments. Any reduction in hardware would require an additional layer of complexity in the software to achieve similar fidelity and scope provided it is not lost altogether with the hardware reduction. Development of a suitable control system would be costly. An initial investment in a control system could pay off in the long run if there are significant imbalances that lead to regular individual early cell failure within the pack.

Given that the large size of the battery back,pack and that a vessel is the often the only thing capable of supporting life for miles around, all onboard safety issues are more than just an expensive inconvenience they. They can, in fact, be life-threatening for hundreds of people. Therefore, battery safety is all the more critical to consider in these instances. While most manufacturers can accept a small margin of failure, even some dangerous ones, catastrophic failures are unacceptable on shipboard. In areas where some commercial companies can be comfortable with a fair amount of uncertainty, certain companies (e.g. the medical field) needs to know more detailed information about the products it deploys.

Due to all the possible avenues of current mismatch, the relative unimportance to other large battery pack applications, the potential cost, and the present shallowdearth of knowledge in the field, the research conducted at UTA PPEL and presented here is vital

for large -fielded battery packs. Therefore, research into examining how cells operate when they are in parallel and discharge at high rates is needed to ensure that the battery pack is supplying power to these high pulse power loads both safely and cost-effectively. It is hypothesized that there will be current mismatch, which at mid-level current demands will decrease as the cells discharge that will cause a small aging increase and for high current loads the current mismatch will increase thereby significantly shortening the array cycle life. The insights gained from this research can be used to optimize large battery pack design for future loads with various energy and power demands.

Nomenclature and Definition

Unless otherwise the below definitions are official Institute of Electrical and Electronics Engineers (IEEE) definitions from IEEE Standards Dictionary: Glossary of Terms & Definitions [4].

Anode: (1) An electrode through which current enters any conductor of the nonmetallic class. Specifically, an electrolytic anode is an electrode at which negative ions are discharged, or positive ions are formed, or at which other oxidizing reactions occur. (2) An electrode or portion of an electrode at which a net oxidation-reaction occurs.

Battery (primary or secondary): Two or more cells electrically connected for producing electric energy. [Common usage permits this designation to be also applied to a single cell used independently.] Primary pertains to non-rechargeable and secondary pertains to rechargeable.

Battery Pack/Battery Bank: Full configuration of electrochemical cells that is viewed as one storage device by the load. For the work presented here one array of parallel cells is the battery pack and will be referred to as the battery or battery pack throughout

Brick: One array of cells either in series or parallel that is often used as the building block for a high capacity configuration of Electrochemical cells. Also called a module in the literature. *

Capacity: Generally, the total number of ampere-hours that can be withdrawn from a fully charged battery at a specific discharge rate and electrolyte temperature, and to a specific cutoff voltage.

Capacity fade: That which pertains to the loss of usable capacity of a rechargeable battery. Capacity fade may be both time and cycle dependent. ^

Cathode: An electrode through which currently leaves any conductor of the nonmetallic class. Specifically, an electrolytic cathode is an electrode at which positive ions are discharged, or negative ions are formed, or at which other reducing reactions occur.

Cell: (batteries for photovoltaic systems) The basic electrochemical unit, characterized by an anode, a cathode, and electrolyte, used to receive, store, and deliver electrical energy

Charge: (storage battery) (storage cell) The conversion of electric energy into chemical energy within the cell or battery. Note: This restoration of the active materials is accomplished by maintaining a unidirectional current in the cell or battery in the opposite direction to that during discharge; a cell or battery that is said to be charged is understood to be fully charged.

Cycle (Cycling): A battery discharge followed by a complete recharge. A deep (or full) cycle is described as the removal and replacement of 80% or more of the cell's design capacity.

The depth of Discharge (DoD): depth of discharge (DOD) (1) (batteries) The ampere-hours removed from a fully-charged battery, expressed as a percentage of its rated capacity at the applicable discharge rate. (2) The ampere-hours removed from a fully charged battery, expressed as a percentage of its rated capacity at the applicable discharge rate.

Electrochemical cell: A system consisting of an anode, cathode, and an electrolyte plus such connections (electric and mechanical) as may be needed to allow the cell to deliver or receive electric energy.

Electrochemical Impedance Spectroscopy (EIS): A method for the non-destructive characterization of electrochemical cells using the frequency response of the system to obtain the impedance and mesoscale dissipation reaction of the cell. *

Electrolyte: A conducting medium in which the flow of electric current takes place by migration of ions. Note: Many physical chemists define electrolyte as a substance that when dissolved in a specified solvent, usually water, produces an ionically conducting solution

Electrolytic cell (1) A receptacle or vessel in which electrochemical reactions are caused by applying electrical energy for the purpose of refining or producing usable materials. (2) A receptacle or vessel in which electrochemical reactions are caused by applying electrical energy for the purpose of refining or producing materials.

Energy: That which does work or is capable of doing work. As used by electric utilities, it is generally a reference to electrical energy and is measured in kilowatt hour

Effective Series Resistance (ESR): A factor such that the conduction current density is equal to the electric field in the material divided by the resistivity. Author note: Also, referred to in the literature as effective resistivity or equivalent series resistance

Float charge: A constant potential applied to a battery to maintain it in a charged condition.

Frequency Droop: (electric power system) The absolute change in frequency between steady-state no load and steady-state full load.

Impedance: (general) (linear constant-parameter system). The ratio of the phasor equivalent of a steady-state sine-wave voltage or voltage-like quantity (driving force) to the phasor equivalent of a steady-state sine-wave current or current-like quantity (response).

Primary cell: A cell that produces electric current by electrochemical reactions without regard to the reversibility of those reactions. Some primary cells are reversible to a limited extent.

Power: The time rate at which energy is emitted, transferred, or received; usually expressed in watts (or in joules per second).

Secondary cell (storage sell): A galvanic cell for the generation of electric energy in which the cell, after being discharged, may be restored to a fully charged condition by an electric current flowing in a direction opposite to the flow of current when the cell discharges.

Self-discharge: The process by which the available capacity of a battery is reduced by internal chemical reactions (local action).

Separator: (storage cell) A spacer employed to prevent metallic contact between plates of opposite polarity within the cell. (Perforated sheets are usually called retainers.)

Service life: (1) (primary cell or battery) The period of useful service before its working voltage falls to a specified cutoff voltage. (2) (storage cell or battery) The period of useful service under specified conditions, usually expressed as the period elapsed before the ampere-hour capacity has fallen to a specified percentage of the rated capacity.

Set: All cycles in between two baselines. *

State-of-Charge (SoC): The actual capacity of a battery expressed as a percentage of a fully-charged capacity. Note: This is based on experience, application (cycling/float service), and charging parameters.

State-of-Health (SoH): An estimation of the condition of the battery expressed as a percentage of the condition of its ideal condition. *

Test: One group of cycles from initial to a 20% capacity fade or failure*

Thermal Runaway: A condition that is caused by a battery charging current that produces more internal heat than the battery can dissipate. This condition ultimately causes cell venting and premature failure.

Trickle charge: A continuous charge at a low rate approximately equal to the internal losses and suitable to maintain the battery in a fully charged condition. Note: This term is also applied to low rates of charge suitable not only for compensating internal losses but also to restore intermittent discharges of the small amount delivered from time to time to the load circuit.

Recommended performance range: The range of voltage, current, capacity or energy, and environmental conditions within which the battery manufacturer recommends to delivering the expected performance in terms of life cycle and safety. *

* Author Definition, ^ [5]

Overview of Electrochemical Cells

Batteries consist of a cathode (i.e., positive electrode, graphite in LFP), an anode (i.e., negative electrode, an $FePO_4$ Olivine with dissolved Li-ions in LFP), and an electrolyte. Electrolytes in batteries are the electrically conducting solution between the anode and the cathode. In Li-ion batteries, the electrolytes have lithium ions dissolved into them. The electrolyte does not itself give up or accept electrons. Instead, it provides a solution through which the exchange of electrons can take place, thereby allowing electricity to flow. It keeps the negative cloud around the cathode and the positive cloud around the anode from slowing down the electron flow. Initially, manufacturers used liquid electrolytes, but gel electrolytes are now the most common.

Constant Current – Constant Voltage Charging

Li-ion cells are sensitive to overcharging and high C rate charging. Their charge rate limits even high-power Li-ion cells. Giving a wide margin for error, undercharging Li -

ion cells or packs is not a workable solution because the Li -ion cannot provide the optimally-rated energy output for a given application. Conversely, pushing Li-ion cells above their recommended voltage limits or apply charging currents that exceed manufacturer-recommended levels will result in a significant loss in cycle life and could drive the cells outside of the recommended operating range. Both overvoltage and charge currents above manufacturer recommendations break down Li -ion cells, reducing cycle life and can lead to catastrophic failures. The challenge is to maximize the charging rate (thereby minimizing charge time) and charge to the cell's nominal voltage (to maximize available capacity) without overcharging the cells.

To fully charge the battery without overvoltage, Li-ion chargers typically follow a two-phase approach. The first phase, called the constant-current phase, is when the cell is charged at a constant current based on the recommended charging current window provided by the battery manufacturer and desired time to full charge. This rate is a generally a 1C-rate charging current based on the ampere-hour rating of the cell. When the cell reaches a specified set-point voltage (3.6 V LFP), cell capacity has generally reached 70 to 80% of its state-of-charge (SoC) but continuing to charge at this current rate risks damage to the cells by overvoltage. Thus, once the cell reaches its nominal voltage, the second phase of the charging is initiated, called the constant-voltage phase. Here, the charging circuit will provide only enough current to maintain the voltage of the cell at the set-point voltage. As a result, the charging current will gradually decrease over time, resulting in a decay of the charging current profile [6].

Lithium-ion batteries

Li-ion batteries are a type of secondary battery that generally have a carbon-based anode and a cathode with intercalated lithium compound that allow li-ions to be exchanged during discharge and recharge. Li-ion batteries are have risen in popularity because of their

relatively high energy-density and cycle life. In Li-ion cells, the positive electrode (or cathode) is the one that starts housing the lithium ions. The negative electrode receives the electrons during discharge. The anode is made of a carbon or graphite collector grid. The cathode is made up of the lithium doped material and using a lithium doped material for the anode resolves the problem with dendrites forming on the anode surface, a familiar source of failure in early lithium batteries [7]. The most notable exception to this configuration is lithium-titinate (LTO) batteries, which have a lithium-titinate coated anode and the cathode is a lithium manganese oxide. There is some parasitic behavior of li-ion cells [8].

Double-layer capacitance, which arises from non-idealities in the mass transport between the electrodes across the electrolyte, is a significant contributor to the short lag seen in pulse power application between the load demand and the battery pack supply. Although this lag is in the order of milliseconds, which is less than one-thousandth of the 30 seconds on pulse cycle, it is crucial to developing a full picture of the aging phenomenon and effects in lithium-ion cells. Diffusion impedance impacts the heat loss of the cells over the longer discharge behavior. It can be significantly different between the same model of cell.

During the first few cycles, the electrolyte in lithium-ion batteries develops a thin passive layer consisting of organic and inorganic material (e.g., solvents, lithium salts and salt degradation products) near the graphite anode. This is the solid electrolyte interphase (SEI), sometimes incorrectly called the solid electrolyte interface [9]. The SEI is essential for the suppression of dendrites, which are thin fibers of lithium that stretch across the electrolyte and can eventually short the battery. It also reduces the exfoliation of the graphite due to the co-intercalation of solvents in the graphite with the Li-ion [10]. As the cells are cycled, the SEI can continue to grow. Although a thin SEI layer is vital for stable

Li-ion cell discharge, thickening increases the impedance of the cell and consumes active

lithium, which results in increased resistance and lower capacity.

Chapter 2: Literature Review

High C Discharge of Lithium-Ion Batteries

A collaborative team from Robert Bosch LLC and the Institute of Automation Engineering found that at high C rates (>5 C) many of the linear and constant assumptions used to model batteries are no longer accurate. At these rates, additional measurements, such as temperature, were needed to produce a precise model of the cells' SoC. A group at Pennsylvania State University in conjunction with a researcher from General Motors ran more symmetrical pulsed profiles on LFP batteries. There were three similar profiles used: X-second discharge / X-second rest / X-second charge / 30-second rest, with X being 2, 10 and 30, depending on the test number. Under these profiles at 45°C, they found that discharge pulse power capability changed little over cycles from 0 to 600. At lower temperatures (0 and -10°C) under these pulsed loads, they observed that there was more significant capacity fade, but that the real limiting factor was the power fade during the pulsed discharge cycles. They found that the increase in the interfacial resistance due to the SEI growth was the primary source of the power fade. So, while the pulsed discharges performed well under mid to high temperatures, they came to the end of their useful life within 600 cycles under cold weather conditions.

Wetz et al. found that using pulsed discharge significantly shortened the overall lifespan of NCA batteries, increasing the capacity fade fourfold. Investigations into aging showed an increase in the passive film formation as well as an increase in the charge transfer resistance, showing that cells undergo different stressors leading to different primary aging mechanisms [11].

Li-ion Aging Mechanisms – Focus on LFP

The aging mechanisms that manifest in various battery chemistries change based on multiple parameters. There is calendar aging, in which the aging that results even if the batteries are not under load. In calendar aging, conditions such as the temperature and storage SoC have the most substantial impact. For cycle life aging that results from use of the battery, the ambient temperature, cell waste heat, current charge and discharge rate and SoC range all have detectable impacts on the aging of the cells [12].

In a study performed on the calendar-aging effect on LFP found that temperature was a more dominant factor of LFP calendar aging than the storage SoC. The primary source of capacity fade observed in this study was the loss of cyclable lithium due to SEI growth. Paired with the capacity fade was a significant decrease in energy efficiency and voltage. These effects increased with decreasing temperatures [13].

In this study, the dominant source of power fade is due to an increase in the discharge resistance calculated from the hybrid pulse power characterization. The discharge resistance increase occurred at cells stored at low temperatures. Studying the EIS of these calendar-aged cells showed that lower temperatures generally led to a lower pure ohmic resistance but a long time constant, which matches with the higher discharge resistance, and charge transfer resistance. The cell aged at 45°C showed the most substantial diffusion limitation [13].

Overall, Dubarry and Liaw found that the most common capacity fading mechanism in cycled LFP batteries was a loss of lithium and loss of active materials. These capacity-fade mechanisms correspond with a similar reduction in peak power. Thus, LFP has an aging mechanism that closely links capacity and power. For high power needs, this link is fortuitous because it means that a producer can size the battery pack by the desired power and capacity—the two predominate sizing metrics—and the pack will age relatively

evenly across power and capacity throughout its cycle life. This implies that a new pack does not have to be significantly oversized to account for future uneven power and capacity aging [14].

Li-ion Characteristics and Aging under Pulse Loads - Focus on LFP

As the usability of Li-ion batteries of several chemistries for pulse loads has become apparent, increased effort has been made to understand the way Li-ion batteries behave under these profiles. There is a desire to know the long-term differences of continuous high discharge and pulse high discharge. Abraham et al. examined the performance of Lithium Cobalt Aluminum Oxide under pulse profiles for transportation applications (e.g., hybrid electric vehicles (HEVs) and battery electric vehicles (EVs)). They found that the batteries could sustain a 17C-rate discharge for 18 seconds without experiencing a significant decrease in power delivery [15]. Smith et al. found that when using Hybrid Pulse Power Characterization (HPPC) they could develop a model that more accurately displayed active material surface concentration for pulses around five seconds in length. The HPPC model, in turn, strengthened the 1D model's ability to predict pulsed 40C capability, a necessary addition to the model for these batteries to be optimally sized for pulsed loads [16]. Huria et al. found that the model of pulse loads requires considering the unique thermal profile of the batteries under these changing loads. Beh et al. found no additional detrimental impacts of pulsed charging compared to constant charging [17]. Popp et al. subjected NCA, NMC, LFP and LMO chemistries to 2C 10-second pulses and continuous discharges [18]. Analysis of the cells throughout the test showed similar evolution in series resistance of the cells for either discharge profile. These papers cover the behavior of batteries under loads that are periodically pulsed but typically operate continuously.

In a 2005 study, Chen et al. found that specially manufactured Li-ion cells could be designed to sustain 2kA for two seconds. This short-term high-rate ability makes these cells good candidates for several different modern loads, such as electric vehicles, and other loads that have intermittent pulsed needs. Using various-sized resistive loads, the researchers tested the limits of the cell. They found that the extreme end is able to supply only about 1% of the total energy available. While this would be adequate for some pulsed loads and might fit the solution space between supercapacitors and other batteries, it is not sufficient for continuous pulsed loads. Many of these would need to be connected to supply adequate power to predominantly pulsed loads. The study presented here did not cover connected cells or the lifetime effect of such pulsed loads on the Li-ion batteries studied.

Large Battery Banks

Regarding large-scale stationary storage, Soloveichik observed that the recent breakthroughs in the LFP batteries have found widespread use for installation. Soloveichik reasoned that the chemistries used for stationary energy storage have similarities to the ocean going vessels' needs. Both chemistries—LFP and LTO—are safer than other Li-ion options, have low self-discharge and are capable of higher discharge and charge rates. This paper reviews only the installation of these battery types and does not observe their long-term behavior [19]. The research team from the University of Michigan Ann Arbor discussed that small manufacturing differences in large battery banks could have acute effects on the charge and discharge of the banks, beyond what they think a BMS can control. Although they did not do any original research at the magnitude of the problem, they propose a framework that allows for online battery pack reconfiguration—a rather expensive solution to the problem [20].

In an invited paper for the Proceedings of the Institute of Electrical and Electronics Engineers (IEEE), Lawder et al. reviewed the need for better BMS models to estimate the SoC and SoH. Consisting mainly of lookup tables, the current models are not accurate for intermittent high-powered discharge used in grid-tie applications. This critique applies to the high pulsed power load covered in this research [21]. A team at Aachen University analyzed the viability of adding renewable energy sources to the grid. They concluded that electrochemical batteries could be a viable way to adjust for the mismatch in renewable power generation, load demand and frequency droop. However, to achieve this in a cost-efficient manner, they suggest pairing the batteries in separate blocks and having an overarching control system decide which blocks to charge and discharge under any given condition. This modular charging reduces the aging effect of system imbalances and shows the research team's concerns about current disparities [22]. Goodenough et al. point out that while LFP along with LTO have reduced the safety hazards of large-scale high-power batteries, a long service life is still a challenge [23]. To add to this, Dunn, Kamath, and Tarascon believe that the price per kilowatt-hour would need to be reduced by half and the energy density double the use of Li-ion batteries of any kind for grid-tie or electric vehicles becomes standardto become common practice. Despite a typical energy density, one of the reasons LFP has become popular is because it is less expensive than other Li-ion chemistries [24].

Manufacture Variations

In two separate papers, Dubarry and Liaw and their team at the Hawaii Natural Energy Institute (HNEI) studied the origins, character, and size of manufacturer variations. In the earlier paper, the researchers at HNEI analyzed a lot of 100 AAA 300mAh LCO cells. From this lot, they measured a ±1.69% weight variation, ±0.45% open-circuit voltage variation, a ±1.9% variation in C/2 capacity, a ±27% difference between the self-discharge

rate and a ±30% difference in DC-ESR (averaged across C/25, C/5 and C/2). They measured a few other variation metrics, which generally showed a magnitude of ±2% variation or less [25]. In the later work, studying cells with the composite cathode of $LiMn_{1/3}Ni_{1/3}Co_{1/3}O_2$ + $LiMn_2O$ also found the DC-ESR to have the most extensive variation across cells. However, in these 18650 format cells, there was only a ±5.7% difference between cells [14].

Pulsed-Power Storage Modules

In "Ultracapacitors: Why, How and How They Work", Burke reviews how there has been a move to use ultracapacitors in conjunction with batteries to provide power to pulsed power applications. The capacitors meet the high-power aspect and the batteries store the vast amounts of energy needed for multiple pulses as the intermediate stage. Herbst, Beno, and Walls reviewed the use of flywheels as a possible power buffer between a generator and a pulsed power load. As a supply, it has several promising characteristics, such as a long cycle life and high power and energy density. It is still an expensive emerging technology, though, and electrochemical batteries are the default [26]. Loads having intermittent, pulsed power requirements have been around for several decades. Therefore, effective means to supply power to these loads has been a research topic since the late 1980s.

Researchers made initial investigations into using lead-acid batteries to supply the power to pulsed loads. LaFollet and Bennion found that they could effectively model thin electrode lead-acid batteries and that thinning the electrode would allow lead-acids to better supply the power for pulsed loads. They found that there was a non-negligible current drop for the first 200us using this battery type. McNab further discussed the challenge of hydrogen production that occurs when using large stacks of lead-acid batteries. Once Li-ion batteries of various chemistries began to be readily commercially

available, they quickly became the battery of choice due to their relatively high energy and power density [27]. Even with the relatively high power density found in Li-ion cells, they still do not meet the needs of mobile vehicles in the emerging high-powered pulsed applications. To fulfill these high-power needs, an energy storage device with significantly higher power density can be paired with the batteries. Otherwise, the battery pack must be substantially oversized compared to sizing needed to meet the energy requirements.

Several papers examine using electrochemical batteries in conjunction with capacitors, inductors or fuel cells. Kuperman reviewed various battery-ultracapacitor energy storage methods. Kuperman found that paralleling ultracapacitors with batteries improved response time. There are several control topologies for connecting batteries and capacitors in parallel. To achieve ideal performance, an extensive control topology is needed, which brings several layers of electronics on top of the underlying system. The battery-inductor energy storage presents a high-energy storage option while also being composed of a more straightforward structure and elementary-to-control alternative to battery-ultracapacitor topologies. There are several different battery-inductor topologies, with the meatgrinder and XRAM topologies featured as the basis on with most are set. Under these constraints, vehicles need to be able to recharge a high-powered device in under a minute using a paired Li-ion battery pack. Discharging the paired battery pack under this strenuous pulsed profile was found to affect the overall cycle performance of the cells [28].

Performance of Batteries in Parallel Arrays

A 2005 study by Chen et al. found specially manufactured Li-ion cells designed to sustain 2kA for two seconds. The high-power, low-duration capabilities of the cells make them good candidates for several different modern loads (e.g., electric vehicles) and other loads that have intermittent pulsed needs. Using resistive loads of varying size, Chen

tested the cell limits. The team found that the cell was able to supply only ~1% of the total energy available at the extreme ends. While this would be adequate for some pulsed loads and might fit the solution space between supercapacitors and other batteries, it is not sufficient for continuous pulsed loads. Many of these would need to be connected to supply sufficient power for continuous pulsed loads. The study presented here did not cover connected cells or the lifetime effect of such pulsed loads on the Li-ion batteries studied.

When placed in parallel, cells naturally maintain the same voltage, but the current provided by each cell varies [29]. The cause for this unequal current sharing is not yet fully understood, but there are several suspected sources. The two discussed and investigated here are the variation in the equivalent series resistance (ESR) of each battery and the resistance between cells due to the tabs used. This phenomenon is necessary to identify because Gong et al. show that once there is an imbalance in the SoH, the whole pack begins to age at an accelerated rate. The authors of that study took used plug-in hybrid electric vehicle pouch cells and evaluated them in 2P, 3P and 4P cell configurations and measured ½C capacity and EIS spectrum of cells for baseline purposes. They found that with four cells in parallel there was a mean current deviation of 3.1% through most of the discharge, with a significant peak at the end, when there was a mean capacity deviation of 2.7%. This data verifies that unbalanced cells do not share current evenly. While the data is useful, it is only for a small number of cells that start at different SoH. Furthermore, they performed only a few tests and primarily investigated how the number of cells in parallel impacted the current imbalance, preventing exploration of the lifetime impact. The data does not cover how new cells share current or how the imbalance in current affects long-term life of the battery [3].

Gogoana et al. studied how cells behaved in parallel by discharging two 2.2Ah cells in parallel. He cycled the cells at a 20A constant-current discharge, which is a 4.5C

discharge for the cells used in the study. They found that a 20% internal impedance could lead to a 40% current difference, with the internal impedance being measured using a 15-second 40A discharge pulse. This current difference led to significant temperature difference and contributed to the premature aging of the cells. They found that the internal impedance mismatch could be quantified using an SEI model [30]. Welsh ran simulations of active and passive battery pack balancing. These simulations showed that unbalanced Li-ion battery packs quickly exhibit voltage drifts, resulting in rapid cell aging and unsafe individual cell voltage conditions. An active balancing system could sufficiently mitigate the problems investigated by the author [31].

Baronti et al. simulated four different series-parallel module configurations. The battery pack was a 24S/4P battery pack in which the smallest manageable unit was a 4S/1P module. The most straightforward configuration only adds parallel connection where the pack meets the load, while the most complex has parallel configurations between each module series connection, leading to five additional parallel bus bars. The two configurations between the least complex and most complex had one additional parallel bus bar and then two additional parallel bus bars. The most complicated configuration produced 3% more available capacity on average. The more extensive the variation between the cell's capacity, the more significant the simulation showed this phenomenon to be. The simulations also showed that the simple configuration was critically sensitive to the module configuration—sensitive to the point where the randomness intrinsic to the battery pack assembly could lead to a 9% difference in the capacity supplied by the cell [1].

Shi et al. found that when discharging two battery modules in parallel, the current small differences experienced during the first 80% SoC (i.e., 100%–20% SoC) of the discharge similarly the first 80% of the recharge capacity (i.e., 0%–80% SoC). The SoC

from the first 80% of the discharge leads to significant current differences between the cells in the final 20%. The current differences experienced throughout the discharge had a direct negative impact on the capacity fade of the individual batteries. To slow down the capacity fade of modules connected in parallel, the authors suggested active current control to suppress the current variation on the individual parallel connections. Specifically, they noted that if there is a substantial SoC difference during the initial 80%, then the current needs to be controlled or suspended to allow the modules to self-balance and thus avoid the significant differences seen in the module currents during the final 20% SoC [32].

The Formula Student team at Imperial College London made two batteries, each consisting of three 12P7S modules of Kokam lithium-polymer NMC pouch cells in series. Upon discharge, they recorded a 7% voltage difference between the first parallel array and the final parallel array. Modeling of the pack showed that a single high-resistance contact (1.9mΩ versus the 0.6mΩ pack mean) would lead to six times more current being drawn from the two cells near the bus versus the other ten behind the high-resistance contact. The source of the high-resistance contact was a small obstruction between an aluminum clamp and its cell, preventing complete contact between the cell's positive terminal and the parallel array positive bus. Once the team reassembled the battery, there was only a 2% difference in the array current. Simulation of this configuration showed that the cells providing the most current in a module provided two times as much current as cells providing the least amount of current during 4/3C discharge.

Highlighting the challenges behind battery module control, the team had one voltage measurement on each parallel array, along with one temperature measurement for each series column, to remain on budget. The placement of the voltage measurement could mean that the voltage or the two current providing cells dropped below the

22

manufacturer's recommended minimum operating voltage. Unfortunately, the team cannot verify this.

The team also noticed a continued rise in temperature within the series column after the removal of the load. They believe this is from passive balancing within the battery pack, but as there were no current measurements, they could not verify this hypothesis. The reasons the students gave for not taking current measurement was the added cost and complexity required for accurate measurements. Therefore, the actual intra-pack dynamics and their magnitude is unverifiable [33].

A team led by So Miyatake at Kyoto University in partnership with CAPTEX built a model to determine the expected capacity from a battery pack built with non-uniform cells. To do this, they initially experimented with two cells in series, two cells in parallel and four cells in two different series-parallel configurations. Both the series-parallel configurations were 2P2S, but one had cross-coupling, meaning this configuration connects each cell to the cell in series with it along with the cell in parallel. In the series-parallel sans cross-coupling, the cells are connected in series and the positive and negative of each series column are connected in parallel. The researchers found different challenges faced by battery packs based on whether they were in series or parallel. In a series connection, they discovered that the weakest cell determined the capacity of the pack, whereas they got the full capacity out of the cells in parallel, but the current was substantially unequally distributed. In the series-parallel, the cross-coupling led to higher overall capacity, higher absolute current differences and smaller voltage differences [34].

A team at the Karlsruhe Institute of Technology studied the impact of circuitry on parallel connected LCO and LFP cells used in home photovoltaic systems. The results showed that the relationship between the cells ESR and the circuitry resistance strongly influenced the current imbalance between the cells. Additionally, they found that LFPs were

more sensitive when it came to current imbalance and life cycle, increasing resistance in the packing circuitry even at discharges as low as 1C and C/2. This sensitivity could be due to the LFP exhibiting more than two times the current imbalance. The most extreme of these current imbalances were at the very high and very low SoC. The researchers concluded that to optimize life cycle cells, selection and resistance-adapted pack design was necessary. [2]

Presented Research Contribution

Research Objective

Research has been performed on two different sized arrays of LiFePO4 (LFP) cells using two load profiles intended to test the cells at a mid-stress point and the upper ends of their capabilities. The array sized are 1S/5P and 1S/30P, the cells have a 26650 form factor (26 mm x 65 mm), and the two load profiles were 46W per cell and 117W per cell.

The objective of this work is to do extensive enough experimentation on a sample of controlled cells as to discover the trends of cells in parallel arrays to a high degree of confidence. To test the hypothesis that cycling cells in a parallel fashion has a detrimental impact cycle life that increases with array size and multiplies the negative impact of high power profiles. It is conjectured that the cells in 30P array will have a measurably shorter life cycle that the cells in the 5P. Furthermore, that instead of the one magnitude decrease seen in comparison to single cell cycle life near the 46W and the three magnitude decrease seen near 117W the decrease in cycle life will 2-4 times that amount [36]. The path of action for this decreased cycle life is that cells within the parallel arrays are expected to age at an irregular rate, which will cause further uneven increase temperature and internal aging symptoms, which in turn imbalances the parallel cell discharge and causes premature aging of the parallel group either due the higher performing cells being stressed significantly what would be expected at the set discharge rate of the poorly performing cells

24

dropping out and obsoleting the rest of the array it is in with the overall result being a shortening of life when compared to the lifetime of a single cell.

In concert with testing this hypothesis is developing an understanding of the most detrimental aspects of the parallel discharge of cells. How to economically mitigate these aspects and to study the changes in aging mechanisms that is seen in highly paralleled cells versus single cells and small arrays of parallel cells. Additionally, an initial cell modeling that could be taken from the literature which could give insight into the initial conditions of the cells and how they impact the lifetime of a pack.

Application and Results

As the modern world becomes more technologically integrated, the need for batteries has increased. In the instance of the small commercial application, the expectation to change out the battery every two years has become the norm. This upkeep cost is often small, given the overall cost of the device's electronics and software in use (e.g., wireless headphones, mobile phones, fitness trackers).

However, in the past few years, batteries have been applied to larger, higher-power, higher-energy applications. The best-known applications are electric vehicles and grid balancing. In the electric vehicle industry, the battery makes up about a third of the car cost. For grid balancing applications, a majority of the cost is batteries, since the simple control scheme is well known, and battery installation requires many work hours. Thus, the batteries become a significant portion of the cost and replacing them every two years is untenable. Fortunately for power transmission companies, grid balancing applications are often inexpensively installed, therefore battery pack size and container brittleness (which would disallow hydrogen venting) are not critical figures of merit. This leads to the solution of using cheap, lower-energy density and lower gravimetric density batteries that has a

long cycle life. However, with electric vehicles, battery pack size is critical to consumer appeal, and it is imperative that the battery pack not significantly deform.

Two major research areas are working to solve this problem. One is the development of better battery chemistries. The second is the optimal use of the batteries presently available. The development of optimal battery use requires a firm foundation on battery behavior, particularly battery pack behavior. It is these large battery installations, with many batteries connected in series and parallel, where this aging rate is most problematic.

The results from this dissertation shows that there is a problem in leaving the batteries uncontrolled, often resulting in the accelerated aging of the batteries. In a time where every increase in the bathtub curve for battery packs increases a company's bottom line, the relatively small phenomenon observed here are of significant value.

Chapter 3: Use and Study of Electrochemical Secondary Cells

General Characteristic

There are a few cells that were used when secondary cells were needed. Generally, the lead-acid cells were used when weight was not an important a consideration as cycle life.

Lead Acid

While this is a cheap technology due to it having been commercially available for 85 years, lead-acid suffers from the shallow specific energy of around 42 Wh/kg, an energy density near 110 Wh/L and low specific power around 180 W/kg [37]. These specifications make them unfit solutions, as the vehicles always try to minimize the total weight added to the chassis as well as the space taken up by the storage module.

Nickel-cadmium

Ni–Cd cells have a nominal cell potential of 1.2 V with it has a long linear portion during discharge. This made if useful for electronics because the voltage was within a smaller window during discharge. When overcharged they suffer from both hydrogen and oxygen outgassing. Similar to the LFP batteries it has low impedance and is therefore capable of relatively high discharges. With a specific power of 150 W/kg, an energy density around 100 Wh/L, and a specific energy of 50 Wh/kg along with the cheap cost made it popular for remote control vehicles. It does have a high self-discharge and suffer from voltage depression [38] [39].

Nickel Metal Hydrides

Battery chemistry that has been commercially available for a relatively long time is that of nickel metal hydride (NiMH). With the specific energy of 60–100 Wh/kg and an energy density of 200 Wh/dm, they would reduce the size of the battery pack required to

meet the energy requirements needed to the supply power to the high-power systems for the specified amount of time. The cycle life of NiMH contributes to them being an appealing choice for the high power applications. For typical discharge regimes, NiMH batteries can maintain over 80% of their battery capacity for 4,000 cycles [40].

However, the safety characteristic and the power density of these batteries do not fit with ocean going standards and needs. With a specific power of 200W/kg, it is an excellent battery for electric vehicles and other commercial mobile application, but for the high-power systems required by future technology, the battery pack sizing would take up a substantial amount of onboard real estate. Furthermore, when overcharged, as could be necessary for the onboard high-powered weaponry or radar, NiMH can vent hydrogen gas, causing the storage room to become a hazardous area. High-power charging of NiMH can lead to thermal runaway [41]. Therefore, deployed servicemen would have to take extra care when charging these cells, leading to an elaborate and expensive control system.

Lithium Cobalt Oxide (LiCoO$_2$)

Lithium cobalt oxide (LiCoO$_2$) are the most common batteries for small mobile applications such as cell phones and laptops. The reason for its widespread use in mobile applications is due to its high specific energy of 500 Wh/dm. At 500 to 1,000 cycles, their cycle life can be on the low side of available batteries, which is exacerbated by high current discharges [42]. This low cycle life combined with ill-suited power demands would mean more frequent maintenance, requiring the ship to be in dry dock. Furthermore, this chemistry suffers from similar problems to the NiMH in that it is more prone to thermal runaway that other chemistries offered and therefore cannot be charged faster than 1C (the ration of current to capacity), meaning a full recharge will take an hour. Also hindering it from being used by the vehicles is that has low power capabilities [43]. Overall, the safety

issues and relatively low power make this chemistry ill-suited to use for the high-powered loads that are needed for future technology.

Lithium Manganese Oxide (LiMn2O4)

Lithium manganess oxide unlike LiCoO2 and NMH is more stable than $LiCoO_2$ and NiMH and is capable of short high-power discharges and can be charged at an elevated C rate. Although they are more thermally stable than leading Li-ion chemistries, they are not as stable as LFP and LTO. In all other characteristics, the cells underperform compared to popular Li-ion chemistries. $LiMn_2O_4$ have a short cycle life of over 1,000 cycles, with the exact number depending on the specific manufacturer, and low specific energy [44]. All these characteristics would lead to overly expensive maintenance and a significant real estate need.

Lithium Nickel Cobalt Oxides (LiNiCoXXO$_2$)

Most common of these types of cells is the lithium nickel manganese cobalt oxide ($LiNiMnCoO_2$ or NMC) and lithium nickel cobalt aluminum oxide ($LiNiCoAlO_2$), which is conventional chemistry for electric vehicles. Because there are different chemistries and chemical ratios used to build the cathode they display some range in their characteristics. They have high specific energy and long cycle life. The fact that they see increased use in the electric vehicle market has seen a reduction in price for the NMC, but the $LiNiCoAlO_2$ are still prohibitively expensive. Their weak point, for ocean going applications, is they have low power capabilities and charging them above their C rate promotes thermal runaway, with $LiNiCoAlO_2$ being the less thermally stable of the two   [45]. Lithium-cobalt oxides have similar characteristics to NiMH cells but with better energy density and can therefore replace NiMH cells in many applications.

Lithium Iron Phosphate (LiFePO$_4$)

Significant advances were made inLithium Iron Phosphate (LFP) cells was by coating the lithium iron phosphate particles. Coating the particles led to the high-power capabilities that, along with their relative safety in comparison with other LIBs, make LiFePO$_4$ optimal cells to use in the high-powered application [42] .With high specific power, cycle life, and thermal stability LFP batteries meet the necessary qualifications to supply power to the high-powered loads needed by future applications. It is midrange economically: It uses a relatively cheap of the cathode material, but it does not have as many commercial applications as other cells listed and therefore is not yet produced on the scale of NiMH and other cells used by electric vehicles or small mobile applications. It has low specific energy at 90–120 Wh/kg and the power capabilities are what determine the size of the pack, which the research here shows to be a critical factor for electrochemical reasons as well as space. In general, the power has been the leading sizing metric for high-power loads and having a chemistry with superior specific power for inferior specific energy makes the energy the main sizing metric but leads to slightly smaller pack sizes. That combined with the safety and cycle life make LFP the best available battery for the Navy. Because the Navy has chosen to investigate the possibilities if LFP cells for shipboard applications, this research focuses on how LFP behave in a pack [46].

Aging Mechanisms

Various battery chemistries have exhibited different aging modes. Typical failure modes are an anodic failure, increased resistance, capacity fade, loss of active cathode materials and voltage depression. Presented here is a brief review of the modes commonly associated with diverse chemistries. This review will acquaint the reader with the shortcomings of various chemistries so that the strengths and weaknesses of lithium iron phosphate (LFP) can be comparatively understood.

Precursors to Li-ion

Under normal operating conditions, nickel metal hydride (NiMH) showed a significant voltage depression, in which the battery voltage drops quickly compared to the available capacity. In modern electronics, this results in a significant disparity between the available capacity and the estimated capacity, causing the device to shut down prematurely. The voltage depression is due to small crystal formations of electrolyte accumulating on the cathode/anode, increasing the internal resistance of the cell. Lead acid batteries commonly experience anodic corrosion, which makes the battery incapable of holding any charge. For nickel cadmium (NiCd), end life is exhibited by faster self-discharge due to the formation of cadmium dendrites.

Lithium-nickel-cobalt-oxides (with aluminum or manganese dopants)

Lithium nickel cobalt oxides (NCA and NMC) display an increase in the interfacial impedance of the carbon anode and the nickel-cobalt oxide cathode, which results in a significant power fade [47]. Under extreme conditions, there is a dissolution of nickel-cobalt-oxides into the electrolyte that occurs when the cells are cycled near their operational temperature limits, particularly if the high temperatures are sustained [48]. Symmetrical reduction in the incremental capacity for NCA shows that there is an equal loss of material from the anode and the cathode. NMC shows a slight tendency towards voltage depression, but this is can be avoided by occasionally fully discharging and then fully recharging the cells.

Lithium-manganese based

In lithium-nickel-manganese-cobalt manganese dissolution with the electrolyte, which leads to high internal resistance. Furthermore, as the manganese dissolves into the electrolyte the cells become more prone to thermal runaway [49]. For lithium-manganese-oxide the incremental capacity curves show a graphite reactivity reduction with lithium. This

31

type of battery chemistry also experiences high manganese dissolution with the electrolyte and therefore shows a significant increase in internal resistance. Of the four Li-ion chemistries reviewed here, LiMO shows the highest increase in internal resistance because of aging [49].

In general, chemistries that use manganese in the cathode show more significant heating than other chemistries. The dissolution of manganese contributes to the overall temperature increase observed in these batteries. LMOs show a more sensitive temperature rise than NMCs.

Lithium-iron-phosphate

The loss of reversible lithium, as opposed to the loss of electrolyte, originating from secondary SEI formation and dead lithium was confirmed by Liaw, Groot, Jin, and Shimpe among others as the cause of the aging for LFP. The team with Ouyang found that the aging due to loss of reversible lithium was especially strong when the cells operated at low temperatures. Akram in his paper "Performance comparison of four Li-ion battery technologies under calendar aging" shows that there is a loss of ions due to oxide particle isolation. The loss of reversible lithium, as opposed to the loss of electrolyte, originating from secondary SEI formation and dead lithium was confirmed by Liaw, Huhman Groot, and Jin, among others, as the cause of the aging for LFP [14] [50] [51] [4] [52] . The Ouyang team found that the aging due to loss of reversable lithium was especially strong when the cells operated at low temperatures [53]. In his paper "Performance comparison of four lithium–ion battery technologies under calendar aging," Akram shows that there is a loss of ions due to oxide particle isolation [49].

Non-Destructive Methods to Study Electrochemical Cells

Electrochemical Impedance Spectroscopy

Electrochemical Impedance Spectroscopy (EIS) is still one of the most promising methods for aging mechanisms investigation of Li-ion batteries [54]. EIS varies between various LIB chemistries. In LFP, EIS has one semicircle at the mid-frequencies which expands with calendar aging, rather than two semicircles [49]. Past investigations have connected the resistance and reactance relationship at low to mid frequencies with the change in cells' electrochemical phenomena, explicitly charge transfer, double-layer capacitance and SEI. In other LIB chemistries, the first semicircle relates to the SEI and the second, larger semicircle connects with charge transfer impedance [55]. Of the aging factors prevalent in Li-ion batteries, many of them stem from SEI growth. As the SEI layer thickens, it consumes some of the active material and increases overall resistance. EIS can be used to study the growth of the SEI layer and even point to the magnitude of the two phenomena [56] [57].

EIS assists in understanding some of the parameters regarding the chemical makeup and structure of a cell without disassembling the cell. This is achieved by perturbing the cell with either a voltage or current sinusoidal signal at a wide range of frequencies (i.e., anywhere between 1mHz to 100kHz) while the other electrical characteristic is measured (e.g., if a voltage sinusoid is used to perturb the cell then the current signal is measured). The perturbing signal is in the mV or mA range to find the linear approximation between the perturbing sinusoid and the measured signal at that frequency. The frequency range for any given EIS is chosen based on the chemistry of the device under test. Using the voltage amplitude and frequency paired with the current amplitude and frequency, the user can calculate the complex impedance of the cell under test. This is further explained by the figure below [58].
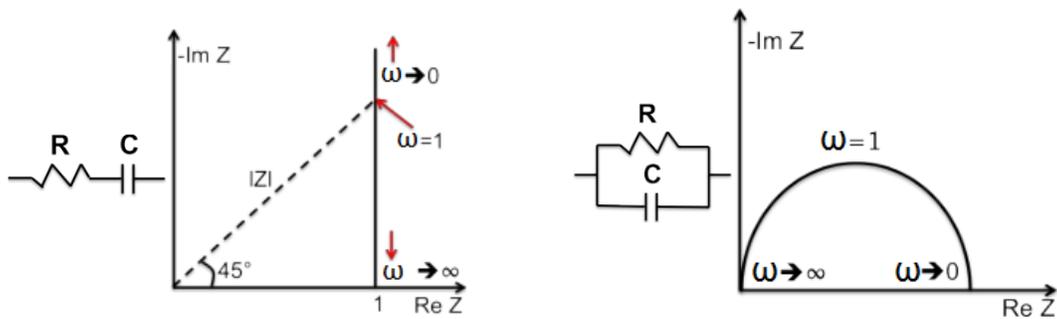
Figure 1: A) Series resistor and capacitor complex impedance B) parallel resistance and capacitor complex impedance [59]

Perturbing a cell with a current sinusoid and measuring the voltage is known as galvanostatic EIS. Potentiostatic EIS was used for this research's testing, meaning that the voltage was perturbed, and the current was measured. For the rest of this background, section voltage is the perturbing characteristic and current is the measured characteristic. There are two methods typically used to present the raw impedance data. One method is both a Bode phase plot and Bode magnitude plot. The other method used to present EIS data for an electrochemical cell is a single Nyquist plot, which plots the real impedance versus the negative imaginary impedance. The Nyquist plot is the most common, and the one used throughout the results section of this dissertation.

There are two main avenues of modeling the battery from the data obtained during an EIS. The first model presented is the electrochemical model. Electrochemical models are meant to represent the electrochemical processes occurring explicitly within the cell. The level of detail provided by these models makes them computationally complex and requires additional information outside of the EIS. This type of modeling is imperative to understanding the endemic flaws of specific chemistry. These models can suggest productive adjustments to current cells chemistries [60], much as was seen when researchers at UT solved LFP's low conductivity problem by using conductive materials to coat the particles and reducing the overall size.

34

The equivalent-circuit model is less complicated: It uses electrical components to represent the electrical dynamics of a specific electrochemical cell type. If an investigator takes EIS at different stages of a cell's discharge and analyses it, the investigator can gain valuable insights into essential changes that happen as the cell ages. These insights can then be used to understand how the changes will influence the battery pack dynamics in the future.

Different applications call for different models are representations, but the versatility of the application shows EIS to be a robust test [61]. The work presented uses significant figures of merit obtained from the EIS and associated with the equivalent circuit model, as this most efficiently give insight into the overall pack dynamics and aging markers. Therefore, an in-depth introduction to equivalent-circuit models is given [58].

The imaginary impedance, also known as the reactance, can be interpreted as a circuit model as capacitors, inductors and constant phase elements. The real impedance, or resistance, can be translated into resistors. Constant phase elements (CPEs) are empirical representations of the non-idealities of the multiple capacitances of the cell. The equation below is a mathematical representation of the CPE where Y_0 represents the capacitance.

$$Z_{CPE} = \frac{1}{(j\omega)^\alpha Y_0} \tag{1}$$

In a capacitor, α would be 1. In resistors, α is 0. In inductors, α is -1. Therefore, in a CPE, α is >1 to best represent the non-idealities recorded in the cells. A limited case of the CPE where α equals ½ and Y_0 equals the Warburg coefficient calculated from the Warburg tail of the EIS shown below. The Warburg diffusion element (or Warburg Impedance) is used to represent the charge transfer impedance (below), where A_W is the Warburg coefficient (or Warburg constant).

$$Z_W = \frac{A_W}{\sqrt{\omega}} + \frac{A_W}{j\sqrt{\omega}} = \sqrt{2} * \left(\frac{A_w}{\sqrt{j\omega}}\right) \tag{2}$$

There is also a finite-length Warburg element to incorporate the properties of the diffusion layer into the impedance equation. It is rare for the properties of the diffusion layer to be known, so this is a rarely used representation, but it provides insight into the general electrochemical relationships in batteries. A commonly used equivalent-circuit model is the Randles Circuit. The circuit schematic for the Randles Circuit can be seen below
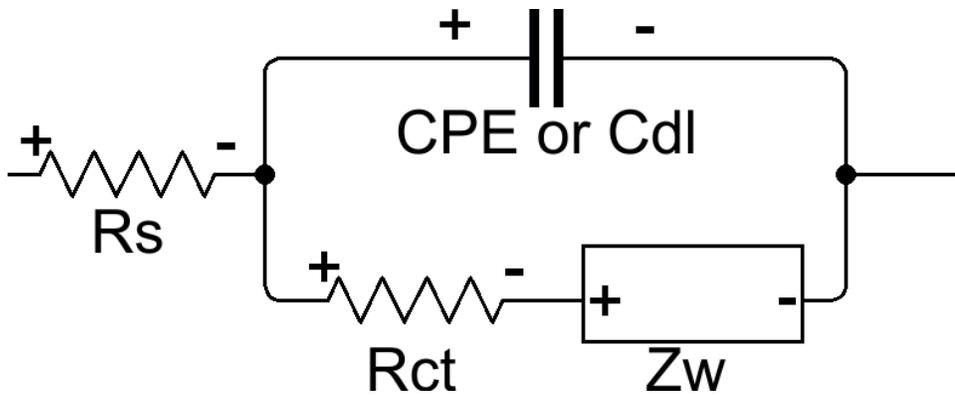
Figure 2: Randles Circuit a basic circuit used to replicate the measured reactance and resistance of an electrochemical cell

In this work, the relevant information can be obtained from a crucial feature in the EIS, and a full circuit model is not needed. For a review of the equivalent-circuit changes observed in parallel cells see work done at the Virginia Polytechnic Institute and State University by Dr. Brett Huhman [52]. Figure 3 is presented below as a reference. Using SEM and FRA/EIS, past research has made a connection between the Nyquist plot and changes in internal chemical structural changes. The author further explains the findings and how they are best applied to electrochemical cells, specifically LFP, in more detail to better acquaint the reader with the important figure-of-merit for the research presented here.
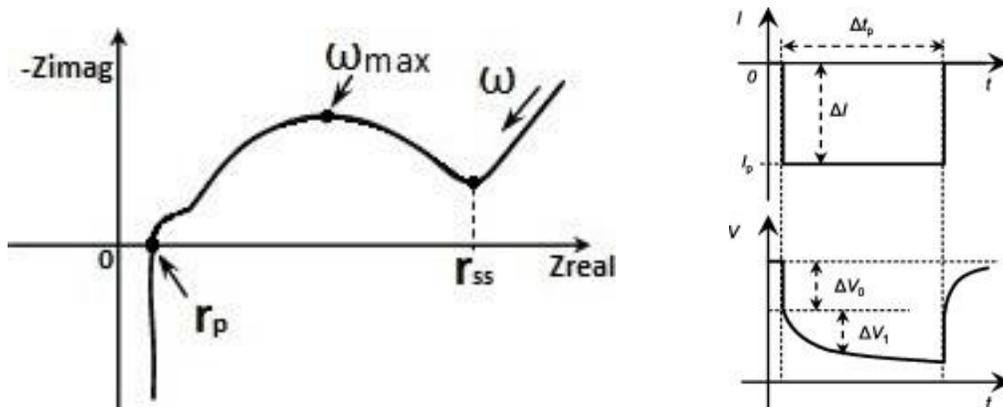
Figure 3: A) Nyquist plot with the key features for this research highlighted and label, B) initial current load applied to a cell and its voltage response, and C) cell's voltage response at the cell ages [62] [55]

The Nyquist plot is an excellent visual representation of the electrical changes relevant to this research. The zero crossing to the imaginary part of the impedance (labeled r_p in the figure above) is the pure ohmic resistance of the battery. Battery manufacturers often use an approximation of the metric r_p to bin cells [63]. The approximation is calculated using the resistance of a cell at 1kHz, where the imaginary impedance of a cell is often at or near zero at this frequency [64]. When the negative of the imaginary part of the impedance reaches a local minimum (labeled r_r), the real part of the impedance corresponds to the battery's direct current resistance or steady-state resistance (SSR). The r_r is not equal to the SSR, but it is an approximation and exhibits similar responses to external effects such as temperature and current [55]. The SSR loosely represents the pure ohmic resistance plus the charge transfer resistance, and therefore the r_r can be viewed as a close approximation of the addition of two. This approximation allows the user to calculate the charge transfer resistance from r_0 and r_s. The first (smaller) of the two semi-circles, seen in Figure 3 (a), relates to the SEI. The second, larger semicircle connects with double-layer capacitance and interfacial charge transfer reaction. If the first semicircle is small, then the SSR is closer to r_r. r_d.

In LFP, the first semicircle is unsubstantial, and therefore r_d can be assumed to represent the SSR with little loss in accuracy. The location where the negative imaginary part of the impedance reaches a local maximum designates the cell time constant. Meaning the angular frequency at which the negative imaginary impedance reaches its local maximum, labeled ω_{max} in Figure 3, is the inverse of the cell time constant. The time constant defines the relationship between current changes and the speed of the cell's voltage response.

Voltage versus Capacity Curves

The two main ways batteries exhibit aging are an increase in ESR and capacity fade. An increase in ESR leads to an increase in initial voltage drop at the same current rate while the linear region is settling at a lower voltage. A decrease in capacity results in a shorter voltage curve. Therefore, if the only aging exhibited in the battery were capacity fade, then the nominal voltage would be the same, but the nominal zone would end at a lower capacity. If the only aging exhibited in a battery is an increase in ESR than the voltage discharge curve will drop, but the voltage cut-off will occur at the same capacity. With an increase in ESR, more of the capacity will be lost to waste heat.

Chapter 4: Setup and Methodology

Setup and Testbed

In most commercially manufactured batteries using parallel connected cells, cells are interconnected using nickel tabs welded directly to the terminals, with no free space for individual current sensors. Given the parallel nature of voltage sensing, manufacturers can place voltage sensors on the outside of the pack. To read individual current, producers must place the current sensors in series with the electrical component they want to monitor. Therefore, the compact method of construction makes it impossible to study commercially assembled batteries thoroughly.

To overcome the instrumentation challenge, Matthew Martin, a graduate member of the Pulse Power and Energy Lab, developed custom printed circuit boards (PCBs) so that all relevant electrical measurements, current and voltage could be monitored on each cell within a parallel array. Furthermore, this open design allowed for easy placement of thermocouples to monitor the temperature of each cell throughout the experiment.

Cells assembled in a 1S/NP pack present an instrumentation challenge because manufacturers pack them in tight bundles with no extra space. This configuration leaves no room for the additional instrumentation needed to measure the current variation within the battery. To overcome this challenge, Mr. Martin a fellow graduate student at the time, designed custom printed circuit board (PCB) and experimental testbed to measure the current, voltage and temperature from each cell. Figure 2 presents a photo of the PCB used for testing. The PCB fits up to five 26650 cells connected in parallel.
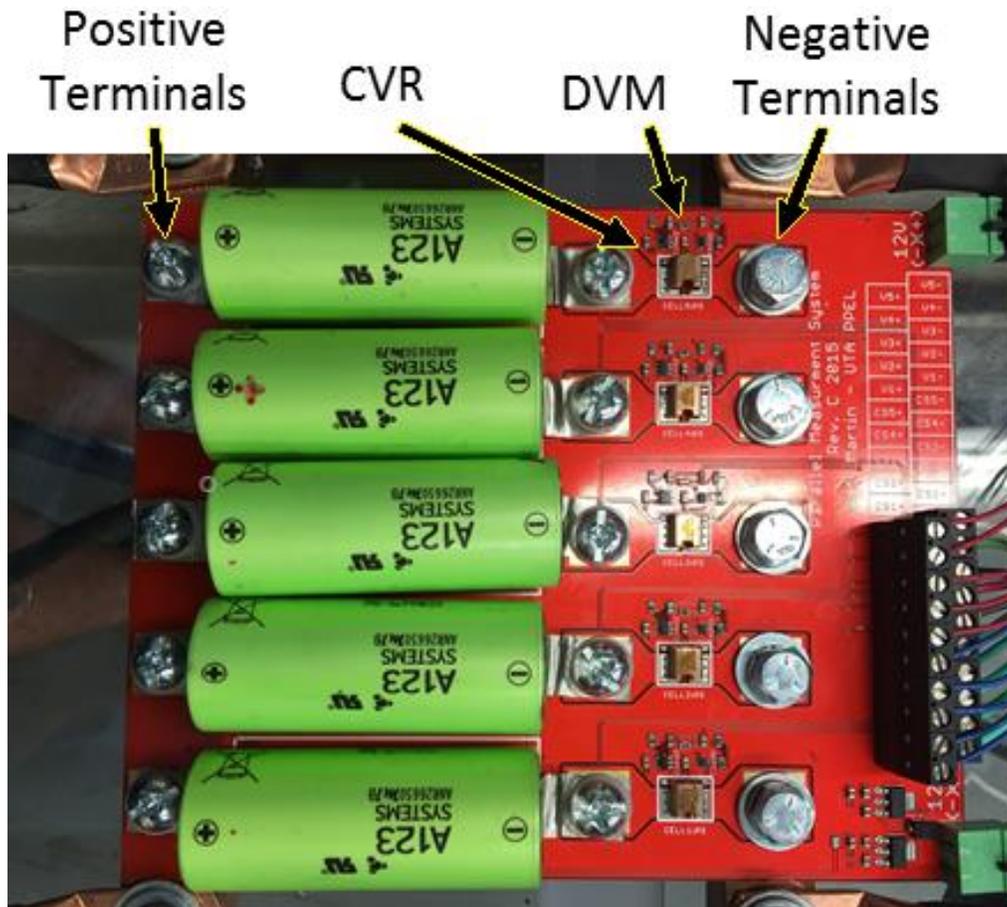
Figure 4: Custom-designed 1S/5P PCB for 26650 cells.

To measure the current in and out of each cell, a 300 µΩ current-viewing resistor (CVR) is in series with each cell's negative terminal and battery's negative PCC. Each resistor has a datasheet tolerance of 1%, which for the current loads here represents a maximum error of 353mA. Differential voltage monitors (DVMs) are connected across each cell's terminal so that they measure fully isolated voltage measurements across each cell. Voltage and current measurements are made using a dedicated National Instruments (NI) CompactDAQ (CDAQ) data acquisition and control system equipped with two NI 9205 CDAQ cards, each of which is capable of measuring 16 differential inputs with a resolution

of 16 bits. Each cell thermal profile is measured using NI 9213 CDAQ cards. The voltage, current and temperature of each cell are sampled at 25 Hz during each experiment.

The intent of the board is to simulate the parallel connections expected in a fielded multi-parallel cell battery. The temperature is measured using Type-T thermocouples attached to the middle of each respective cells body, plus one measuring ambient temperature. Six boards are connected in parallel to evaluate a 1S/30P battery. The cells were each assigned to position 1 to 30 (Figure 3), and those numbers are used throughout the results to identify the cells. The testbed connects the boards in parallel by having them bolted into copper bus work with a cross-sectional area of 1.27 cm x 1.27 cm (6.5 cm^2 copper bus bar). The actual negative terminal of each cell is attached to the board through a bolted connection into a threaded plastic bar to ensure good contact with the PCB pad. Electrical connections from each end of the positive and negative copper bars are made to connect to them to the programmable power supplies and loads. From there, the copper bus bars are connected to copper blocks (4.5 in x 11 in x 1 in) via seven 3/0 cables on each side. This was done to minimize location dependency of resistance within the testbed. From the copper blocks, two 1/0 cables connect to the loads and two 1/0 cables connect to the supply. The last cables were kept to 5.5 feet, the shortest distance possible, to reduce the energy lost over the cables.

Figure 5: 1S/30P battery and thermocouple input ports

Programmable loads and power supplies are utilized to discharge and recharge, respectively, the 1S/30P battery under profiles of interest to ONR. Up to three Chroma 63209 (80V/1000A/15.6kW) loads connected in parallel and two Ametek 80V/188A/15kW power supplies were available for this research. Even at the highest power levels, only needed two of the programmable loads and two of the power supplies. For the 5P test, only one load and one supply were required. Figure 4 shows the full experimental setup.
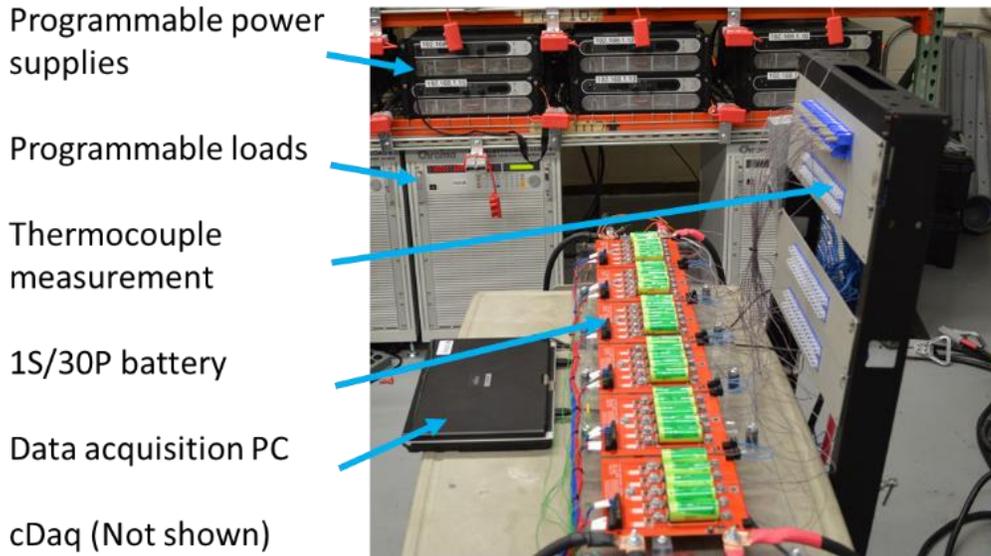
Figure 6: 1/30P battery experimental setup. The laptop was later changed to a PC, but the setup otherwise remained the same.

Four versions of the PCB were fabricated throughout the testing, two of which collected data for the experiments presented here. To reduce high-frequency noise in the second revision (red boards shown in Figure 4), a low pass filter was added to the output stage of the buffers used to measure the voltage and current of each respective cell. However, this revision suffered from significant impedance differences based on the location of the five different cells. The impedance of each channel's trace was measured using a Megger DLRO-10X micro-ohm meter. The trace resistance was measured across three boards, and each measurement was taken five times. Any outliers were thrown out and then the average was taken. Figure 7 shows the approximate impedance of each location between the positive cell terminal and the copper bus bar based on these measurements.
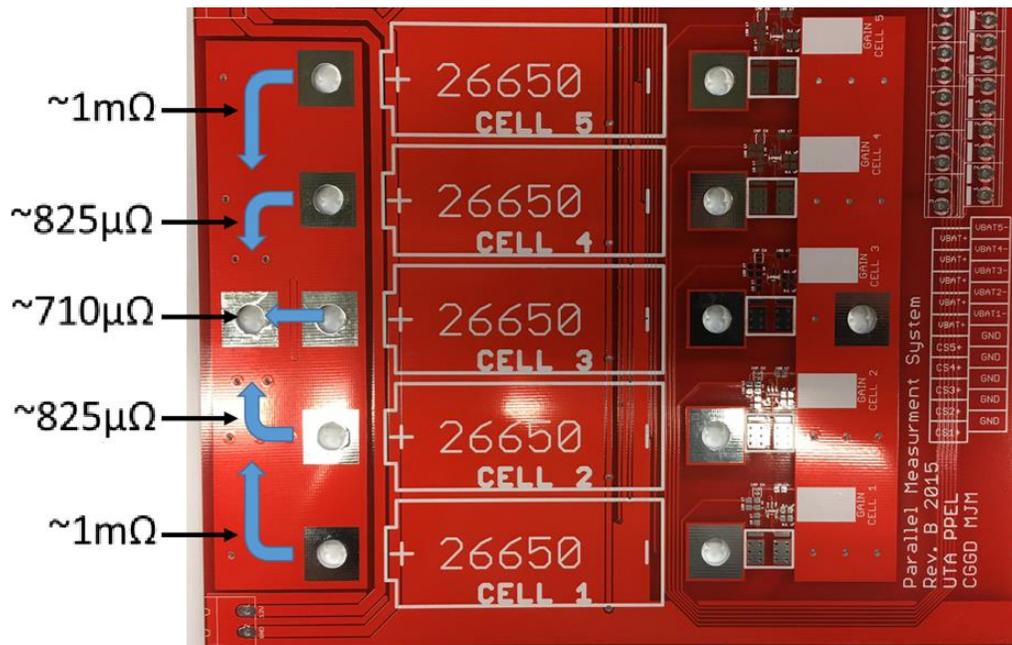
Figure 7: Relative impedance seen by each cell based on board location

In the results presented here, the experiments presented here used only the second and fourth revision of the board. In the third revision, the negative PCC was removed. Instead, each CVR terminal was tied directly into the large copper bus bars that carry current to the programmable loads and supplies. These boards are designed to conduct roughly 50 A per cell while introducing as little additional impedance as possible. The mask on these boards was found to be delicate and caused a short to the ground plane. The fourth revision was identical to the third except in shortening the ground plane, meaning that the positive terminal could not easily short to the ground and revert to the red mask.

The experiments presented here use 2.5 Ah cells manufactured by A123 Systems. The team chose these cells due to their cylindrical, 26650 form factor, their low ESR of ~7 mΩ and their ability to source high continuous power of ~170W. The lab purchased 110 cells in total across three difference shipments. From those 60, the author chose the cells being

cycled together at random. The random selection was made on purpose, as it simulates a worst-case scenario of impedance mismatch within a multi-parallel cell battery.

Because the difference between current in and out of cells should be small, it is critical that each current measurement made across the CVR be as accurate as possible. To achieve a high level of accuracy, the author carefully calibrated the gain of each cell's current monitoring circuit by running a -40 A to 20A ramp through each one. The ramped current was measured using a highly calibrated oscilloscope probe simultaneously with the NI CDAQ. The scale factor for each channel was calculated using the data from both measurements.

A custom LabView Virtual Instrument (VI) panel Figure 8 was created to collect this data and control the programmable cycler, discussed later.
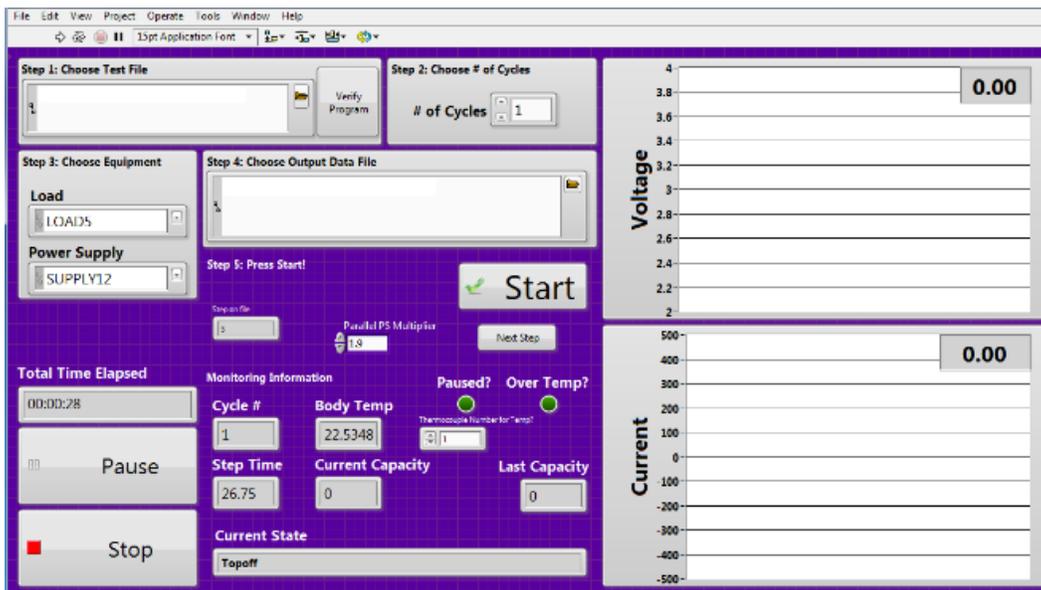
Figure 8: Front panel of the LabVIEW program used to measure the testing metrics in situ.

The cells were each assigned to position 1 through 30 Figure 9, and those numbers are used throughout the results to identify the cells. Chroma 63209 programmable loads (80V/1000A, 15.6kW) are utilized to load the cells under standard pulsed profiles. Ametek

45

SG series power supplies (80V/188A, 15kW) are utilized to recharge the cells after each discharge. The LabVIEW VI shown in Figure 2 is used to control the loads and supplies in real time while recording data from the CompactDAQ.

Figure 9: 1S/30P battery and thermocouple input ports

The testing uses 26650 cells manufactured by A123 Systems (model number ANR26650m1-B). The cells have a usable 1C capacity of roughly 2.5 Ah, a 1 kHz impedance of internally 6 mΩ and are rated to conduct approximately 70 A, 28C, continuously. The cells are optimal for these applications due to their high rate capability.

Experimental Test Plan

The power profiles were pulsed profiles at either 46 W per cell or 117 W per cell followed by a 3C recharge. After a specific number of cycles, which was based on test power level and type, the cells were baselined. The first type of test periodically baselined the cells to gain insight into progressive aging mechanisms. The second type of test only baselined at the beginning and end to see the current sharing of uninterrupted cells. The group of cycles between each baseline is a set, and the all the cycles from 100% capacity to 80% capacity are tests.

Pulsed Profile

Six experiments have been performed and reported here. The first tests involved a power level of 1390W, or roughly 46 W per cell, and 2,000 cycles were completed, with baselines

approximately every 200 cycles. At this power level, each cell provides power at around 6C. The second test included 313 cycles at a power level of 3500W, or 117W per cell. This last rate is approximately a 15C discharge rate. Periodically, throughout each series of experiments, the cells were removed from the array and baselined at the C/2 and 1C rates, respectively, for evaluation of the capacity fade induced during the intervening cycles. The author ran FRA measurements to assess the cells' internal structural changes across cycles with the cells at 50% state of charge (SoC). From this data, the author can evaluate the current variation and its overall impact. In the studies performed and the data presented, a negative current measurement indicates that the current is flowing into the battery (charge), while a positive current represents current flow out of the battery (discharge).

Baseline

Initially, all cells were put through a baseline procedure in which their 1C and ½C capacities were measured using constant current (CC) discharge and constant current / constant voltage (CC/CV) recharge procedures, respectively. These measurements were used to track each cell's capacity as well as make an estimated low-current DC ESR measurement. After these procedures, the baseline moved to the EIS measurements of each cell at 50% SoC.

To calculate the usable capacity of each cell versus the practical capacity obtained during cycling, a C/2 and 1C discharge was performed on each cell individually before the array was cycled. These curves were then used to calculate the low C DC ESR using the following equation:

$$R_{DC} = \left| \frac{V_{1C} - V_{\frac{C}{2}}}{I_{1C} - I_{\frac{C}{2}}} \right| \tag{3}$$

Next, the cell was recharged and discharged to 50% SoC and was run as part of a frequency response analysis-based (FRA) EIS measurement, which is used to obtain a quantification of the cell's internal impedance before experimentation. Finally, a top-off charge brings the cell back up to 100% SoC. These steps all constitute the baseline procedure. A baseline was conducted periodically, with the number of cycles between baselines changing based on the test run. Once baselined, the cells were cycled in the 1S/30P or 1S/5P array using the pulsed power profiles described above.

There are six tests presented in this dissertation. The first test baselines were at 50; 150; 300; 700; 900; 1,000; 1,250; 1,500 and 2000. The second test was baselined at 107, 170, 227, 253 and 313. The third test was baselined at 25, 53, 78, 103, 128, 153, 178, 203, 228, 253, 278, 304, 329, 354, 379, 404, 429, 455, 480, 505, 530, 555, 580 and 607. The fourth, fifth and sixth tests were baselined initially and at the end only. Running baselines at the beginning and end allowed a clear understanding of what would happen in fielded operation where the cells would not be partially reconditioned electrochemically by baselines.

Metrics Studied

Mean Current

Industry standard assumes that in-parallel cells have voltages that are so close to one another they can be treated as identical. That assumed dynamic held true for the voltages of the cells discharge in the below experiments. With this assumption, the voltage measurements taken during the testing reaffirms that little accuracy is lost in regard to SoH and SoC. Thus, current difference is the primary symptom of the manufacture discrepancies between cells. Because mean current is to be the leading manifestation of manufacturing variations between cells in parallel, due to locked voltage and temperture

variations stemming from current variations, packs, it is vital to see what the dynamic changes in the mean current the cells are experiencing throughout the cycling.

Four discharge windows were investigated to develop a full picture of the current dynamics between cells. The mean current for all the pulses in discharge was chosen to see the absolute difference between the cells. The researcher chose the mean current between 80%–20% SoC because this is the most linear are of an LFP's discharge curve. Using the linear region reduces the noise from the frequency of the cell-based internal dynamics, such as the charge transfer time constant [55], leading to a better understanding of current differences more inherent to any system and whose only solution is a BMS. Additionally, this is the optimal SoC window for battery performance, balancing runtime with cycle life; thus, it is a SoC window of interest to many readers [5] [65].

Presenting the mean current for the full discharge (i.e., from 0%–100% SoC) was chosen to see how variation change beyond the optimal window. Any applications where reliability and cycle life are more important than weight avoid the final 20%–0% of the SoC curve (e.g., temporary bases of operation, medical equipment, electric vehicles). This area of the SoC discharge curve is avoided due to being the area where real-time SoC calculation differs from the rest of the discharge curve [66] and that it has an outsized negative impact on cycle life [67] (Ramadass, 2003). Furthermore, this area reflects how the time constant and SoC affect the current imbalance. Knowing the magnitude of the impact these two parameters have allows the user to optimize a battery pack based on individual needs. The five-second rest period between pulses is examined to see whether the dynamics are seen when the cells are stressed (i.e., under discharge) and how this plays out when the cells are electrically connected but not under stress. The recharge is useful because understanding the potential asymmetry and how it varies from cell to cell is essential given

that, like most Li-ion chemistries, LFP is asymmetrical and requires lower charge currents than discharge currents.

Because the cells were discharged in a pulsed fashion, the mean current was calculated first by getting rid of the undesired portions of the discharge. For the mean "on" current, the rest periods were removed from the discharge before the mean current was calculated, and vice versa. To limit the mean to a specific SoC span, the overall capacity for that cycle was obtained from previous calculations and normalized based on the final capacity to get a SoC from 0 to 1. The start and end SoCs were then associated with array indexes on the individual current profiles. This method of SoC windowing reflects the SoC of the battery pack rather than each cell's SoC. Due to the difficulty of accurate in situ capacity calculations and clear ramifications of undervoltage, various cells within the battery pack can be at different SoCs, so using the pack SoC allows for clear insights into how this research applies to real-world situations.

Percentage Difference of Temperature and Current between cells

It is useful to look at the individual current supplied by each cell because it gives a full picture of the individual current levels the cells are providing. Examining the descriptive statistics of the salient electrical characteristics of the overall battery pack throughout its cycle life brings into focus how the parallelization of the battery pack contributes to the overall stress the cells experience during discharge.

There are several commonly used statistical indices available to describe the overall behavior of each data set. Percentage deviation provides insight into the impact of uncontrolled parallelization. If the load was either provided by one cell, or if a BMS was controlling the current supplied by each cell, the percentage deviation would be zero or near zero. The percentage deviation allows the reader to know whether allowing the current to remain uncontrolled is likely to push some of the cells in an LFP array beyond the

manufacturer limit. Furthermore, percentage difference allows for a comparison between various current levels.

The range of the current and temperature difference shows the magnitude of the current and temperature experienced by the cell throughout the cycling. The strength of the relationship between temperature and internal resistance is well documented [55][62]. Thus, knowing the difference between the minimum temperature and maximum temperature can help readers can determine whether the temperature of individual cells is a major cause for concern. Likewise, datasheets generally include current dependence on cell cycle life (e.g., A123 m1-b). The range of the expected current difference could be added to a model to predict the expected aging acceleration on the current supplying the most current in comparison with the mean or the cell providing the least. This expected aging acceleration is then compared to the actual differences in aging rates.

The percentages of current deviation, expressed as a percentage deviation from the mean, and the current range considered either the mean on current at the 80%–20% capacity or the 20%–0% capacity ranges in the calculations. The percentage temperature deviation and temperature range were calculated using the mean of the temperature within the 80%–20% SoC and 20%–0% SoC. The percentage temperature deviation and temperature range were also calculated using the unedited temperature within these SoC windows. This means that the current during the five-second rest was included therefore the same on time was used to ensure that current and temperature could be easily matched and correlated. The author chose these ranges because they are of interest to most readers. Many high-power commercial packs have electronics to keep the battery between 80%–30% SoC in early life and 80%–20% SoC later in the battery cycle life to get the most extensive cycle life out of the battery, with similar capacity available to the user throughout [5,59,63]. Therefore, looking at this area of the discharge curve shows importance for typical

applications. By looking at the outside this SoC window, the overall negative impacts caused by this SoC area are presented. If the negative impacts are small for LFPs, manufacturers could find it worthwhile to use this area of the discharge to allow for smaller battery packs or allow users to tap into this reserve under less critical conditions. Knowing the exact magnitude of the effect allows manufacturers to make economically optimal decisions.

Correlation of Various Figures-of-Merit and Current Supplied

One way to mitigate the imbalances seen in parallel packs is to classify the cells using a specific characteristic or set of characteristics. For classifying to be used, the chosen characteristics must be indicative of the current that will be supplied by the cell and easy to measure. A common characteristic used by manufacturers is the 1kHz impedance. This characteristic was chosen because it is commonly at or near this frequency that the imaginary impedance crosses zero. When the imaginary impedance crosses zero, then the real impedance at that point indicates the pure ohmic resistance. At this point, the manufacturer can quickly obtain the pure ohmic resistance within ±0.0X% error using a piece of equipment that only needs to produce a single frequency. Additionally, it takes less than a second to perturb the cell at this frequency, making it a quick metric to measure and therefore a useful metric for commercial use.

The conduction voltages recorded from a cell's ½C and 1C baseline procedure are used to calculate the low-C DC-ESR. The calculation (shown in Equation 3) is made by mapping the conduction voltage to the cell's SoC. Next, the 1C voltage is subtracted from the ½C voltage, and that voltage difference is divided by the difference in the two CC values—in this case, 1.25 A. Because the two CC baseline values are low, it is safely assumed that the cell's temperature rise is negligible during the discharge and that it does not play a role in affecting the cell's impedance.

Using the conduction voltage of each cell during the high-rate pulsed discharge procedure, the observer can calculate the high-C DC-ESR. The high-C DC-ESR is calculated in the same way that the lower-C ESR was calculated. First, the pulsed discharge conduction voltage of each cell is mapped to its SoC. The measured pulsed discharge current and the baseline ½C conduction voltage curves from each cell are then used to calculate the ESR. The high-C DC-ESR reflects the impact of elevated cell temperature on the effective ESR. At the power levels presented here—46W and 117W per cell—the temperature generally reduces the effective ESR for each cell. Consequently, the high-C DC-ESR is expected to reflect the cycling state of the cells more accurately than the low-C DC-ESR.

Electrochemical Impedance Spectroscopy

EIS was chosen for parallel array analysis is because it provides a broad range of insights while resulting in a minimal change in the cell characteristics. Furthermore, it does not require destructive testing of the cells, which would make it impossible to continue cycling them. Therefore, by choosing EIS, the researcher was able to take an intermittent diagnostic test of the cell and then continue the cycling. The frequency window, perturbation amplitude and battery SoC at testing are all chosen by the user based on the individual battery under test, allowing the user to tailor the testing to the battery and the phenomenon under study.

For the experiments done here, the EIS was obtained as part of the baseline procedure. A potentiostatic EIS was taken at 50% SoC with a 10mV perturbations taken between 10kHz to 10mHz with a data quality of four. That is, for each data point on the EIS, four measurements and the average value are reported to the data collecting software. The EIS was conducted using a Parstat 4000 developed by Princeton Applied Research in conjunction with a Maccor Series 4000 battery cycler. When deemed necessary by outlying number or Nyquist plot shape the FRA was repeated. Occasionally this resulted in a

notable change in the Nyquist but most often the outlying numbers were indicative of actual difference in the cells and no statistically significant changes were observed.

Difference between recharge capacity and discharge capacity

The directional change of the SoC, combined with the EIS, can indicate how the loss of capacity is happening. A capacity fade occurs at both the anode of the cathode through a handful of different processes. By assessing how the capacity absorbed changes from recharge to recharge and comparing it to how the capacity released changes from discharge to discharge, the observer can make inferences on the aging mechanics inside the cells [57]   Lu, 2007). It is essential that this single metric is paired with the understanding gained from the EIS. The EIS impedance spectra show subsequent shifts throughout cycling that has are related to the intercalation of lithium in the graphite cathode. The connection between the impedance shift and the internal cell structure is supported by the incremental capacity analysis, especially with the LFP chemistry [53] . Based on this strong foundation and Li-ion aging literature, the researcher points to the most likely modes of aging in the cells. These modes and the relevant internal changes contribute to the understanding of unbalanced current causes in future cycles. By assessing the environmental conditions and electrical measurements recorded during the discharge procedures and aligning them with the literature, the likely chemical changes occurring within the cells can illuminate how the parallel array alters which aging mechanisms are predominate. In cycles with multiple baselines, the researcher develops a timeline of these mechanisms and the feedback loop they create [70].

The difference between recharge and the discharge capacity was arrived at by calculating the capacity of the recharge from the start of recharge to the end, calculating the discharge capacity from the first pulse to the end of the ten-second rest with the five-second "off" periods included, then subtracting the discharge capacity from the recharge

capacity. A negative difference suggests that there is more of an anodic loss in that the active materials are trapped in the SEI or the graphite matrix, whereas a positive difference suggests more of a cathodic loss with the Li-ions not being released from the lithium iron phosphate Olivine matrix. The current measurements result in a precision of ± 5mAh, therefore the overall pack statistics are compared to determine whether there a significant enough difference between the two capacities exists. The metric that gives the researcher the most insight into the overall pack experience without resulting in cancellation is the most common capacity difference seen in individual cells or the mode of the capacity difference. The mean between the cells leads to error rates in either combining or an outlier causing the median to be unrepresentative. The mode, taken out to an accuracy of 10mAh, pulls individual cells out and allowing the frequency to verify that the behavior is typical and therefore representative.

Chapter 5: Experimental Results and Analysis

Test 1 – 46 W per Cell, 30P/1S, Intermittent Baselines

Given the rich amount of information available for all thirty cells in this test, it is imperative

to look at the data from multiple angles. As the following sections explore the data from the

cycles, a foundation of the metrics explored by the author is established for the reader.

Then the findings are summarized for the full 2000 cycles. The summary establishes the

key metrics. The key metrics are chosen because they are the most insightful and concise

metrics for establishing an accurate overview of the phenomenon seen in this research. In

the presentation of future tests, the author then relies on the key metrics established as

insightful and concise, with few updates, and in those sections. An extensive overview of

the data available is important to immerse the reader in the richness of the data available

and establish the veracity of the key metrics chosen. After the reader becomes acclimated

to the terminology and data landscape, then a summary of each test can be truly insightful.

Overview of the cycling data and available figures of merit

Initially, all thirty cells were baseline procedure established in chapter 2 section 2.2, which

included a 1C (2.5 A) and ½C (1.25 A) discharge and an EIS on each cell. [14] [15] CSSW.

Figure 10 presents the EIS measurements made of each cell before the 1389 W cycling.
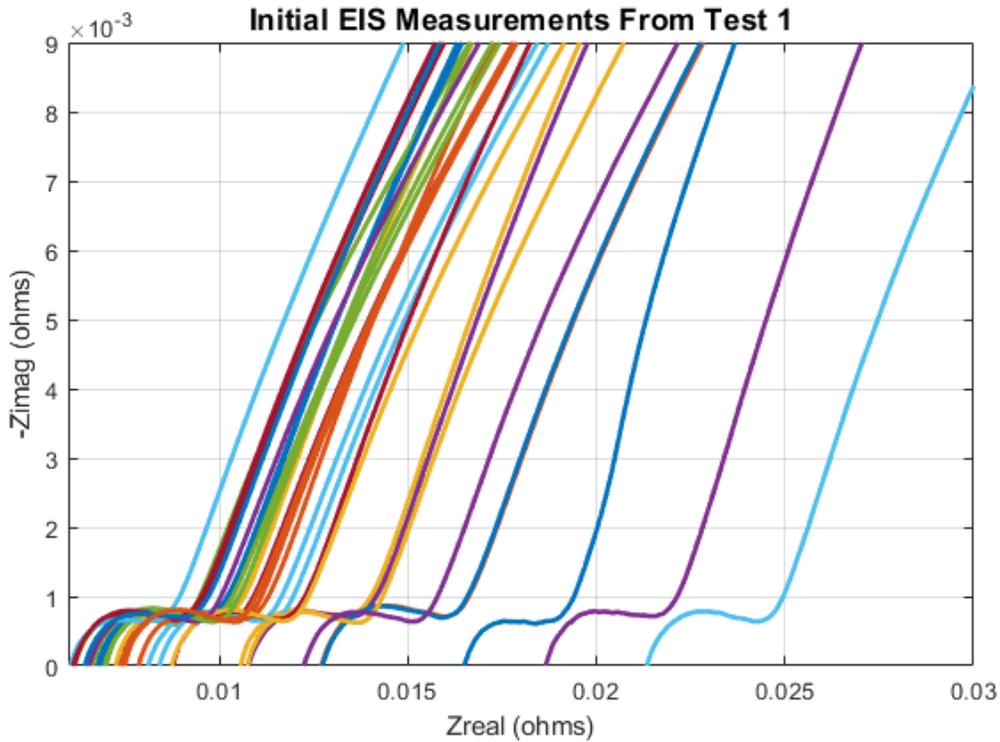
Figure 10: Test 1 electrochemical impedance spectroscopy (EIS) measurements made before any cycling

In addition to the EIS impedance measurement, the DC ESR of each cell was calculated. Since operation at a high temperature significantly increases the electrolyte's ionic conductivity, higher cycling rates lead to a reduction in the DC ESR. A histogram of the 'low C DC ESR' values measured among the thirty cells, between 20% and 80% SoC, before any high rate cycling is shown in Figure 6. In the figure, the reader can see that the 'low C DC ESR' values are between 13 mΩ and 18 mΩ. The 'low C DC ESR' value along with the 1 kHz ESR value is most often used by industry to define cell impedance [71].

Next, the thirty cells were assembled into the 1S/30P experimental setup, and they were pulsed discharged fifty times according to the discharge profile established in section 2.2 then baselines and then pulsed discharged one hundred times. Eventually the cells were cycled for 2000 cycles, these initial 150 are used in the next several pages to explore the

data made available by the cycling and baseline. The discovery of the increased PCB trace resistance does not reduce the usefulness of the data presented. Rather the data leading to the discovery of the increased trace resistance points to the richness of the data available from the cycling. Each cell should supply 46 W which results in between 13 A and 19 A (5C-7C) to the load at the 1389 W level. Ideally, they all share current equally, but that does not occur, as will be shown soon.
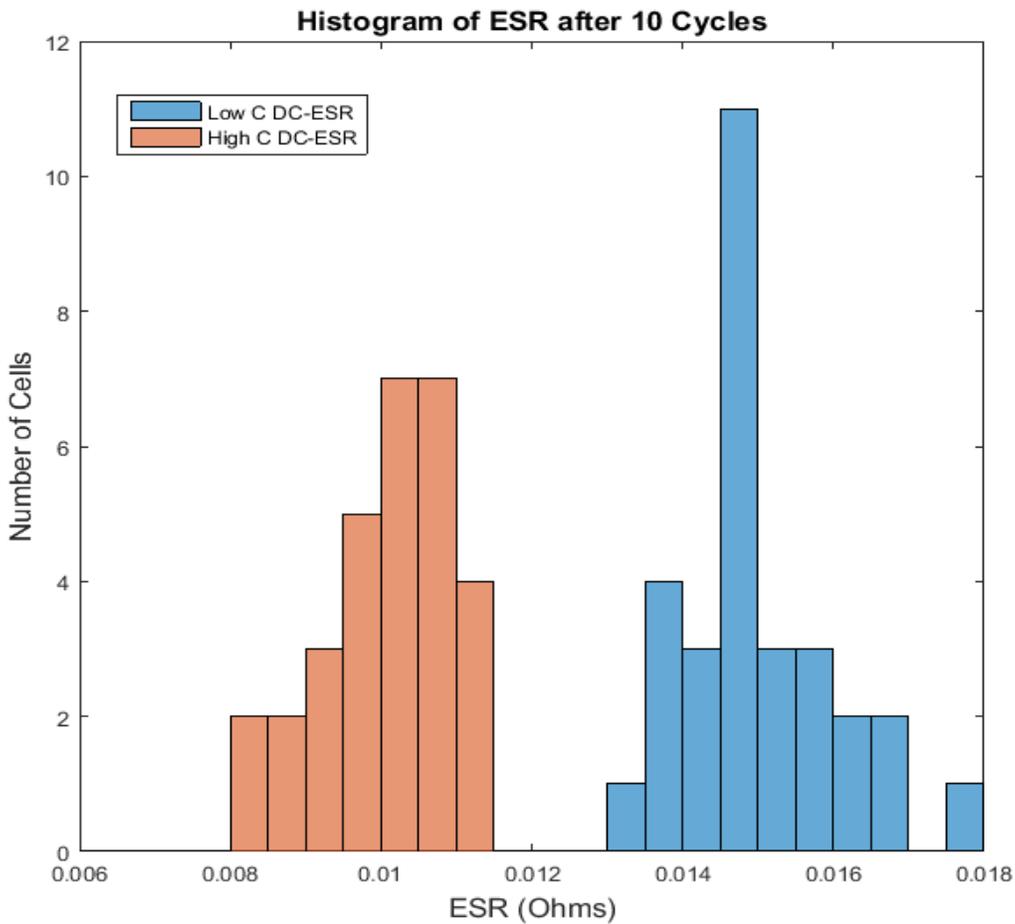
Figure 11: Test 1 histogram of the low C DC ESR and high C DC ESR calculations

Figure 11 shows the 'high C DC ESR' values measured during cycle 10 of the pulsed discharge procedure. As seen in Figure 6, the 'high C DC ESR' values are significantly lower than the 'low C DC ESR' values, eight mΩ, and 11 mΩ. The 'high C DC ESR' values

are lower because the cells are operating at higher temperature at the higher C rate. It is also important to notice that the variation in the thirty 'high C DC ESR' values is significantly less than that seen in the 'low C DC ESR' values. Seeing both histograms, as well as the difference between them, brings up a dilemma of what ESR value should be used to assemble a battery of similar ESR cells and also of which one should be used to understand how impedance affects the sharing of current in a battery made up of multiple parallel cells.

The one hundred fifty cycles discussed here occurred over two periods. During the first period, fifty cycles were performed, and during the second, one hundred cycles were performed. Figures 7 through 11 are a sample of the electrical and thermal data collected during twelve of the 30s on/5s off pulsed discharge cycles. Figure 10 shows a zoomed-in view of the current measured from each of the thirty cells during the last three pulses of a discharge cycle. From Figure 10 it is easy to see the variation in the current amongst the thirty cells. The cell sourcing the highest mean current supplies roughly 5 A more than the cell sourcing the least mean current. Given that the mean cell current is roughly 15 A, the variation between cells is quite significant. The thermal data plotted in Figure 11 shows how the variation in current leads to significant variation in the thermal heating of the cells. A peak variation of almost 5°C is measured. Although 5°C does not seem like much, keep in mind that the cells are being operated at only 20% of their maximum current rating. If the cells are operated at higher currents with a 20% variation, the deviation in heating will rise, as is verified in a later test.
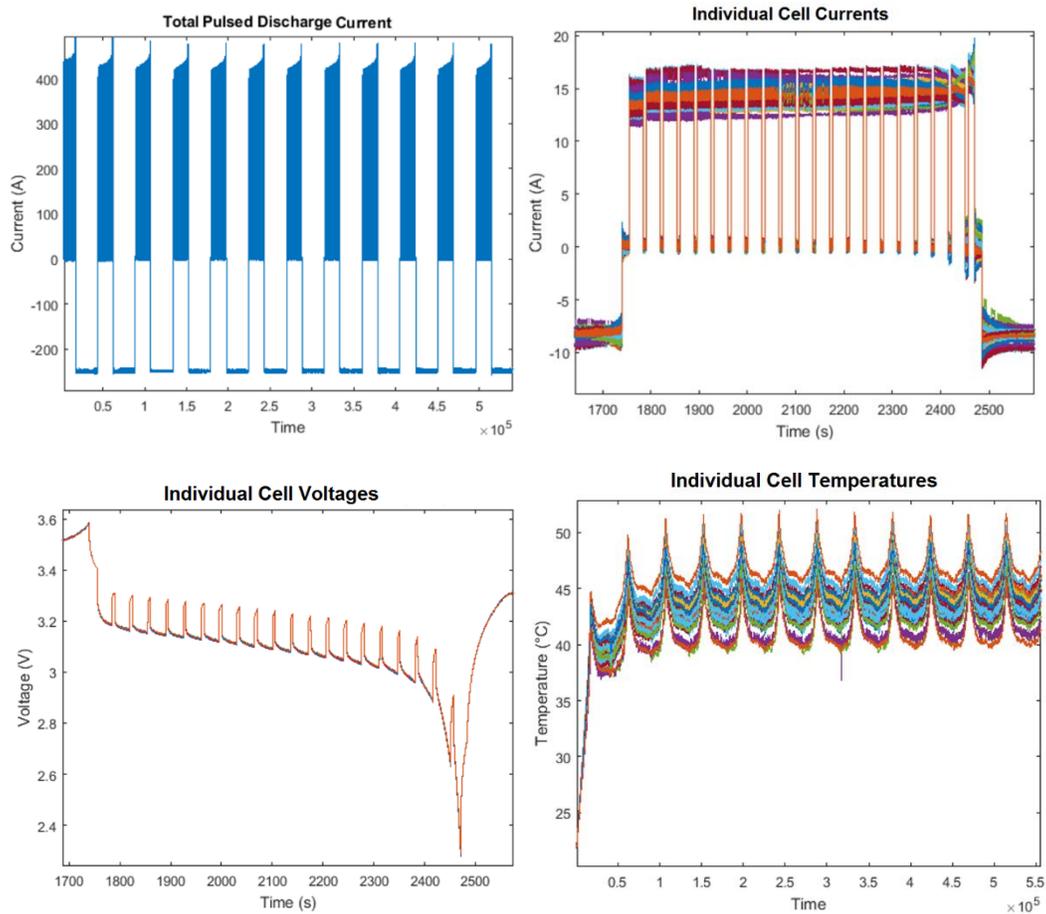
Figure 12: Clockwise from top left test 1 A) The plot of the total battery current vs. time during twelve cycles. B) The plot of each cell's current vs. time during one discharge C) Plot of each respective cell's temperature vs. time during twelve pulsed discharges D) Plot of each respective cell's voltage vs. time for one discharge

The results show that significant variation, roughly 25%, is present when multi-parallel cell batteries are operated at elevated rates. One question that arose when evaluating the results concerned the impact that PCB trace impedance, especially the variation amongst the five cells on each respective board shown in figure, has on the uneven current sharing observed in figure 4. The impact of trace resistance was studied further and will be discussed in depth later, but these figures show the richness of information embedded in the cells current when paired with the EIS measurements. The similarities of the current

for identical board position, knowing the random distribution of the cell, pointed to similarities in each positions trace resistance. After the one-hundred fifty pulsed discharge cycles were completed, the baseline procedure was repeated so that the impact on cell aging can be measured. Figure 11 shows a histogram of the calculated 'low C DC ESR' and 'high C DC ESR' values, respectively. The 'low C DC ESR value was calculated using the ½C and 1C baseline discharges measured at the completion of one-hundred fifty cycles. From this plot, it should be noticed that the median ESR values have stayed roughly the same, but the variation has decreased slightly in both respective DC-ESR categories. An initial decrease in the impedance variation, measured as/the equivalent low C, high C and 1kHz, is expected early because these first cycles allow the solid-electrolyte interphase (SEI) layer to property develop and stabilize. As cycle life continues, the electrolyte will start to break down and the electrodes, especially the anode, will begin to degrade resulting in impedance growth. The EIS measurements made during the most recent baseline procedure are shown in Figure 13. Those measurements also show tightening of the variation in cell impedance.
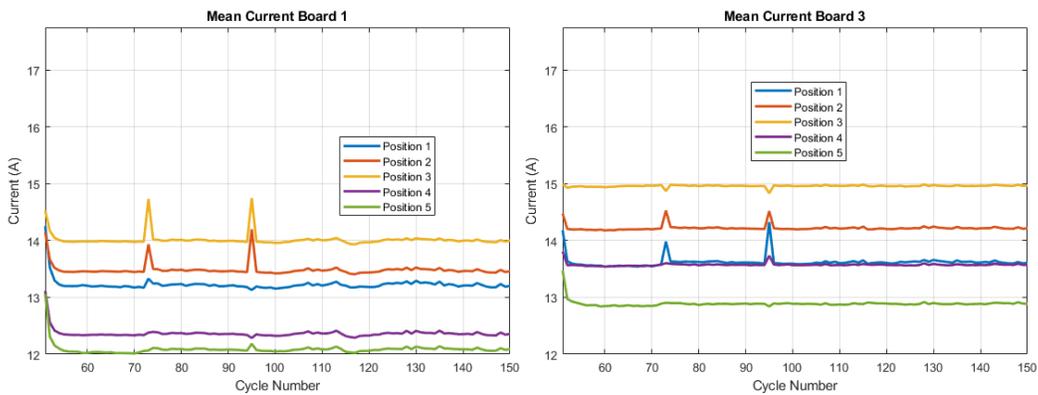
Figure 13: Test 1 normalized current for cycles 50-100 for board 1 and board 3, which shows the similarity in the current supplied by cells in the same board position, despite lack of other similarities.
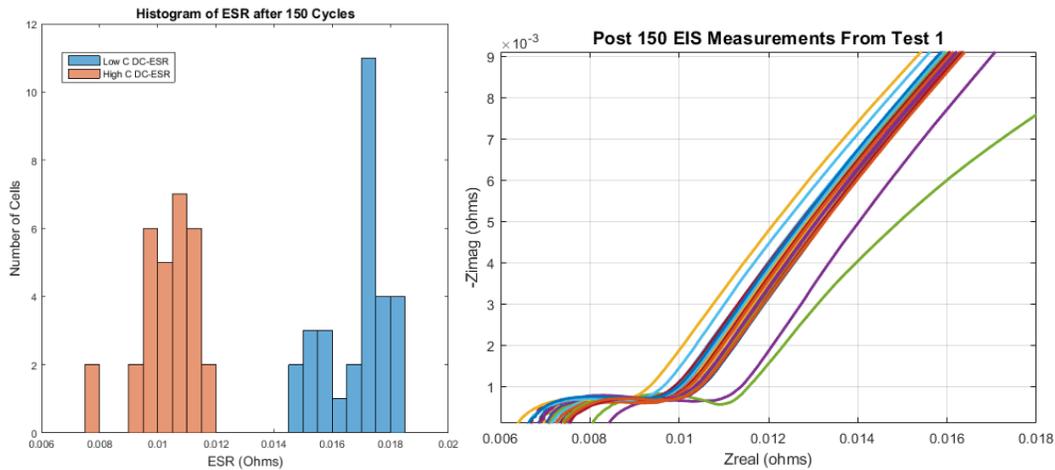
Figure 14: Test 1 A) Histograms of the DC ESR calculations made from the post 150 baseline procedure discharges and the 150th cycle of the pulsed discharges B) Electrochemical impedance spectroscopy (EIS) measurements made before the 150 pulsed cycles

Using the DC- ESR measurements, a study of the correlation between current variation and cell impedance can be made. It would be expected that the cell with the lowest internal impedance, as measured by the initial baseline, would supply the most current whereas the one with the highest impedance would supply the least current assuming that all other impedances external to the cell are the same for all of the cells. Figure 14 plots the mean current measured from each of the thirty cells during the tenth pulsed discharge cycle vs. each of their respective initial 'low C DC ESR' and 'high C DC ESR' values. Figure 15 plots the mean current measured from each of the thirty cells during the 150th pulsed discharge cycle vs. each of their respective 'low C DC ESR' and 'high C DC ESR' values measured during the second baseline procedure. From the plots, it is clear to see that there is a direct correlation between the mean current measured and their 'high C DC ESR' but not much of a correlation between the mean current and their 'low C DC ESR'. The 'low C DC ESR' is a common metric used by industry to assemble batteries using multiple cells and the lack of correlation suggests that it would be difficult to use that value to predict how cells

will share current or to properly assemble a battery for that matter. The plot does suggest that better prediction could be made if a battery is assembled using their 'high C DC ESR' value however more still needs to be studied before that can be said with a high degree of certainty.
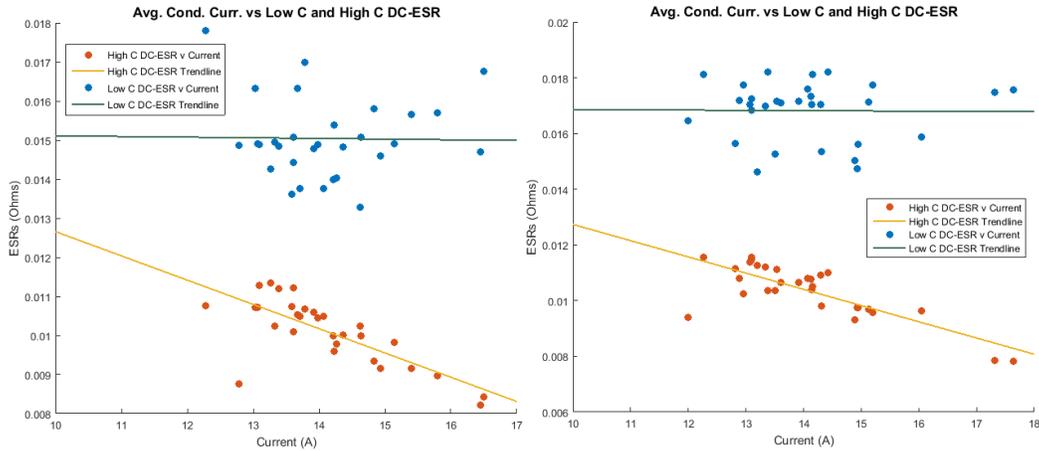
Figure 15: Test 1 Current from the A) 10th and B) 150th pulse correlated with low and high C DC ESR

One thing that the data presented thus far does not show is how the impedance of each cell changes as cycle life evolves. The data in Figures 14 and 15, respectively, show values representing each cell but does not indicate what cell it represents. A plot showing how the 'low C DC ESR' and 'high C DC ESR' varies for each cell between the first and last pulsed cycle is shown in Figure 16.
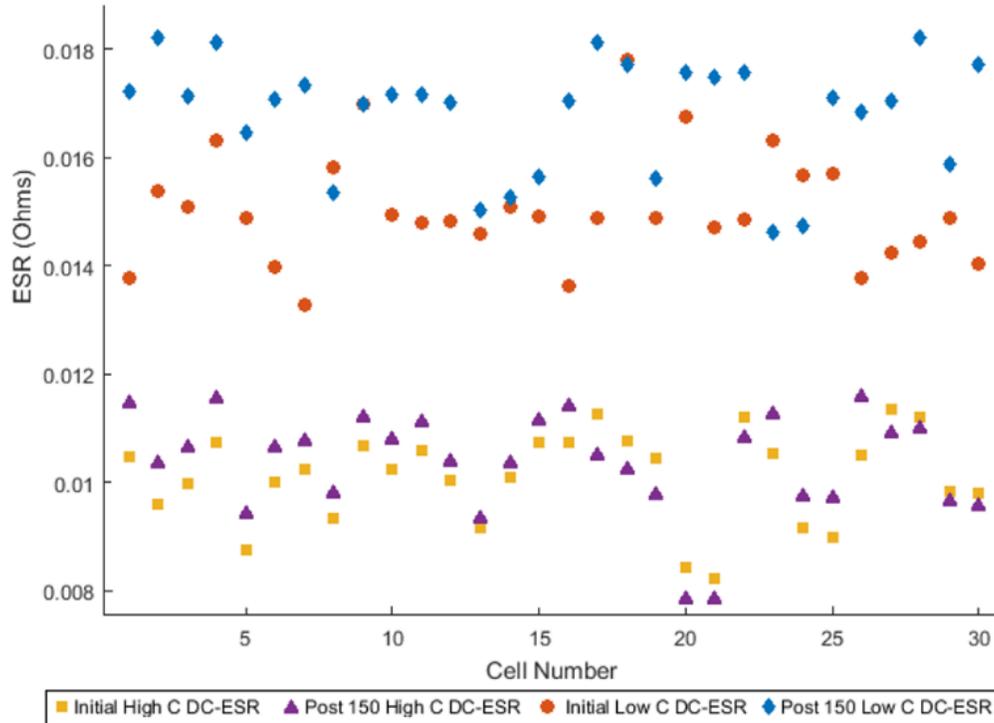
Figure 16: Test 1 The plot is describing how the 'low C DC ESR' and 'high C DC ESR' of reach respective cell varied between the measurements made earlier (initial baseline and cycle ten) and later (second baseline and cycle one-hundred fifty)

Figure 16 points to several trends which a reader can notice. First, it appears that both the 'low C DC ESR' and 'high C DC ESR' generally increase over the 150 cycles, with only a few outliers. Given that 'Low C DC ESR' is not a good indicator of current sharing, it is more important to pay attention to the variations in the 'high C DC ESR values.' Cells 17 through 22 and 27 through 30 each have a slightly decreased 'high C DC ESR' value during cycle one-hundred fifty than they do during cycle ten; however, all the remaining cells have a slightly decreased ESR later in the cycle life. Though cells 17 through 20 appear to have a more significant decrease in their 'high C DC ESR,' there is no good indication from the

data as to why this would be the case. What the data presented thus far does not provide is the long-term impact that the uneven current sharing will have on each cell's SoH. The literature does not fully answer the question if uneven current sharing will lead to uneven degradation; or, if somehow the degradation rate of each cell will vary throughout its life and lead to even degradation over the long-term. This work through the full six tests presented here answers that question more thoroughly and with a more accurate statistical representation of full cells discharge than has previously been presented.

Early investigations into trace resistance

Early in the analysis of the results presented previously, questions arose concerning the impact that board trace impedance has on the level of current imbalance observed. Measurement of the negative trace impedance on each of the six PCBs reveals that cells 1 and 5, the outer two cells respectively, have roughly 1 mΩ of trace impedance between the output of each CVR and the negative PCC. Cells 2 and 4 have roughly 0.83 mΩ of series impedance respectively, and cell 3 has roughly 0.71 mΩ of series impedance.
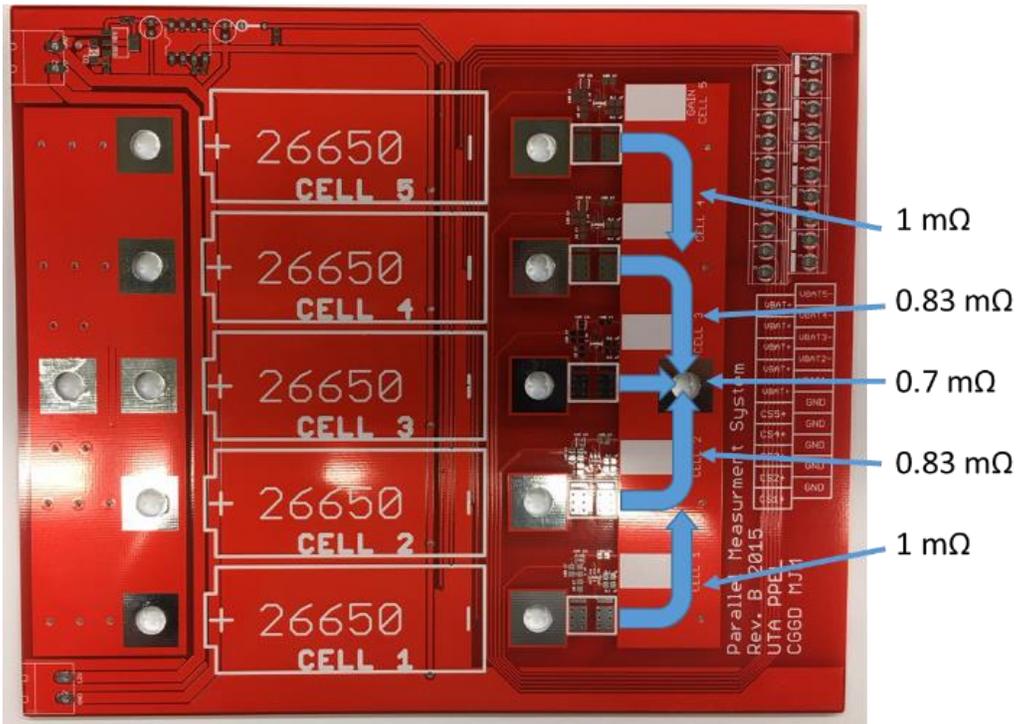
Figure 17: Original board used for cycling the parallel cells with each channel's internal impedance imposed on top

There is roughly 3 mΩ of variation in the DC-ESR impedances measured amongst the thirty cells. Therefore, the 0.13 - 0.3 mΩ variation in trace impedance is a maximum 10% of the difference in the DC-ESR variation. The magnitude differential means that even if the cell with the lowest DC-ESR impedance was in a position with the lowest trace impedance, it would only add marginal differences to the ESR compared to what the cells alone contribute. Thus, at the time, it was concluded that cell position should not play a dominant role in the results observed here and that the current variation measured is mostly a result of the cell's own ESR variation and the data were useful for analysis. Despite it not seeming to have a dominant role, testing was stopped to allow for further investigation into the data from the first 150 cycles to see if this assumption was correct. While the author was working on the analysis, Matthew Martin revised, fabricated, and

populated a board that eliminated the variation in board trace impedance. The new board shown in the test bed section removed trace resistance differences by removing the negative PCC and instead the negative terminal of each CVR is connected directly to the negative copper bus using a bolted connection. The revised board eliminated the position dependent impedance, and all further tests presented in these chapters were performed using these boards. It is essential to keep in mind that in the laboratory the position dependent impedance can be eliminated, yet it will be present in constructed batteries and therefore the manufacturers need to include it in their design for a truly accurate understanding of how their parallel arrays will behave once they are installed in fielded batteries.

The analysis of the following cycles revealed that small differences in trace resistance for each cell position had a significant impact on current sharing. This discrepancy in trace resistance contributed more to the current imbalance than the manufacturer variations in the cell, despite being a smaller added resistance than the calculated 'low DC-ESR.' One attribute of the trace resistance, which is different from internal cell impedance, is that the circuit resistance is a constant. It impacts all stages of the cycle equally whereas the impedance of the cell varies based on the time constant of the reaction. The goal of this research did not involve the effect of circuitry on the performance of parallel-cells, but research done by others does show that the constant nature of circuit voltage combined with the relatively low impedance of LFP makes them vulnerable to poor circuit design [35]. From the analysis of these 150 cycles, paired with other literature, points to an economic exchange between careful and expensive pack assembly vs. shortened cycle life.

After this new board was designed, the cells completed a further 1850 cycles with baselines taken at 300, 500, 700, 900, 1k, 1.25k, 1.5k, 1.75k, and 2k. Figure 4 presents a summary of the current and temperature imbalance calculated using the mean absolute deviation,

for all 2000 cycles. The seven times larger current difference for the first 150 cycles shows how the trace resistance impacted the current imbalance.
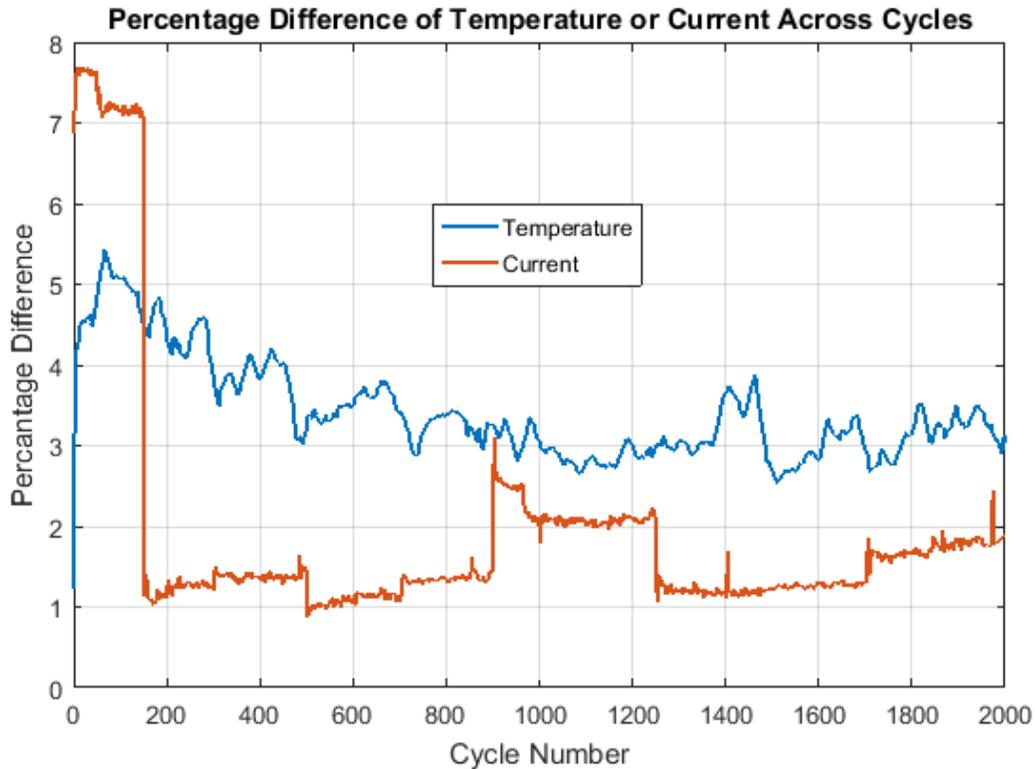
Figure 18: Test 1 Percent absolute deviation between individual cells' current and temperature, based on the mean values between 80% and 20% SoC of each discharge cycle.

The sharp changes in the percentage difference mark the point at which the cells are baselined. These 1C discharges done as part of the baselines procedure were used to measure the 1C capacity. The capacity measurement, or capacity fade, are presented throughout the paper in conjunction with other metrics to give a complete picture of the overall performance of the cells. As this figure shows, there are small current imbalances throughout the 2000 cycles. There is a ~1.5% mean current difference between cycles 150-2000, with a corresponding ~3.6% temperature difference between cells. The temperature is noisy, with T type thermocouples having an accuracy of ±1ºC. Therefore the ~11%

68

change between the highest and lowest temperature difference, which correlates to about ~5ºC, is near the noise threshold of the thermocouples. Therefore, unlike what was initially presented the temperature is not significantly contributing to the aging. Furthermore, the aging mechanisms in these batteries are not due to increase resistance, because that would result in measurable temperature differences. Other literature on LFP also finds that capacity fade rather than increased resistance is the primary form of aging [46]. The sharing and subsequent stress on the cell changes throughout the discharge, mainly as the cells get to the end of the linear portion of their voltage curve. The next section investigates these changes and the overall current sharing across the whole discharge

Dynamic Changes across the discharge

To better explore the current imbalance, an in-depth look at the last three pulses in a cycle are presented along with a look at variations in the cell's SoC. The previous three pulses give a good overview of what is happening throughout because the first pulse in the series shows individual currents like the rest of the discharge whereas the last two pulses show what happens as the cells are pushed past 20% SoC, a customary cutoff for commercial applications. The SoC and the end of recharge can indicate whether potential loss of capacity come from anodic or cathodic reactions.

Figure 19: Test 1 Individual cell currents during the last three pulses of the 500th discharge

Initially, after fixing the board problems, the current imbalance decreased significantly. For the next 350 cycles, there are no significant changes in the cell current and temperature. Due to the unrepresentative nature the first 150 cycles and that the initial trends from these cycles were not reflected to immediately following the end behavior of those cycles is not covered in depth. The insightful end behavior begins at the 500th cycle after the 4th baseline. By the end of the 3rd set, cycles 300-500, the cell capacities have faded, and the end current imbalance has increased. The 1C capacity showed that there is a mean of 0.14 Ah fade from the first 2.56 Ah. Furthermore, after fixing the boards, there was an overall decrease in current imbalance. The increase in current inequality for the last two pulses has become significant and a cause for concern by the 500th cycle. Specifically, Figure 3 shows that the

70

cell(s) providing the least amount of current during the conduction period then sink current from the other cells during the rest period between the conduction periods. The following figure 4 shows that the cell providing the most current during the on-time recharges the low performing cells during the rest.

Individual Cell Currents During the Last Three Pulses of a Single Pulsed Discharge Cycle
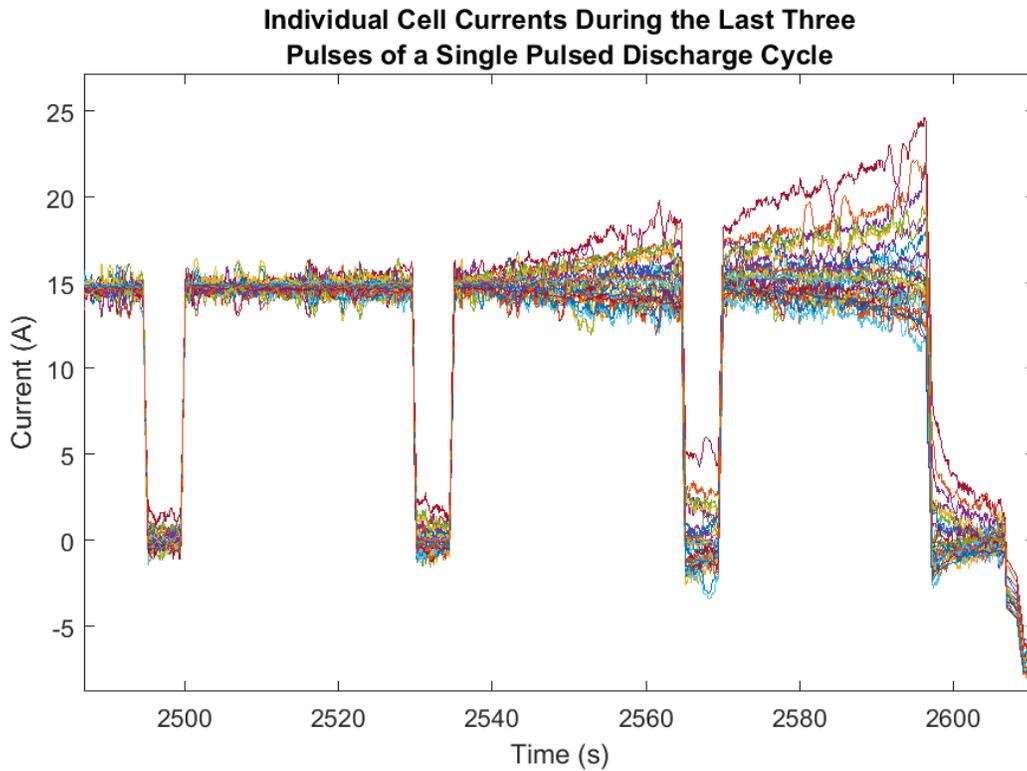
Figure 20: Test 1 Individual cell currents during the last three pulses of the 900th discharge

By the end of the 900th cycle, the separation at the end has become so significant that during the last rest period, cell 14 sources 5A while cells 12 and 29 sinks 2.4A each. Other cells are seen in either sink or source current, cells 14, 12, and 29 are pointed out as extreme instances of this trend. Current imbalance between cells increased as the low functioning ones continued to source near 12A, but the high performing cell began source ~24A. Previously, there was a more even distribution of current provided at the end of discharge. There was a near even split of cells below the mean current as above it, and

these were similar distances away from the median. By the end of the 500th cycle, the cells were already starting to show an increase in the current imbalance for the final 20% SoC, to the degree that two of the cells were sinking current from the rest of the cells during the off period. By the 900th cycle, as the capacity faded, discrepancies increased to 4.08%. By this cycle, instead of most of the cells sourcing a small amount of current to compensate for the low capacity cells, one cell is sourcing a significant portion of the current needed, while the low capacity cells sink current.
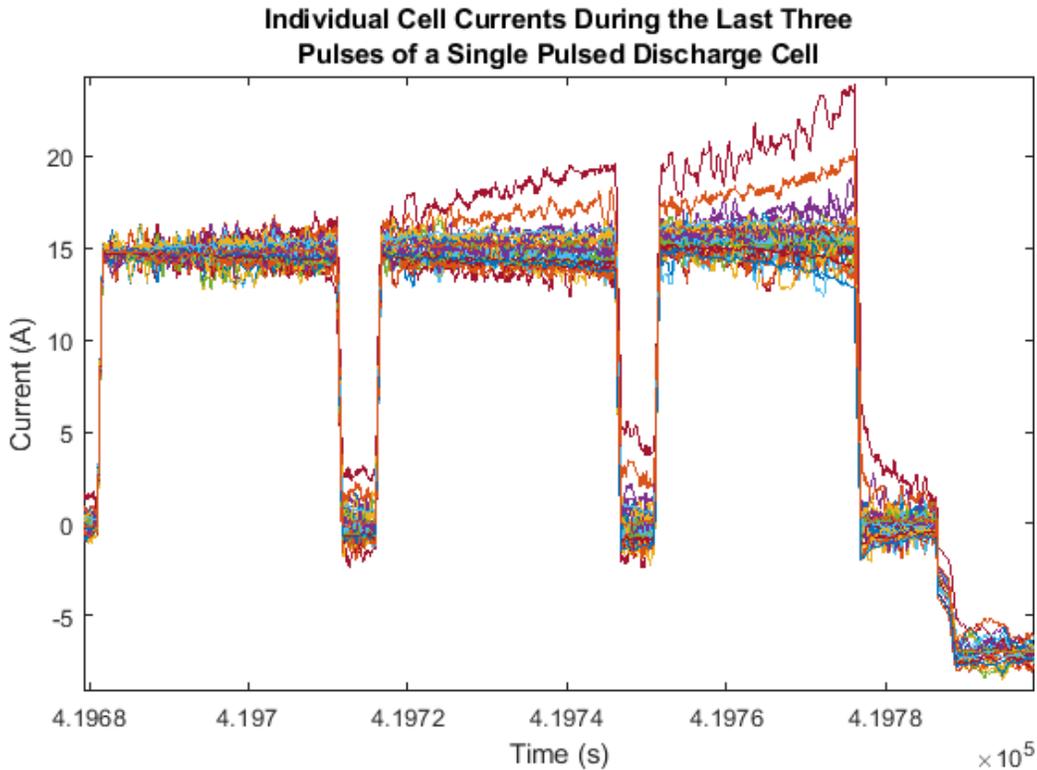
Figure 21: Test 1 Individual cell currents during the last three pulses of the 1500th discharge

This trend of strong cells compensating for weak ones propagates throughout the rest of the testing. Eventually, a few of the high performing cells' end current are 10% above the median; and, several low performing cells' end currents are at 10% below the median. Instead of one cell contributing ~8A above the median two cells individually contribute

72

~4.5A above median. Therefore, there are long-term balancing effects. The balancing, and its positive effects, comes later than would be seen with a BMS. Much of the adverse effects could be mitigated by reducing Amp-hours during each discharge cycle so that the cells stay at or above 20% SoC.
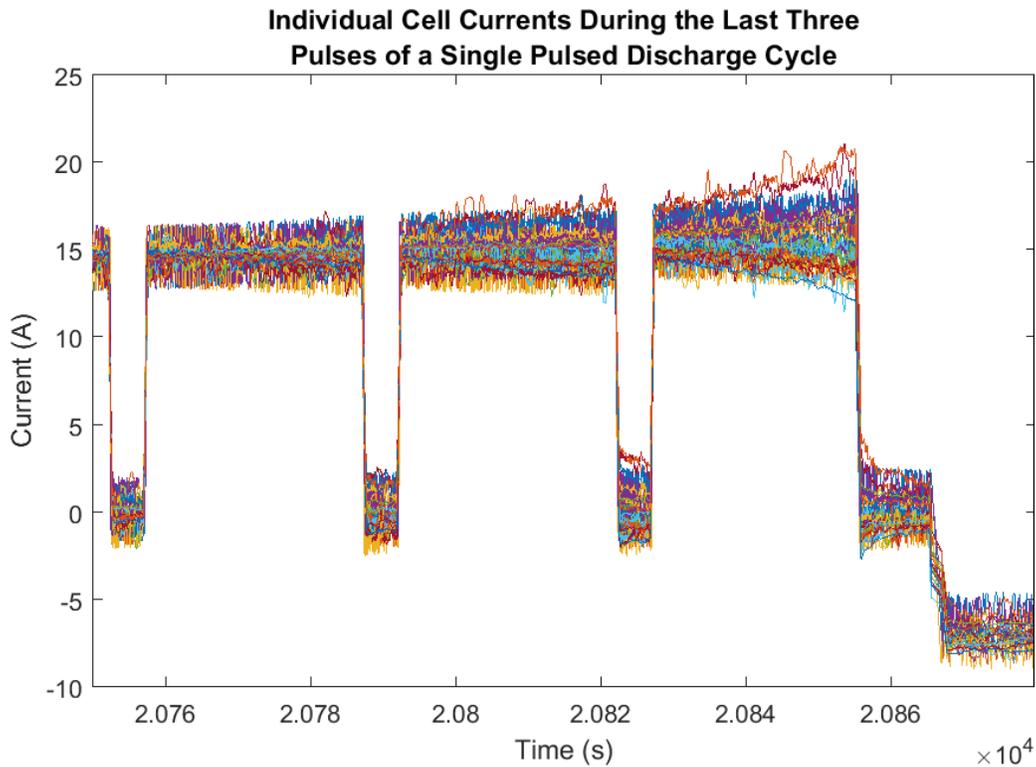
Figure 22: Test 1 Individual cell currents during the last three pulses of the 2000th discharge

After 2000 cycles, as the capacity fades, the current imbalance overall increases with a standard deviation current of 1.82. With the increase of the overall current imbalance, the end of discharge imbalance is less noticeable because it is not as substantial a percentage increase. This trend would cause a more significant impact except for the fact that it does not begin until the cells have reached a mean capacity fade of 15.7%. With only 4.3% capacity fade left until the battery is at the end of its usable life, the increase in current imbalance only modestly contributes to decreased cell lifetime.

Recharge and Overall SoC Balance

The directional change of the SoC, combined with the EIS, can indicate how the loss of capacity is happening. Capacity fade occurs at both the anode of the cathode through a few different processes. By accessing how the capacity absorbed changes from charge to charge and comparing it to the capacity-released changes from discharge to discharge. This paired with understanding how the EIS lines up with the typical impedance spectra of intercalation electrode some concept about what might be affecting the aging of the cells and contributing to the unbalanced current. By accessing the environment, and the overall discharge behavior then comparing to the aging mechanisms commonly found in literature at similar environments and power levels, can help illuminate how the parallel array alters which aging mechanisms are predominate.

The median and mean for the difference between recharge and charge are slightly positive at 1.8mAh and negligible, respectively. Looking at the mode of the difference between recharge and charge, what individual cells are experiencing most often is a general negative trend.
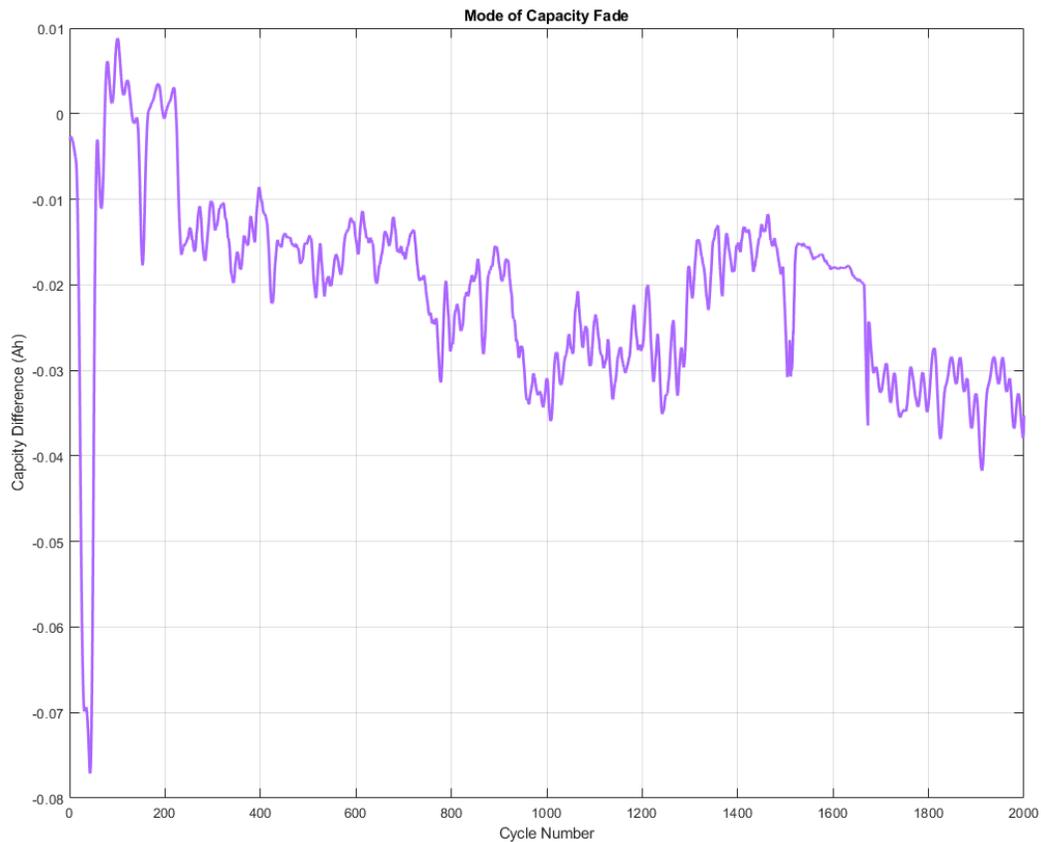
Figure 23: Test 1 the mode of the difference between recharge and charge for each cycle. The smooth portion of the plot is due to a different way to store the data which divided the discharge according to the LabVIEW command making the data less noisy

The general trend shows that although generally the capacity is returned to the pack on the individual cell level for any given cycle the cell is more likely to give up more capacity then is returned during recharge. Therefore, this suggests more anodic losses. Looking at literature for other Li-ion cells, to supplement the LFP literature, this could be due to loss of active material due to volume changes during cycling or loss of lithium due to SEI formation.

75

DC Impedance measurements

After an additional 750 cycles were run, making for a total of 900 cycles, the 'high C DC ESR' from those baselines is compared to the 'high C DC ESR' from the initial 150 cycles. Clearly, the trace resistance was contributing to this overall 'high C DC ESR' as seen by the load.
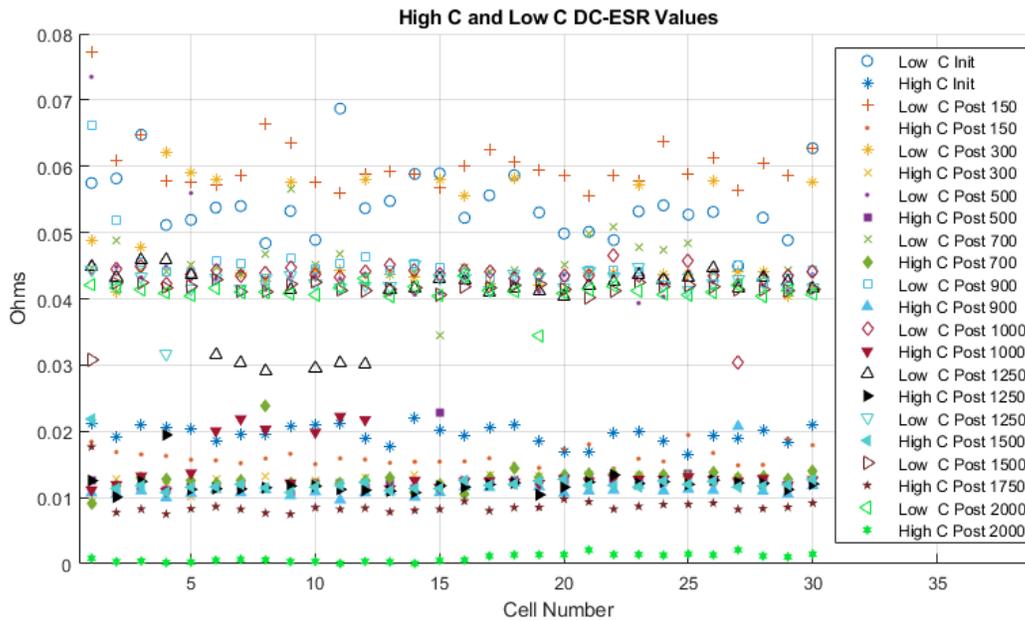
Figure 24: Test 1 all the High C DC ESR value and Low C DC ESR values from test 1 scatter plotted for quick comparison

Although the relationship between the 'high C DC ESR' and the current diminishes without the additional trace resistance, it is still a weak indicator; and the 'low C DC ESR' has no practical relationship to the mean current. The 'low C DC ESR' is a metric used by industry to assemble batteries using multiple cells; and the lack of correlation to the mean cell current suggests that it would be difficult to use that value to predict how cells will share future current when deciding how to assemble a battery pack.
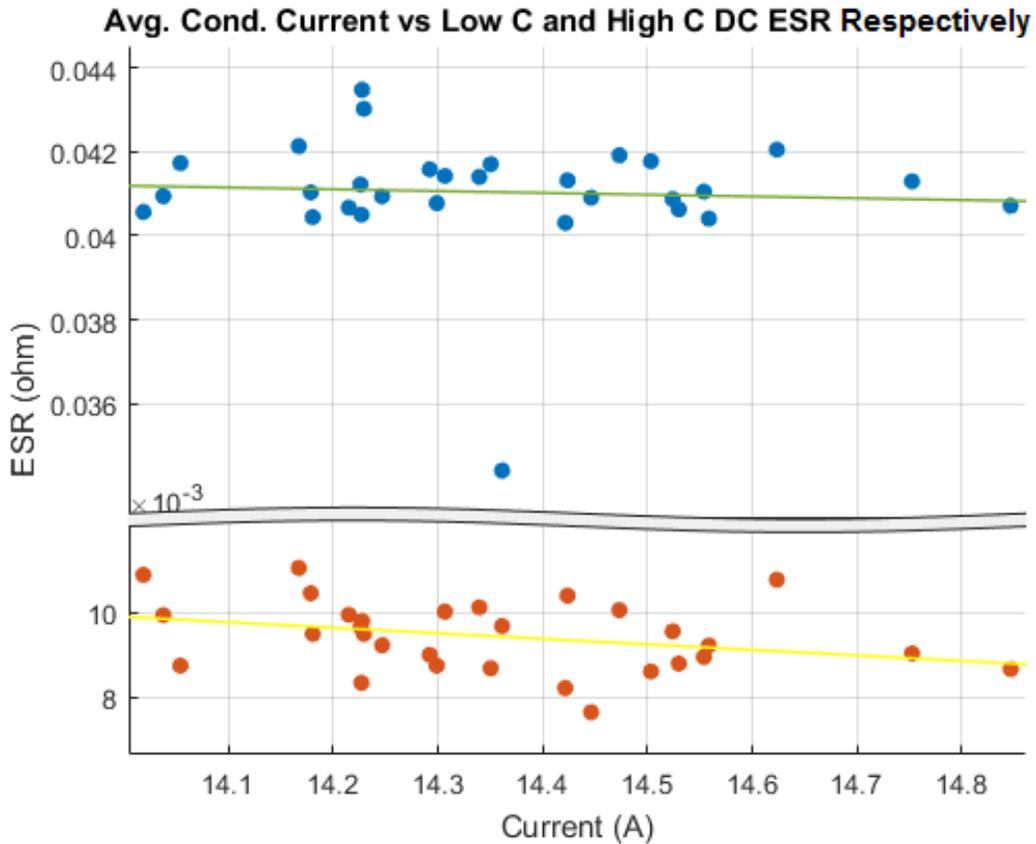
Figure 25: Test 1 Low C and High C DC ESR's predictive ability as it applies to current at cycle 1936 of the 46W cycle test

Given the above findings, the author decided to calculate the correlation of the initial, low C DC ESR, high C DC ESR and 1 kHz impedance, another common binning metric, on the future current provided by each cell. The results presented in figure 17 shows that initial high C DC ESR does have a weak correlation with how the cells share current over the long term. Therefore, better predictions could be made if a battery is assembled using the cells high C DC ESR value; however, it is a time-consuming metric. Also, the initial 150 showed that part of the strength of the correlation between the High C DC ESR, when the measurements are taken in-situ as done here, and the current provided is dependent on the difference in trace resistance. If the difference in trace resistance is an order of

magnitude smaller than the highest internal impedance, whether that be the Rss, pulse resistance, or 1 kHz impedance; then this relationship should hold and binning according to the high C DC ESR would lengthen the pack cycle life. Yet if the trace resistance is near the largest internal battery impedance the trace resistance will dominate, negatively impacting the cycle life. These calculations further show that for high-power applications the 1 kHz ESR and low C DC ESR have little impact on the current shared between cells. Therefore, one commercial application from the research performed here is that assuring uniform resistance between the cell and the point of common coupling (PCC) can be of more value than binning the cells based on their internal resistance. The magnitude of these relationships suggests that for a high-power pack, generally considered 5C and above for more than 20% of the discharge, it would be better to invest in high conductivity tabs rather than high-resolution cell binning.
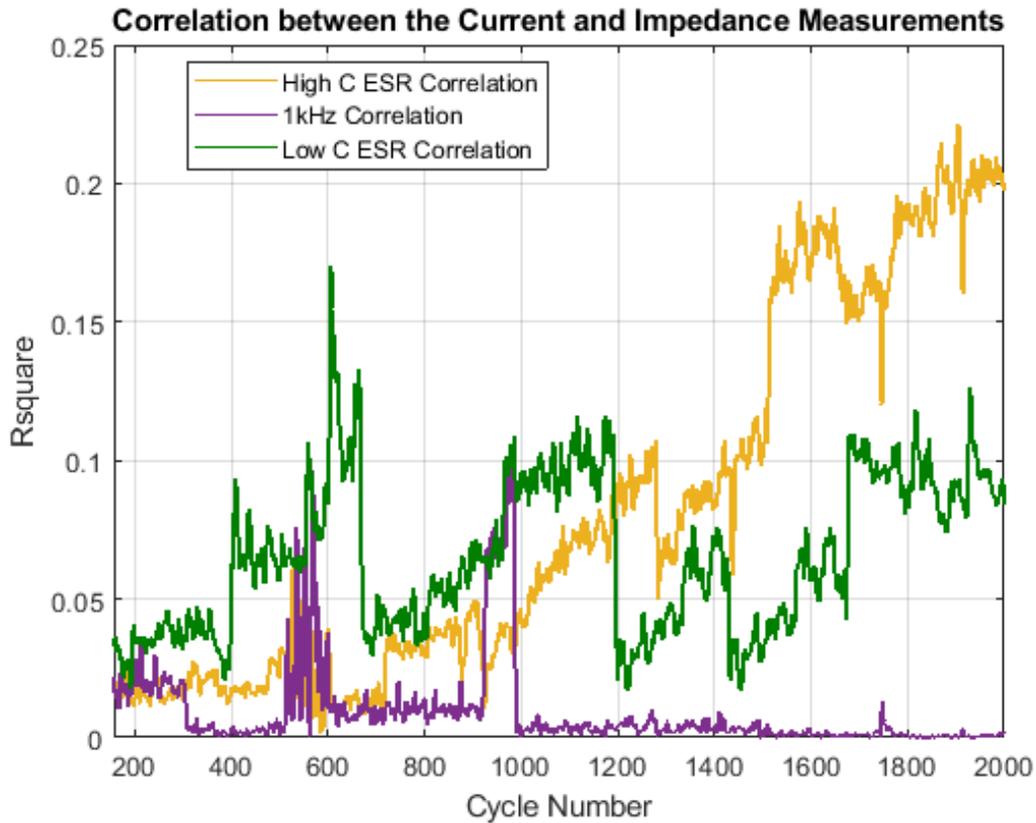
Figure 26: Test 1 Correlation of the initial 1 kHz impedance, Low C DC ESR, and High C DC ESR

If the cells are kept above 20% SoC, the initial High C DC ESR is an initial metric which could be used to bin cells with greater effectiveness than either 1kHz or the typical low C DC ESR used for cell characterization.

EIS and 1 kHz

Electrochemical Impedance Spectroscopy has multiple regions of interest, which gives in-depth insight into the chemical changes occurring within the cells without destroying the cell. These chemical changes can then be compared to the behavior seen in the cells during cycling.
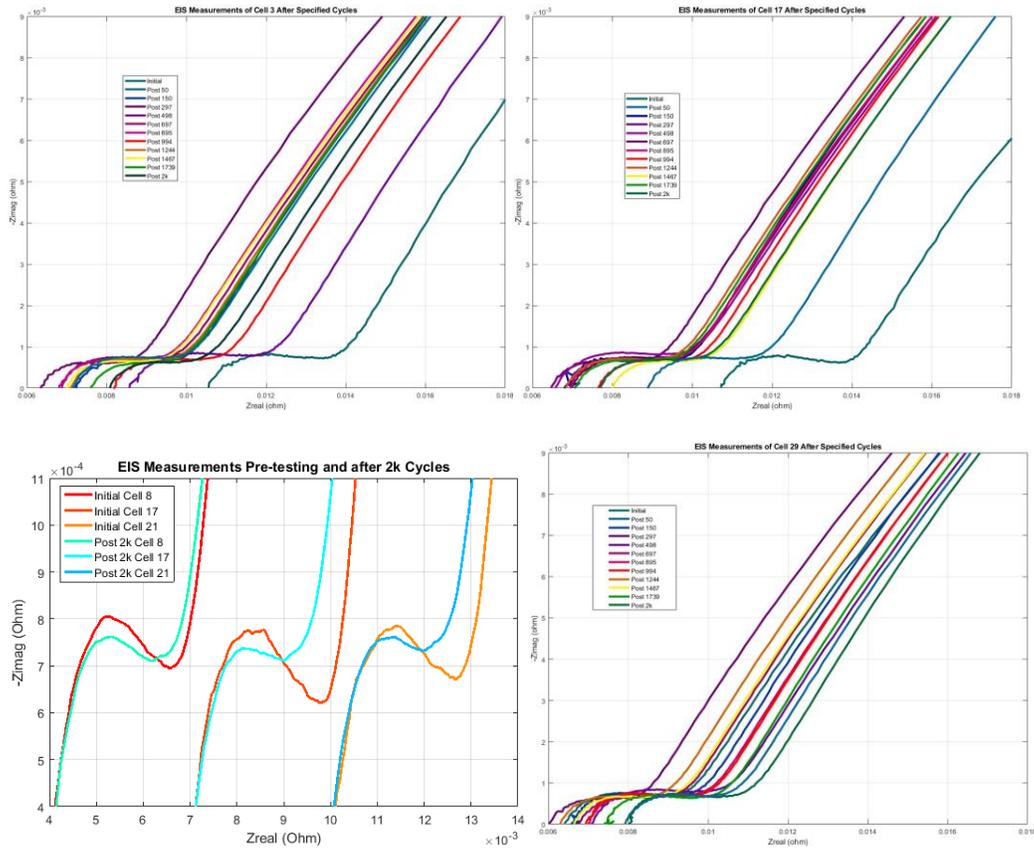
Figure 27: Clockwise from top left, Test 1 EIS measurement of A) cell three, B) cell seventeen, and D) Cell twenty-nine after each baseline procedure. D) EIS measurement of cells eight, seventeen and twenty-one from initial and end baseline with the Nyquist plots lined up along their 1 kHz real impedance

The above plots show that there is a 1kHz ESR increase, which leads to a right shift of the entire EIS plot. With the capacity fade of the cell contributing more to the aging than the amplitude of the semicircle, which is typical in LFP cells [56] [66] [67]. Capacity fade contributing more to aging that impedance growth is more typical of cycle-aged cells, as was the occasion with these cells, rather than calendar-aged cells where the semicircle is depressed by aging. Therefore, with this pattern of aging, the 1 kHz ESR is a decent stand-in for the internal cell dynamics because the magnitude of the shift in the 1 kHz ESR is closely mirrored at the other frequencies, thus reflecting significant changes to the internal

80

materials comprising the cell. However, it is not a precise enough predictor to indicate the SoH of the cells from that measurement alone [52]. The EIS measurement gives additional information into what kind of breakdown is occurring within the cells. The higher frequencies of the EIS show what is happening between phases in the SEI layer and the double-layer capacitance. The double layer capacitance corresponds with the charge transfer behavior. The lower frequencies (called the Warburg frequencies or Warburg "tail") show the mass transport of the electrode. The overall shift in the EIS seen as the life-cycle increases, as opposed to significant and consistent alterations in shape, suggest that the sources of aging are close to evenly distributed across the major causes of aging:

- Morphological changes (lower porosity, particle cracking and loss of active material)
- Increased local resistance/ electrode impedance (electrode electrolyte decomposition and resistive surface film formation)
- Particle Cracking
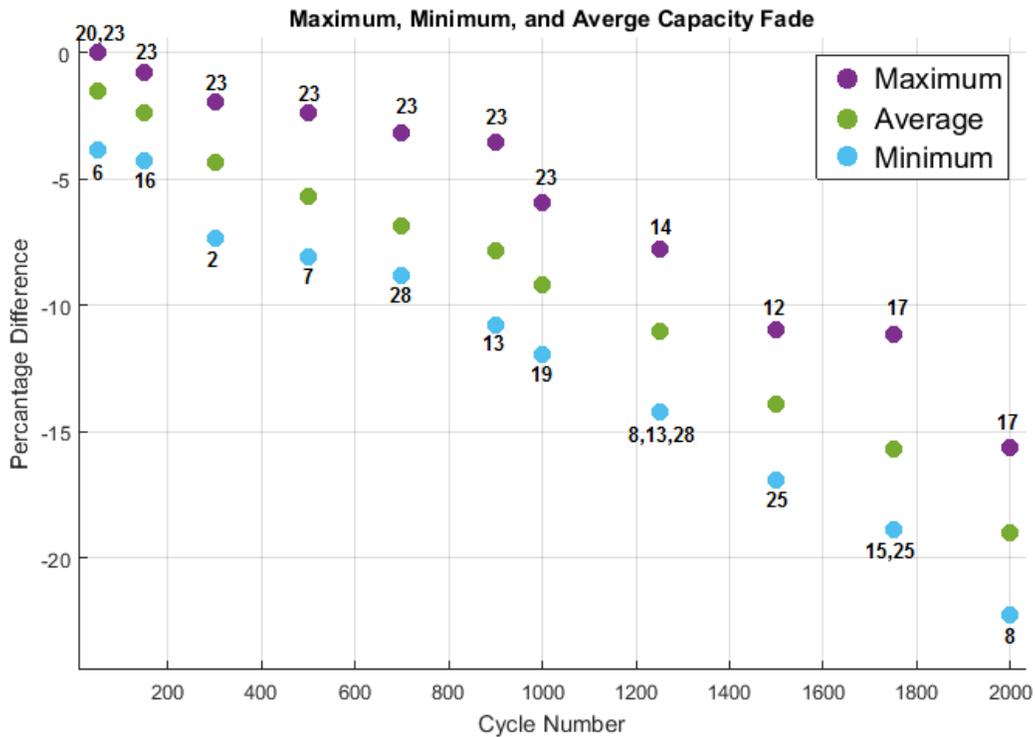
Figure 28: Test 1 Capacity fade highlighting the max, min and mean capacity fade at each baseline

Usually an individual cell begins to show increased capacity fade prior to the rest of the pack, these cells can then act as a catalyst for the degradation of the rest of the pack. If these cells could be identified and replaced with cells with similar electromechanical characteristics, the pack cycle life could be extended. Unfortunately, these cells cannot easily be replaced in a manner that slows down the failure of the whole pack. Not only are they compactly configured in the pack, but also the vast disparity between old and new cells can increase the circulating current and results in limited net gains in pack longevity [3]. Therefore, the early decline or failure of one cell is a strong indication of a shortened life cycle for the whole pack.

Potential Causes of Capacity Fade

Cells provided a similar amount of current throughout the test (i.e., if they offered current within the top 25% for the first cycles after 150, they provided current in the top 30% throughout). This trend is then reflected in the amount of capacity fade experience by each cell for any given cycle set. Although there is not a direct correlation between temperature and capacity fade, it does appear that there is a loose correlation, which will be represented in this section.
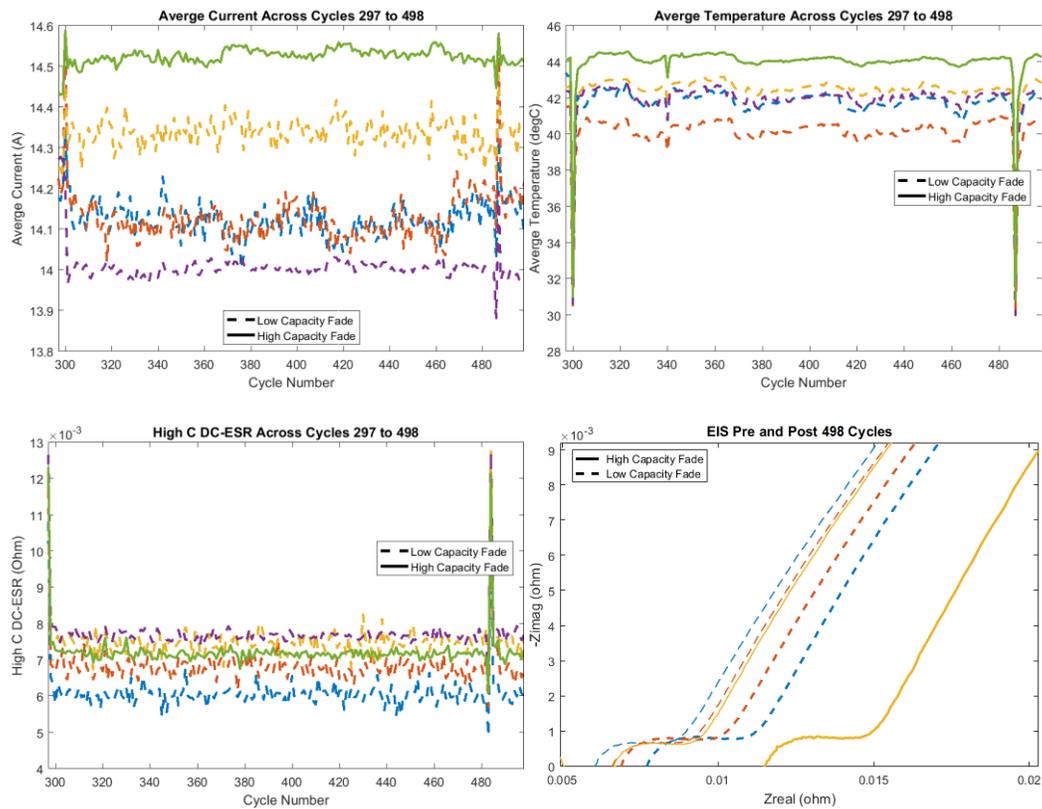
Figure 29: Clockwise from the top left test 1 A) Mean current and B) mean temperature supplied by the cells that exhibited the maximum or minimum capacity fade for cycles 300-500 C) from those cells EIS both before and after the cycles and D) High C DC ESR from cycle 297 to 498

Looking at the cycles from 300 to 500 shows that one cell shows a significant difference in the amount of current across cycles and that higher current correlates with a higher

capacity fade. The correlation between the current supplied and capacity fade further borne out by cycles 900 to 1000, not represented, where cell 19 provided significantly less current but has a 40% increased capacity fade.
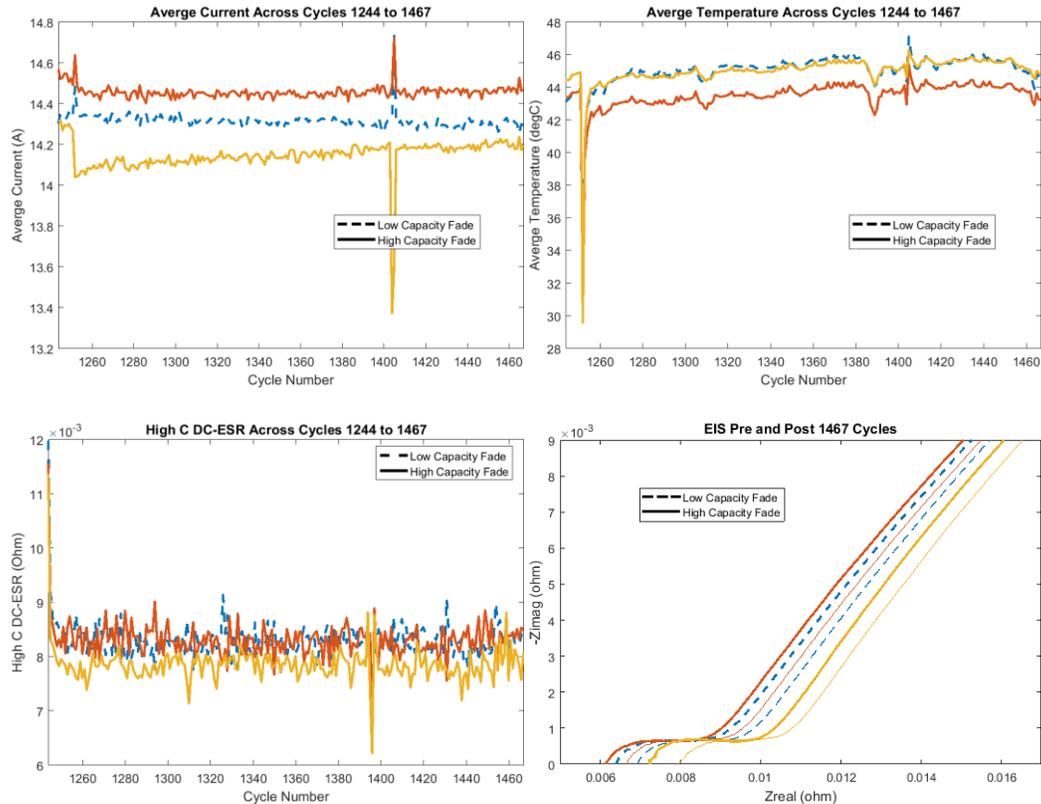
Figure 30: clockwise from top left test 1 A) Mean Current B) Mean temperature supplied by the cells that exhibited the maximum or minimum capacity fade for cycles 1.25k – 1.5k and C) the cell's Nyquist plot from before and after the cycle set C) the High C DC ESR across those cycles

After looking at all cycles, it can be shown that the cells that diverge a significant amount from the norm do not negatively impact the following cycles. The capacity fade across time suggests that there is some stochastic process that shows itself through the cycles. The other aspect is that the cells run for a certain number of cycles before being removed from the board, run through a baseline, and then reassembled. It is not known whether this stopping and disconnecting could be preventing what would otherwise be the start of a

84

destructive behavior cycle. Further tests in this report will be run without the baselines to see if there is different battery dynamics if the cells are not reconditioned.

This trend continues to the very last cycle. The loose proportionality between mean current and mean temperature suggests that the small variation in current does not result in a squared difference in temperature, which would be the expected source of disparities in the capacity fade. Furthermore, there does not seem to be a consistent causal relationship between the mean current or mean temperature.

Test 2 – 117 W per Cell, 30P/1S, Intermittent Baselines

After the 1389W test, the 1S/30P setup was used to cycle a new batch of 30 cells at 3500W. The new cells were selected at random from the remaining 40. At the end of the testing, the data were used to produce an identical current and temperature analysis. Due to the new power level the cell current, temperature, and voltage for the first 12 cycles of this test is plotted, along with the overall power.
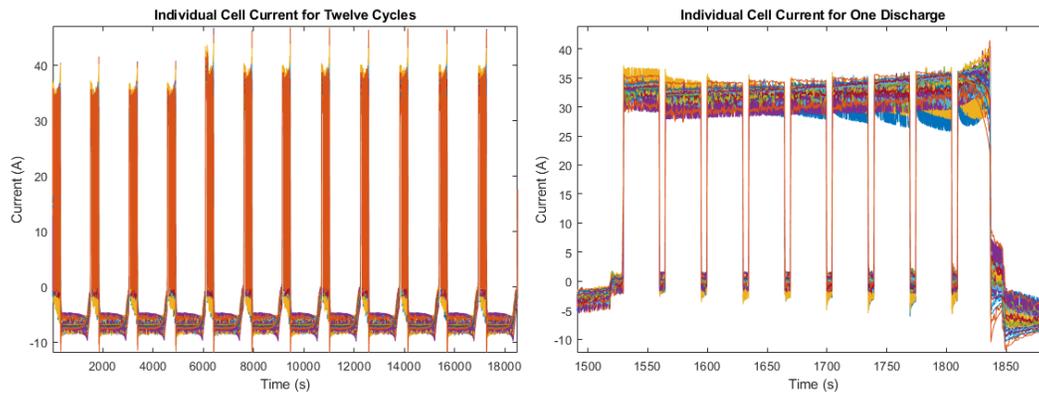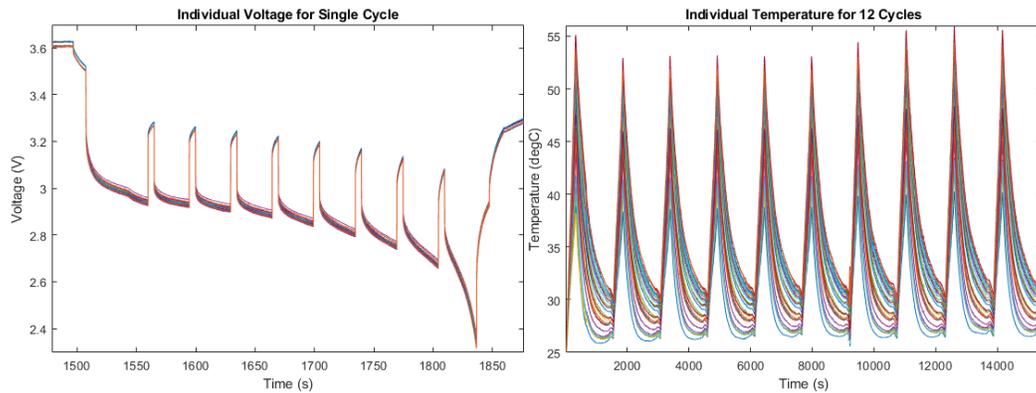
Figure 31: Clockwise from the top left test 2 A) Individual current for 12 discharges B) Individual current for one discharge C) Temperature and D) Voltage all these measurements are from test 2

The most noticable difference is that the temperature immediately reaches equilibrium and then stays there. With the 46 W test it took two cycles for the cells to reach equilibrium. Furthermore, the equilibrium is between 26 and 56 instead of 38 and 52. The lower threshold is due to the forced cooling whereas the upper is contributable to the high-power level.

Figure 11 is a presentation of the percentage difference between the temperatures and currents of all 30 cells. It shows erratic behavior. The sharpest changes appear after the baselines or a pause in testing. The erratic behavior suggests that the stress experienced by the cells under 117W, even with forced air cooling, make internal changes to the cells that reflect in the next set of discharges. These more permanent cycle differences potentially reflect the changes in the SEI formation that are encouraged by high cycling rate and high temperatures around 60°C (Vetter, 2005).

Percentage Difference of Temperature and Current across Cycles
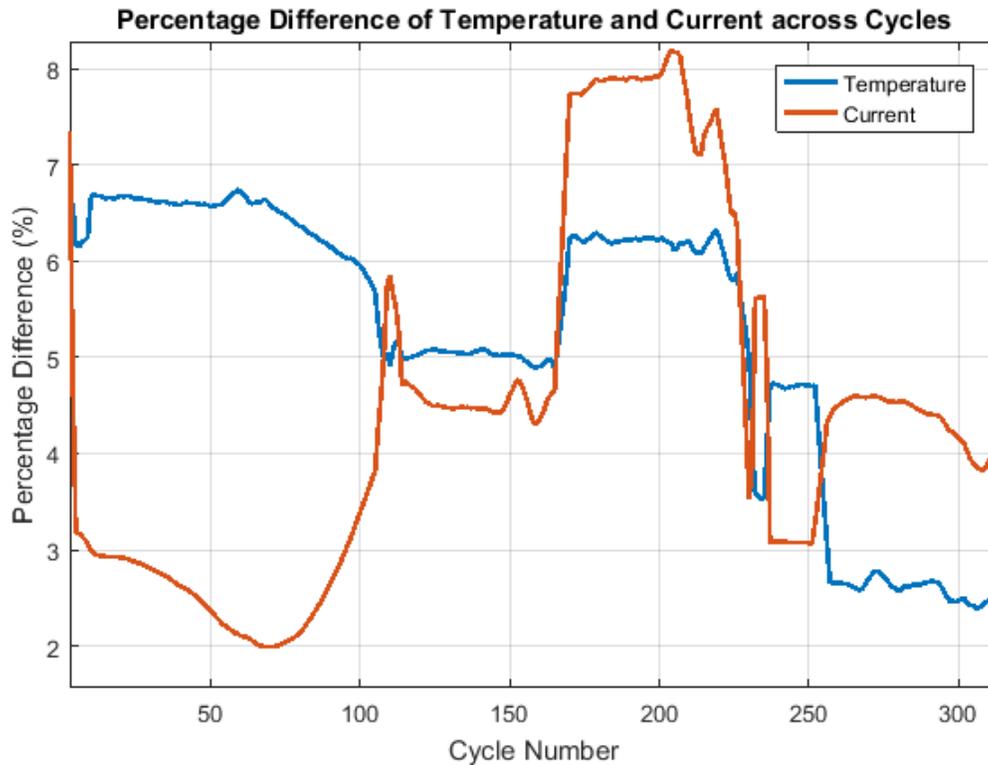
Figure 32: Test 2 Average percent difference between individual cell's current and temperature, based on the average values of 80% and 20% SoC of each discharge cycle in the 1S/30P test.

Before testing, initial baselines were run to establish the starting capacity and EIS for each cell. The 3500W test was stopped and baselined after cycles 107, 128, 253, and 313 before an end of test condition was reached.

Initially, the proposal was to stop testing when the average ideal capacity was at 80% - the typical cut off of allowable capacity degradation for batteries used in commercial operations. However, after cycle 313, visible inspection of the cells suggested that cell 18 had experienced significant thermal stress and that some venting of electrolyte had occurred along the positive terminal of the cell. Analysis of the test data showed that the test cycling started and stopped abruptly twice after the completion of cycle 257. Although the battery monitoring system did not record an individual cell failure, the electrical load

data showed that the overall system voltage dropped below the test cut-off voltage threshold. The battery end cap seal then presumably cooled down after two rest cycles, and the pulsed discharges continued as usual.

Many of the potential mechanisms for failure have been studied. Two critical mechanisms are increased temperatures, and end of SoC stress. It is desirable to understand the mechanisms that led to the cell rupture event and how the current imbalance affects the cell aging at the rates seen in the high rate test. Since the percentage difference in the temperature is relatively small, a further investigation is done on the end of SoC stress.

Dynamic Changes across the discharge

Figure 33 is plot of a full recharge and discharge with the 80% and 20% SoC points marked out to show the reader the area of the discharge being discussed. Then four plots present the final three pulses of the discharge and the author analysis the end of discharge behavior.
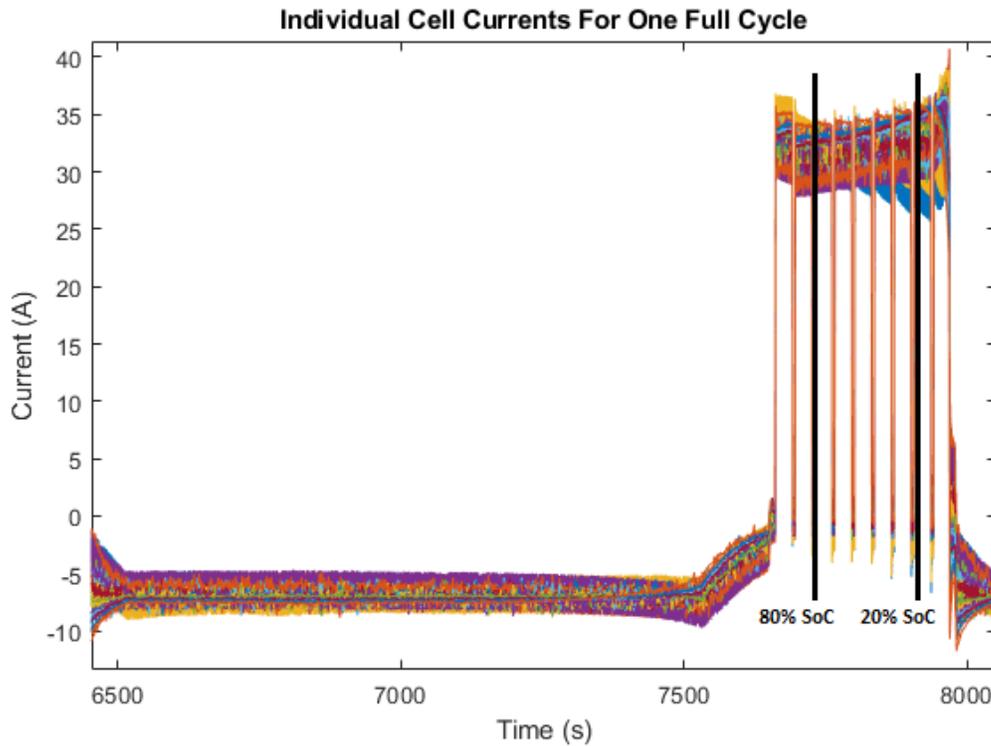
Figure 33: Test 2 one full recharge and discharge from the 6th cycle set with the 20% and 80% SoC points
set out by black lines

The above plot demonstrates how the current changes throughout cycling even though the
resolution is low. At this resolution the dynamic behavior of cells represented by yellow and
blue can be seen at the start and end of discharge. This cycle is at the beginning of the
test and already current differences are observed and cell trends are perceived. The below
plots investigate how these trends evolve of the length of the test.
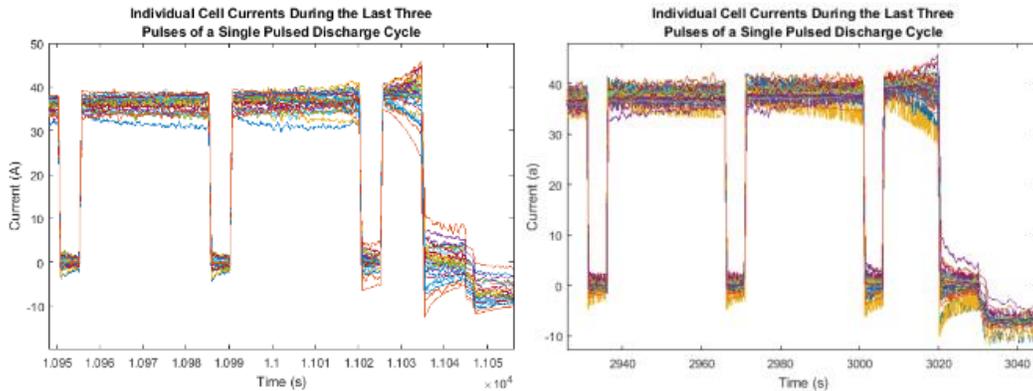
Figure 34: Test 2 last three pulses from the A) 107th discharges and from B) 158th

One difference that stands out in these plots in comparison to the 6C is that the current spike has a significantly reduced amplitude. Part of what contributes to this phenomenon is the fact that the current load is severe and leads to an initial 0.38v drop in the cell voltage. In the 6C test there is an initial voltage drop of 0.18v. In the 15C test the current is already contributing a more substantial portion to the power because the voltage cannot have increased with the increased power, in fact the voltage is initially closer to the cut-off voltage of 2.25 v. Therefore, once it gets toward the end of the discharge where the voltage curve is no longer in the linear region, it is a proportionally smaller difference, leading to a smaller voltage slope for the final two pulses. In turn the differences in the current slopes at the end of a discharge for 6C are smaller compared to 15C. For 6C the voltage has a change of 0.254V and 0.5V for the last two cycles where 15C only has a slope change of 0.39V and 0.44V. The decrease in overall voltage drop leads to a significantly decreased end current spike, which then contributes to a decrease in the current difference at the end.
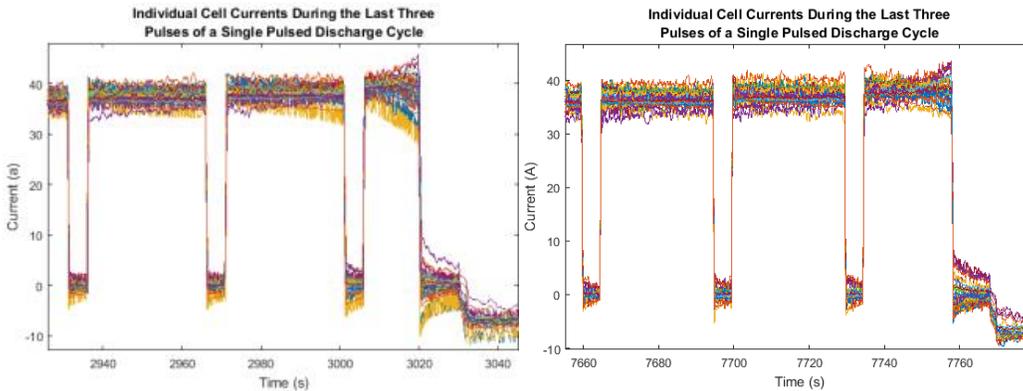
Figure 35: Test 2 last three pulses from the A) 228th Discharge and B) 313th

There is a notable change in the current supplied by the individual cells at the end of the discharge, with the pulses presented above being representative of the typical end of discharge behavior. As the voltage drops below the linear region of the voltage discharge curve the current must increase significantly to maintain the required power. This significant increase in required current combined with the varying SoC, due to different total capacity of each cell, leads to some cells significantly increasing in current while others drop off. This behavior can begin to be seen in the rest prior to the final on pulse. Already some cells are recharging from the other cells during the off pulse. This behavior then continues during the 10s rest between the discharge and recharge. During the final pulse there is an initial 0.38 V drop in the cell voltage, leading to a total of 11.4A that is needed from the battery pack to maintain the power level. Shared evenly this would not be significant; but, since several cells drop off to varying degrees as the voltage is dropping, it leaves the remaining cells amperage to increase in varying magnitudes. The most substantial increases being around 9A and the top 10% of cells experience a 6A or above increase by the end of the discharge. 6A is a significant increase and if the battery pack is not built for it the cells can go beyond their manufacturer limits. However, this extreme behavior can

91

be avoided if the limits are put on the battery pack to keep it at or above 20% SoC as is conventional in many commercial applications.
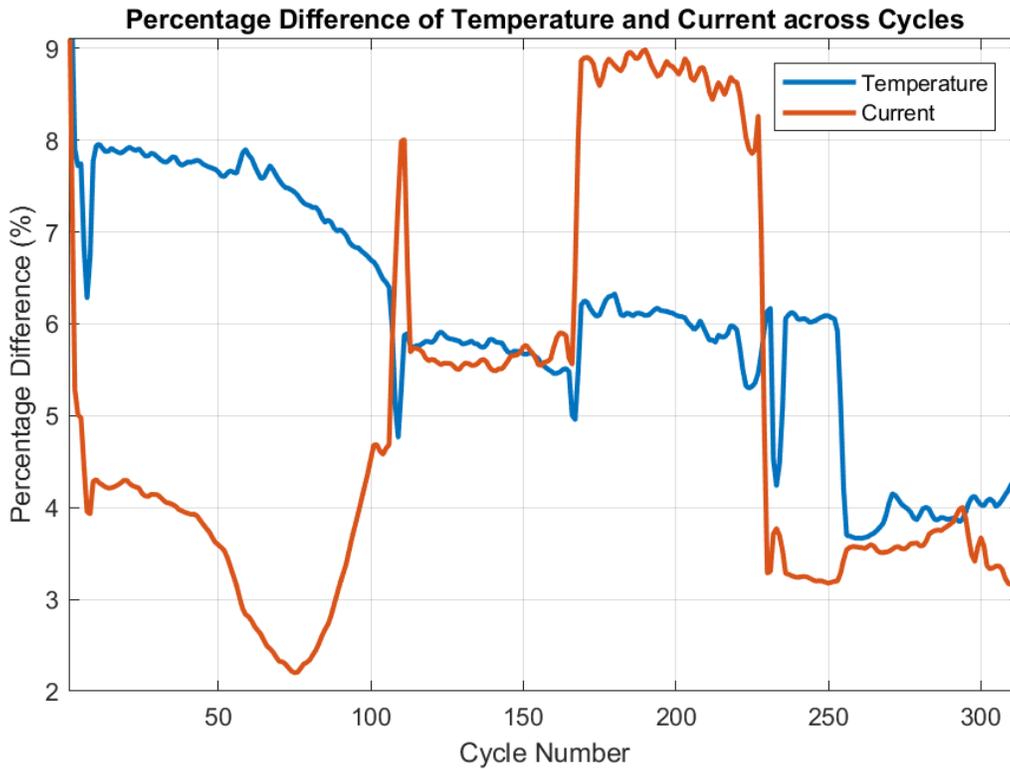
Figure 36: Test 2 average percentage difference between the current supplied by each cell compared with the average percent difference of the temperature of each cell for the final 20%

The increase in current from ~260-313 is from cell 18 venting. Decrease in temperature overall leads to a decrease in percentage difference. Maybe this should be thrown off because of the adjustments in the way the cells are cooled. The general trend seen here is that as the current difference increases so does the temperature difference, with a notable exception of the first 100 cycles. This strong correlation, for most of the cycles, between the current difference in the temperature difference suggests that current imbalance seen in batteries discharged at high rates becomes a significant source of aging.

Capacity Fade Trends throughout Cycling

Presenting 30 cells capacity fade in one plot presents the reader with an overwhelming amount of information. To highlight the trends occurring in this 30P/1S array the capacity face of the cells with the minimum and maximum capacity fade are presented along side the average pack capacity fade.
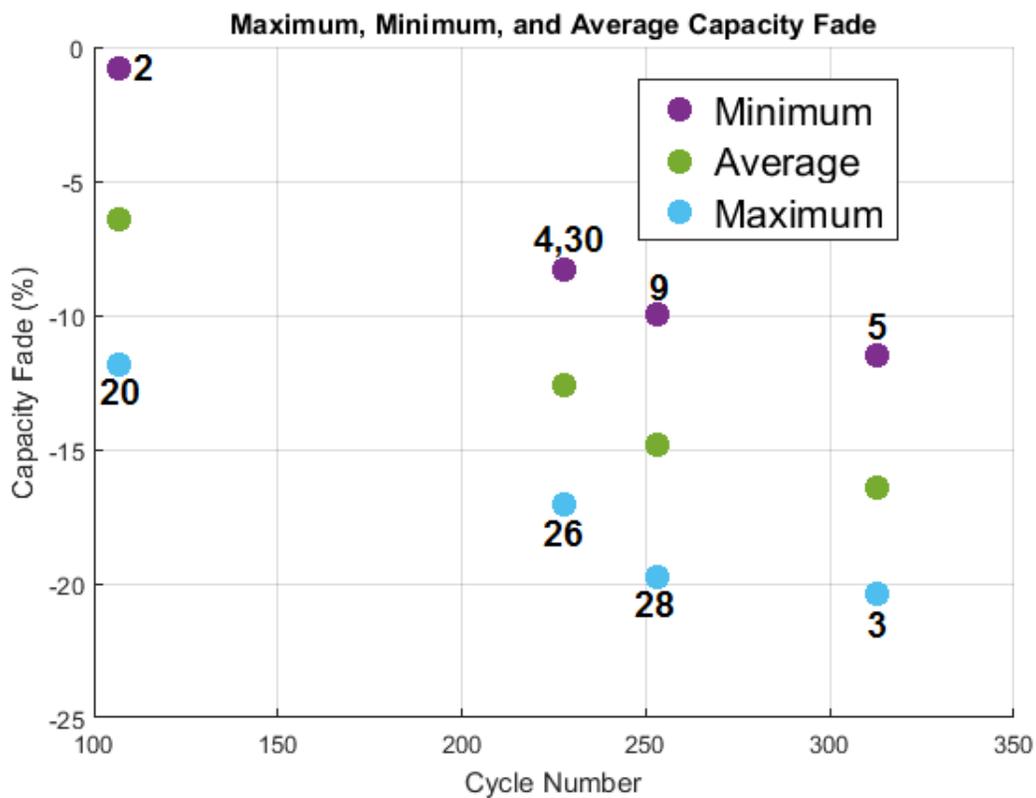
Figure 37: Test 2 Maximum, Minimum and average capacity fade exhibited by the 30 cells during each set of cycles of the high current discharge

The temperature difference relation to capacity fade is not clear from the rate of capacity fade shown in figure AG. It can be challenging to tease out the impact of cycle life and temperature. Further investigation is underway to address the impact current imbalance has on the capacity fade, especially at these higher currents.

Before testing, initial baselines were run to establish the starting capacity and EIS for each cell. This test was stopped and baselined after cycles 107, 128, 253, and 313 before an end of test condition was reached. The baseline procedure consisted of discharging and recharging each cell individually at C/2 and 1C rates to measure its ideal usable capacity, versus the practical capacity obtained during cycling. Then the cell was recharged and discharged to 50% SoC, and a new EIS test was run. Then a final top off charge brought it to 100% SoC. The baseline values along with the in-situ measurements were analyzed using similar methods seen in the analysis of the above 1389W tests.

Initially, the proposal was to stop testing when the average ideal capacity was at 80%, the typical cut off SoH for batteries used in commercial operations. However, after cycle 313 visible inspection of the cells suggested that cell 18 had experienced significant thermal stress and that some venting had occurred at the positive end of the cell. The mechanism for the venting was an overheating of the electrolyte that led to the seal at the negative end cap of the battery to melt allowing the heated electrolyte to escape. The investigation into when in the cycle set this might have occurred showed that there were two cycles that started and stopped abruptly after cycle 257. Although no individual cell reached the cut-off voltage according to the measurements output by the LabVIEW programming, it is presumed that the cells dropped to below the cut-off voltage long enough for the load to pick up the drop-in voltage and stop the discharge. The seal then presumably cooled down after two rest cycles, and the pulsed discharges continued as usual.

Many of the potential mechanisms for failure have been studied. Some of these mechanisms are increased temperatures, end of SoC stress, and quick changes to operating conditions that can cause chemical stress in the internal structure. It is not known what each mechanism's amplitude of impact is, and only one mechanism can be known at a time and can be considered economically. It is desirable to understand the mechanisms

that led to the cell rupture event and how the current imbalance generally affects the cell aging at the rates seen in the high rate test. To investigate this phenomenon, the author made comparisons of the capacity fade to the other measured variables. Also, the EIS was analyzed to understand better the type of degradation happening in the batteries. At high rates, it is common for lithium-plating on the surface of the anode to be prime cause of capacity fade, but periodic EIS of the cells will give a clear picture of how well this hold for the cells, and if the imbalance of current leads to different mechanisms of degradation.

Binning Mechanisms

As with the 6C test, an investigation was taken of how the initial cell parameters influenced and predicted the long-term current sharing of the cells. The correlation was found between the High C DC ESR, Low C DC ESR, and 1 kHz impedance, and the current provided by each cell at each cycle.
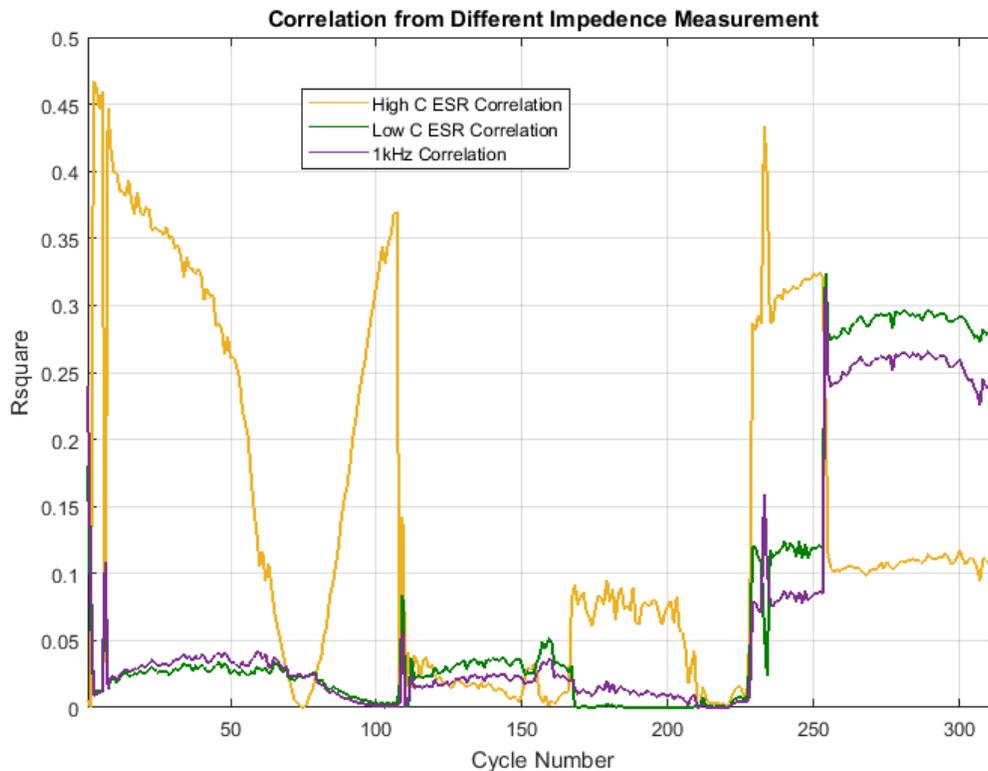
Figure 38: Test 2 Correlation of the initial 1 kHz impedance, Low C DC ESR, and High C DC ESR

The above plot, Figure 23, shows an inconsistent correlation between either of the common binning metrics of 1 kHz impedance and low ESR for the higher discharge rates being analyzed in this research. The lack of correlation suggests that other mechanisms of correlation need to be investigated. Unfortunately, between high C DC ESR value as a binning metric for test one and as a binning metric for test two it proven to be an inaccurate predictor of supply current. This conclusion along with other research that has investigated parallel cells [52] [30], suggests that the electrochemical processes internal to the battery are challenging to predict and probably need to be approached stochastically. However, the researchers still suggest future work in this area in finding another binning metric or confirming the stochastic nature of these processes.

Review of EIS and Potential Causes of Capacity Fade

Baseline measurements are used to characterize capacity fade of each cell periodically. After cycles 108 and 228, two cells, one with the highest capacity fade and one with the lowest capacity fade, are singled out; and plots of their respective average current, temperature, and before and after EIS are shown in the plots below. Between cycles 0 to 108, current imbalance is present, but it is not all that significant; the current supplied by the cells stay within a few percentage points of each other (0.2%-8.7% specifically). As cycling progresses, the current imbalance is more consistently significant. The spread for cycles 108-228 is 3.1%-8.8%. It appears that the cells that have a higher capacity fade are trending towards supplying less current while the cells with lower capacity fade seem to be trending toward supplying more current for the first 107 cycles. After the first 107 cycles the cell current levels, off with the average current being supplied after the first 5 cycles being a good predictor of what will happen for the next 95 cycles. After cycle 108, the EIS plots show some small increase in DC ESR, this increase could be within the margin of

error and is not enough to confidently say that it is the cause of the trends observed. There are significant changes in the mid-frequency semicircle indicating changes in the charge transfer impedance. However, that change is for the mid-frequency semicircle to decrease in amplitude, which is a more challenging result to interpret because aging typically causes the mid-frequency semicircle to increase in amplitude.
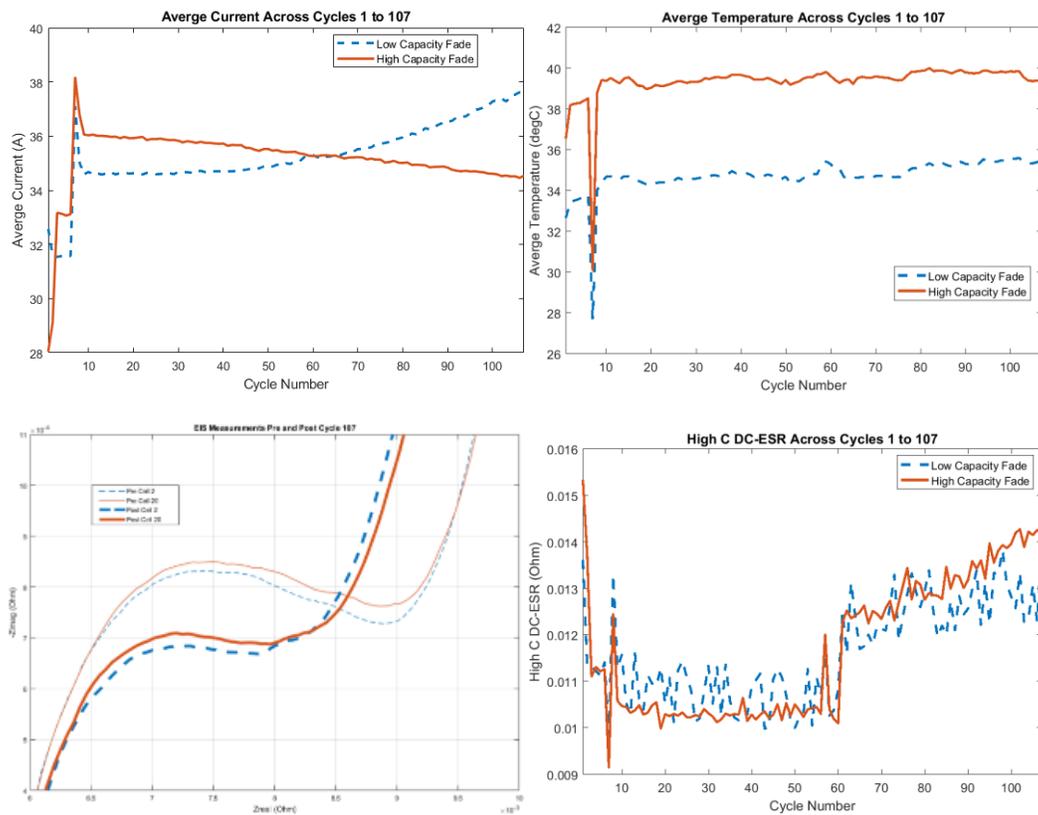
Figure 39: Clockwise from top left Test 2 A) current B) temperature, and C) High C DC ESR for test 2 cycles 1-107 D) EIS taken before and after the cycle set

The average current seen from cycles 1 to 107 show a dramatic change in behavior. There is a change in the cells that are strongly performing with the ones that are weakly performing at the cycle 60 mark. A majority of the cells in the array show a significant shift in their mean but the shift is most dramatic in the cells with the highest and lowest capacity

97

fade, which are cells 20 and 2 respectively. The behavior points to the aging behavior presented in the Brand and coworkers' paper, the SoC imbalance near the end of cycle cause those that start with a high initial capacity, source near threshold currents as cells with a low initial capacity abate. Therefore, packs that start with relatively small imbalances in the first 60% of discharge can began to show current ranges where the upper bound stretch beyond the manufacturer recommended discharge area. For the first ten cycles of this test, only two cells reach the recommended limit of 40A, then the number reaching the limit spikes to 13-14 until cycle 60 at which point in the cycling it levels out to 6 cells reaching the limit. These fluctuations impact the current and temperature difference seen in Figure 32 and Figure 36. Importantly, this shift is not immediately mimicked in the temperature. Although the temperature experienced by cells in all the tests run here are within margins of each other to suggest little impact on the overall aging, it still provided some useful insight into the quiescent nature of the cells. The disproportional behavior of the temperature to the current seen in cycles 1 through 107 paired with the near identical semicircle changes suggest that the changes are coming from some other internal source of resistance rather than the dissipation properties of the cells. Cell 2 shows a 0.4m increase in 1kHz ESR while cell 20 shows a 0.8m decrease, this is paired with a decrease in ω_{max} in cell 2 but no change in cell 20. Cell 20 does have other markers of capacity fade. Where cell 2 has steady recharge resistance, cell 20 shows a jump at cycle 37 where other markers do not otherwise indicate significant deviation between the cells. Between cycles 7 and 71, cell 20 shows a slight downward trend in the capacity it receives on recharge in comparison with the mean capacity received on recharge. Starting at cycle 72 cell 20 grows closer to the mean until it is within 30mAh of the mean by cycle 93 and stays within a 30mAh of the mean until cycle 107. The dynamic behavior of these two cells show the multiple levels of chemical changes that occur in the cells simultaneously. It is these

98

constant and multifaceted nature of the cells' aging mechanisms that make them particularly susceptible to the long-term impacts of current imbalance. Theses many aging mechanisms complicate the SoH estimation in the pack that can have make the current imbalance economically significant.
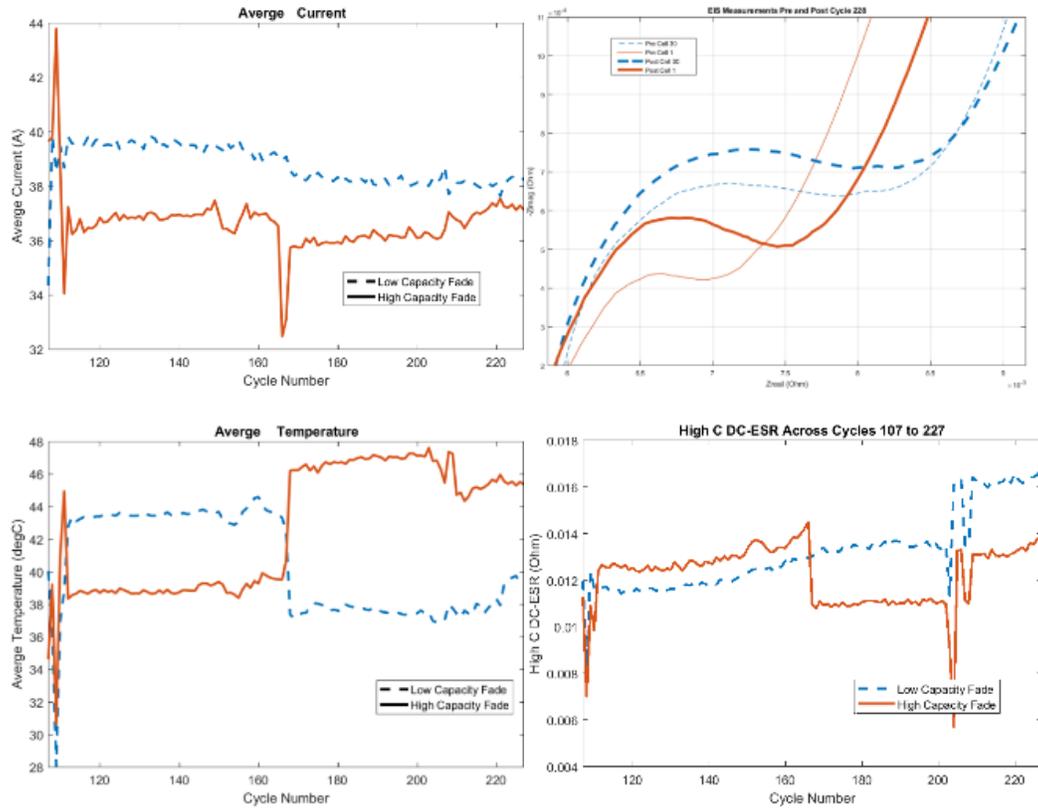
Figure 40: Clockwise from top left Test 2 current, EIS, temperature, and High C for cycles 107-228

Investigations into EIS have often indicated a trend where the mid-frequency semicircles increase in length causing the Warburg frequencies to begin later. Several investigations have been made into the way LFP batteries age--both under calendar aging and cycled [74][72][55]. The trend, starting after the initial EIS, seen in this analysis is that the mid-frequency semicircle flattens out and is shortened. It does appear that cells under thermal stress are more likely to experience a shortening and decrease in amplitude of the mid-

frequencies semicircle [32] [11] [75]. The earlier onset of the Warburg tail points to the diffusion distance that the reactants experience, and lower amplitude of the mid-frequencies suggests a lower relative charge transfer resistance. The overall shift to the left shows an increase in resistance, which with capacity fade are the main parameters that indicate declining state-of-health of a battery cell [46].
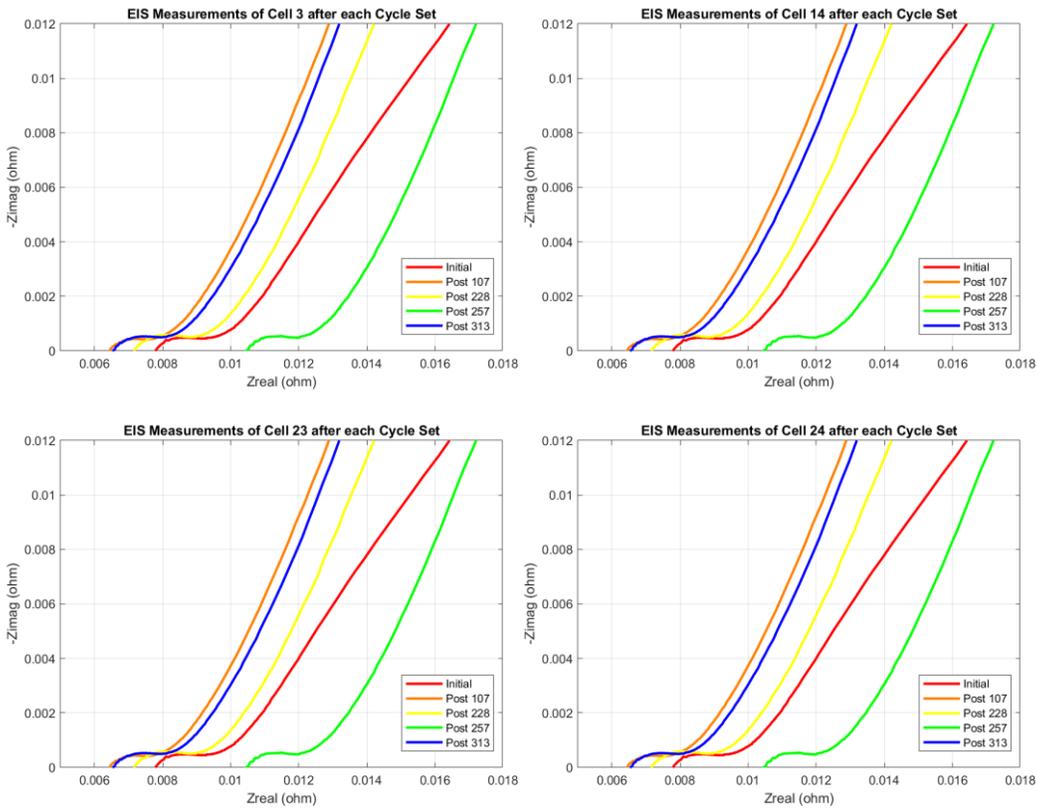
Figure 41: Clock wise from top left Test 2 EIS measurements taken at each baseline for A) The EIS measurements of cell 3 that experienced an average capacity fade and ended with the least 1C capacity B) The EIS measurements of cell 14 the cell that experienced the minimum capacity fade and ended the cycles with the most remaining 1C capacity C) The EIS measurements of cell 24 the cell that experienced the most capacity fade and ended with a below average 1C capacity D) The EIS measurements of cell 23 a cell that experienced a normal amount of capacity fade

There is an initial settling, where the SEI stabilizes, which shifts the real impedance back from the initial value, then the real impedance begins to steadily increase. During settling, the cells show, as a general trend, a decrease in impedance of all kinds. This decrease in impedance does not provide much additional insight into what is happening internally that causes current imbalance than what was already known from previous research. It does strengthen the argument that the initial binning done in commercial settling does little, if anything, to mitigate the issue of current imbalance. The initial 1 kHz impedance is used by many manufacturers to bin the cells only holds for the initial 50 cycles and is not strongly indicative of where the cell will end up after settling. The increase in the real impedance after the initial SEI formation and settling period is steady and consistent. Therefore, there appears to be a consistent decrease in Li-ion diffusion and active mass capacitance. It is not yet known how much of that would happen even with ideal current sharing. Future tests should investigate the aging rate and mechanism for cells discharged at exactly 1/30 of the power of the whole array of parallel cells. As the cells cycle, there is not a steady increase in the mid-frequency semicircle. It is not clear, therefore, what is happening at the surface film solution interface. It would be beneficial to investigate the changes at the film surface via battery dissection, but that is left to further research.

The differences between the mid-frequencies are stark, with cell 3 experiencing significant changes between initial and 107 cycles, but cell 14 and 24 both show a less significant shortening to the curve. However, these differences are only loosely correlated with the capacity fade experienced. The cell with the least capacity by the end, although it experienced an average capacity fade, has one of the steepest curves and highest absolute value at the mid-frequencies.

Recharge and Overall SoC Balance

Although many tests are necessary to gain valuable and reliable insight into array phenomenon running test with 30 cells in each array does make each test closer to statistically represented of individual cell behavior than firm conclusions based on small test batches. Due to this large test-bed size the understanding that cells are exhibiting mostly anodic behavior is well founded. The previous literature available support this claim. However, to best understand how the parallel nature of the array is affecting the capacity fade mechanisms one must compare the overall behavior of each test. Both similarities and differences provide insight into the parallel behavior of battery packs.
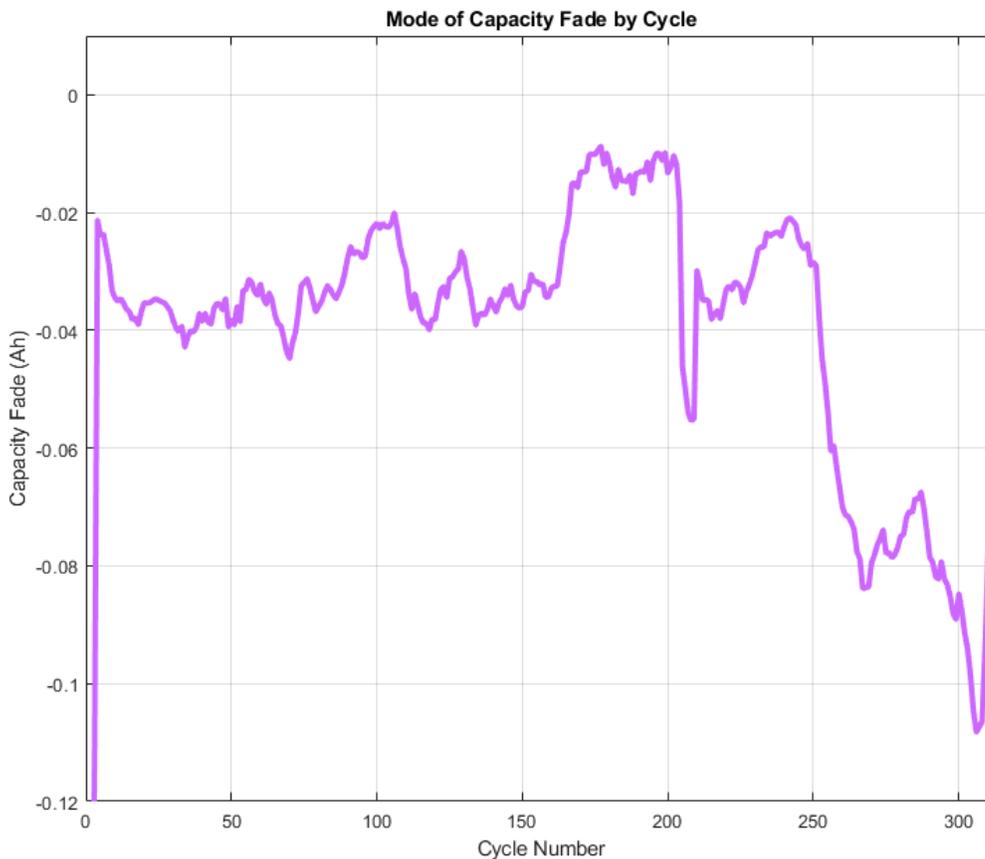
Figure 42: Test 2 mode of the difference between the recharge and the discharge for the High C cycles

While the mean and median are slightly positive, at 3.5mAh and 1.8mAh, respectively, the mode shows a consistent negative trend in the 5-10mAh range. This negative trend in the mode is seen here for the 3500W test as was seen earlier in the 1390W tests. Furthermore, in the 1390W tests, the negative trend significantly increases towards the end of the test. The direction of this trend suggests a more consistent aging mechanism due to stress, whereas the 1390W shows a different trend across time.

Internal cell structure insights from EIS and Capacity Difference

Baseline measurements are used to characterize the capacity fade of each cell. After cycles 108 and 228, two cells--one with the highest capacity fade and one with the lowest capacity fade--are singled out, and plots of their respective average current, temperature, and EIS before and after cycling are shown below. Between cycles 0 to 108, current imbalance is present, but it is not very significant; the current supplied by the cells stay within a few percentage points of each other (0.2% to 8.7%, specifically). As cycling progresses, the current imbalance is more consistent and significant. The spread of cycles 108-228 is 3.1% to 8.8%. It appears that the cells that have a higher capacity fade are trending towards supplying less current while the cells with lower capacity fade seem to be trending toward supplying more current for the first 107 cycles. After that, the current cell levels off, with the average current being supplied during the 6th cycle being a good predictor of what will happen for the next 95. After cycle 108, the EIS plots show a small increase in real impedance. There is a significant decrease in the mid-frequency semicircle amplitude, a portion of the EIS diagram associated with the charge transfer impedance. The decrease in amplitude is a denotive result because aging under normal condition typically causes the mid-frequency semicircle to increase in magnitude. Initial studies have shown that under thermal stress the mid-frequency semicircle decreases and shortens suggesting that thermal stress is the cause of much of the aging [74] [72][55]. The thermal

aging is due to the high-power discharge and not due to additional thermal stress from a wide temperature spread among the cell.

Review of EIS and Potential Causes of Capacity Fade

The overall shift to the left shows an increase is shown, which with capacity fade are the main parameters that indicate declining state-of-health of a battery cell. The aging mechanisms in these batteries are not due to increase resistance, because that would result in measurable temperature differences. Other literature on LFP chemistry cells also finds that capacity fade rather than increased resistance is the primary form of aging [46].
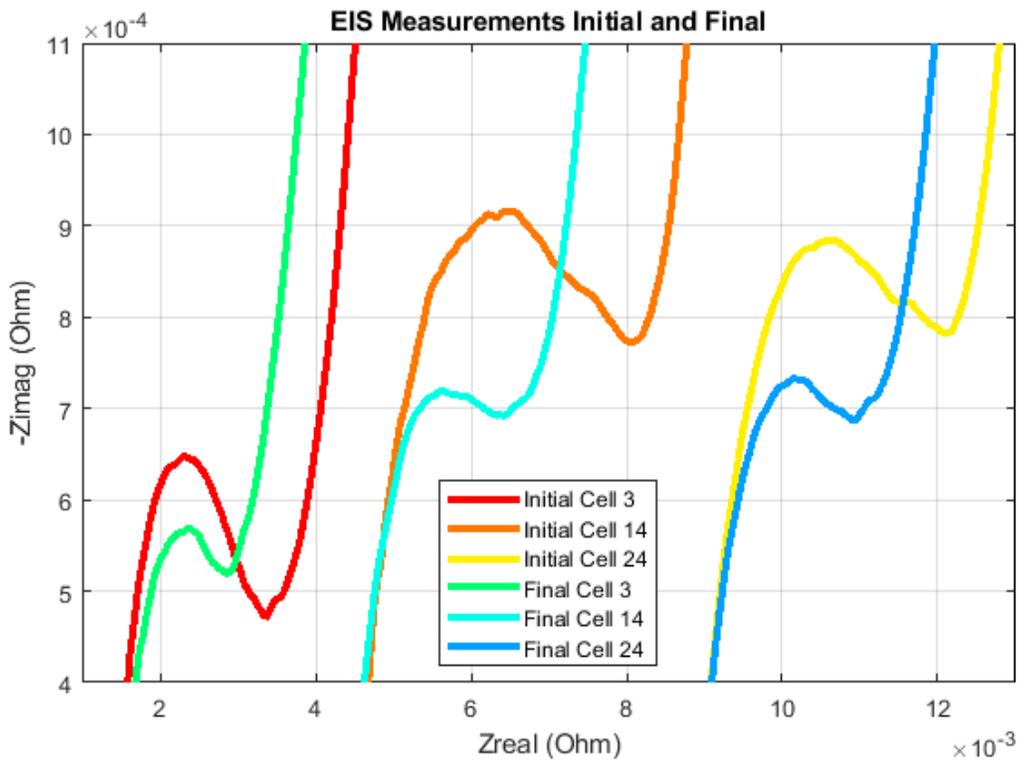
Figure 43: Test 2 A) EIS measurement of cell 3, 14, and 24 measured before and after testing with a focus on the mid-frequencies and shifted to same 1kHz impedance for better comparison

There is an initial settling during which the SEI layer stabilizes, which shifts the real impedance back from the initial observed value. After this stabilization, the real impedance

begins to increase steadily. During settling, the cells show, as a general trend, a decrease in impedance of all kinds. This reduction in impedance does not provide much additional insight into what is happening internally to the cell -- specifically what could explain current imbalance – over what was already known from previous research. The lack of correlation between the impedance and the current imbalance does strengthen the argument that the initial binning done in commercial settling does little, if anything, to mitigate the issue of current imbalance. The initial 1kHz impedance used by many manufacturers to bin the cells only holds for the initial 50 cycles and is not solidly indicative of where the cell will end up after settling over the first few cycles. The increase in the real impedance afterward is steady and consistent. Therefore, there appears to be a regular decrease in Li-ion diffusion and active mass. It is not yet known how much of that would happen, even with ideal current sharing. As the cells cycle, there is not a steady increase in the mid-frequency semicircle. It is not clear, therefore, what is happening at the SEI. The differences between the mid-frequencies are stark, with cell 3 experiencing significant changes between initial and 107 cycles, but cells 14 and 24 both show less significant shortening of the curve.   Moreover, cell 3 started with a shortened EIS curve. Although for these three cells the EIS mid-frequency semicircle changes correlate well with both the start capacity and the capacity fade the EIS changes are only loosely correlated with the capacity fade experienced when looked out across all 30 cells. The cell with the least capacity by the end, although experiencing an average capacity fade, has one of the steepest curves and highest absolute values at the mid-frequencies. The complicate factors of initial capacity, final capacity and capacity fade make system identification challenging. However, the loose correlation does suggest that if the mid-frequency was combined with other key merits that change with aging an outline of optimal battery pack construction.

Test 3 – 117 W per Cell, 5P/1S, Intermittent Baselines

The third series performed cycled five cell at 583.5W, which is 117 W per cell. The 1S/5P setup was used to perform this test, a single PCB board attached to the test bed and the other 5 removed. Five new cells were chosen randomly from the among the second order of 53 cells. Figure 44 shows a summary of the current and temperature imbalance calculated using the mean absolute deviation between the cell's current and temperature divided by the mean of that parameter for all cells, for all 607 cycles. The abrupt changes seen in the current difference is due to the baselines taken at cycles 28, 54, 79, 104, 129, 149, 174, 203, 253, 324, 374, 419, 454, 519, and 567. For Cycles 203 – 419 the cells were charged and discharged from 0% - 50% SoC. This was due to one of the supplies dropping out of communication with the computer LabVIEW that was not noticed for five sets. This discharge regime has a small enough change on the aging mechanisms and the researcher will evaluate the testing under the same guidelines as previous test. This array end cycle number was on the high end for what is seen for five cell arrays cycled at 117W per cell, but still within range. The aging rate of the cells for these cycles, relative to full discharges, suggest the it is discharging cells at the end of their voltage is a part of the accelerated aging experiences by cells that are fully discharged and not only due to the stress due to the length of time spent discharging. Future work could investigate the exact magnitude of this impact by repetitive extensive testing within different SoC windows. Given that the last test was at the same power level per cell, there are no plots of the overall current, temperature, and voltage before discussing the descriptive statistics.
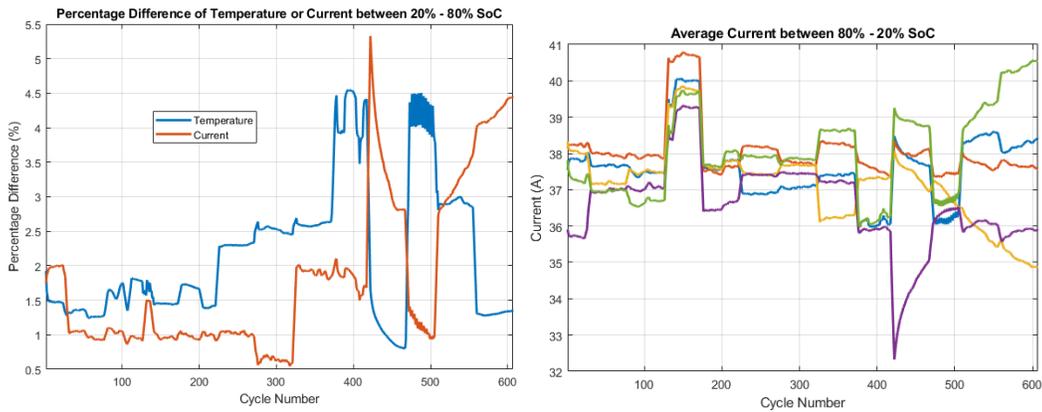
Figure 44: Test 3 A) Average percent difference between individual cells' current and temperature B) Mean current of each cell, both A and B use the mean values between 80% and 20% SoC of each discharge cycle.

As this figure shows, there are small current imbalances throughout the 607 cycles. There is an ever-increasing temperature difference between cycles 0-354 going between 1.75%-4.25%, on the other hand, the current difference floats around 1.75% between cycles 28-374. Like earlier tests, there is little connection between current and temperature. The strongest link is that they mark the baselines, which gives insight into the impact the of baselines conditioning but does not suggest a strong link between the current supplied by the cell and the waste heat produced by the cell. Significant changes in the current difference correlate with some notable changes in temperature. These changes are at times of different magnitudes, with the temperature decreasing when the current difference increases or vice versa. The change between the sets does not consistently show similar amplitude, or magnitude shows that they are not proportionally related to each other. Rather the location of the changes is an indication of substantial structural chemical change occurring due to the conditioning happening from the baselines. The spike in temperature difference seen between 374-419 is due to the fan that was providing the forced air cooling was not optimally aligned. This non-optimal alignment caused the cells to be cooled differently, hence the large difference between the temperature, and caused two

temperature-based cutoffs between these cycles that led to the two dips in temperature difference.

Full Discharge vs End of Discharge

Figure 45 plots data collected during one complete discharge and recharge with the 80% SoC and 20% SoC portions of the discharge are indicated by the black lines. Figure 6 presents the regions of a single discharge that is of interest, the last three 30-second pulses measured during a single discharge. At the power levels used here they represent approximately 25% SoC, with changes based on the overall capacity supplied by the cell in that given discharge.
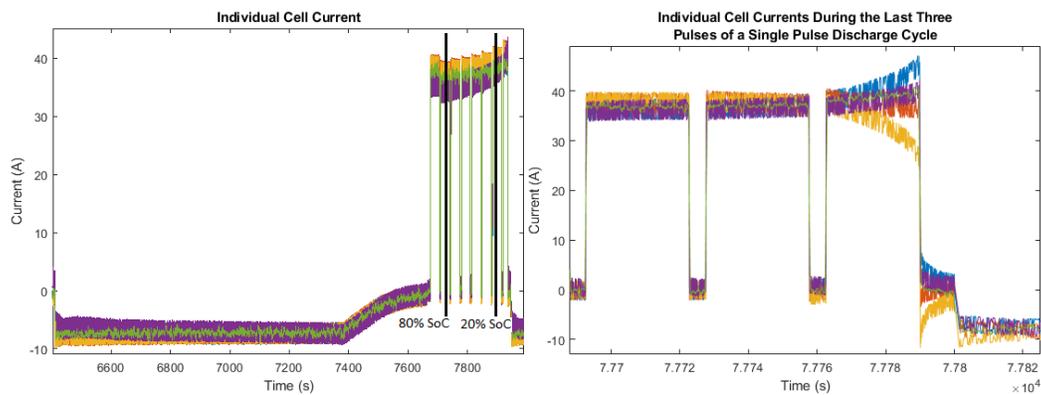
Figure 45: Test 3 A) One full recharge and discharge from the 8th cycle B) Individual cell currents during the last three pulses of the 419th

The last three pulses in the above and below plots show an overall increasing difference between the current for the last 20% SoC. By the 419th cycle cell 5, represented by the green line, is supplying a minor amount more current for initial 100% - 25% SoC, then at the start of the last pulse cell 5's current sharply drops out at the end and cell 1, blue line, provides a significant amount more current. Unlike in previous tests the higher performing cell for the initial 85% SoC recharges during the final 5s rest and the 10s rest between the discharge and charge. During the end rest cell 3 pulls 10A from the rest of the array. While

this behavior shows distinctive dynamics, this plot presents data from one cycle only and no meaningful conclusion can be drawn at this scale. To understand what impact this has in the long run and gain meaningful insights into the final 20% SoC an analysis of the final 20% SoC for all cycles is needed. Therefore, the author calculated and plotted the percentage difference between the temperature and current during the final 20% SoC for all 607 cycles, as well as the average current during the final 20% SoC.
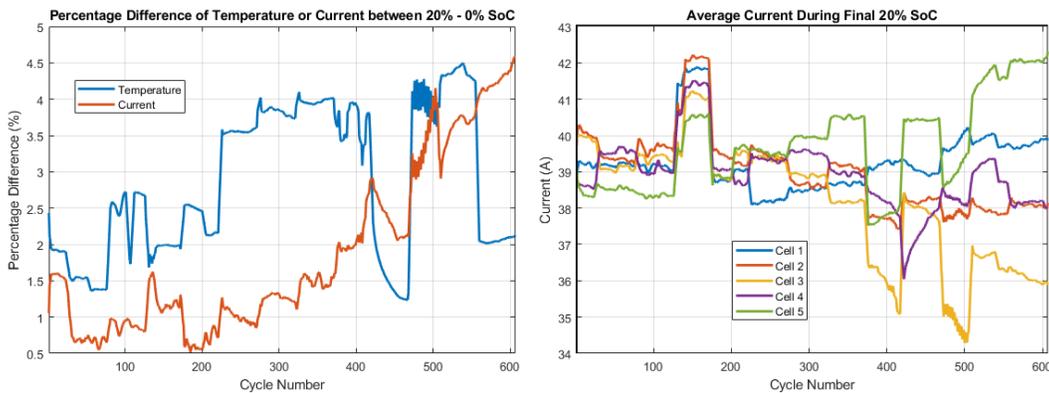
Figure 46: Test 3 A) percentage difference between temperature and current for final 20% SoC B) Average current provided by each cell for the final 20% SoC

The behavior of the temperature and current difference are significantly difference between the linear region and the final 20% SoC. The differences indicate that there are impact differences between the linear regions, but their magnitude of the percentage difference is similar. It is critical to consider that the mean temperature and current are higher in this region so although the percentage difference is similar, the maximum values are still elevated. There is a median 11°C increase between the mean cell temperature at 50% SoC and the 10% SoC. The temperature of one cell increases a median 2.9°C increase between 20% SoC and the cutoff. The high temperature and current are the reason this area contributes heavily to aging in power discharges. For current discharges the temperature at the end of discharge is still higher at the end, but the varying SoC

contributing to larger current differences between cells increase the damage sustained to the cells in this region of discharge. For the A123 cells used here the maximum allowed continuous current (defined as more than 10s) is 50A, the maximum recommended continuous current is 40A. Given that the cells supply above 40A current for 30s or less the modest increase in the aging effects already underway should accelerate the end of cycle life by 30% based on the manufacturer recommendation and test carried out in [68] [69] and [78]. Furthermore, as the cells age, this region of the discharge is the most likely time for the cells to fail as they are at their more elevated temperatures.

Recharge and Overall SoC Balance

The next electrical measurement to assess is the capacity difference. This measurement is the difference between the capacity supplied to the battery on recharge vs the capacity conducted by the battery on discharge for the 5 cells cycled. This comparison uses the mode of each cells capacity to find the general trend.
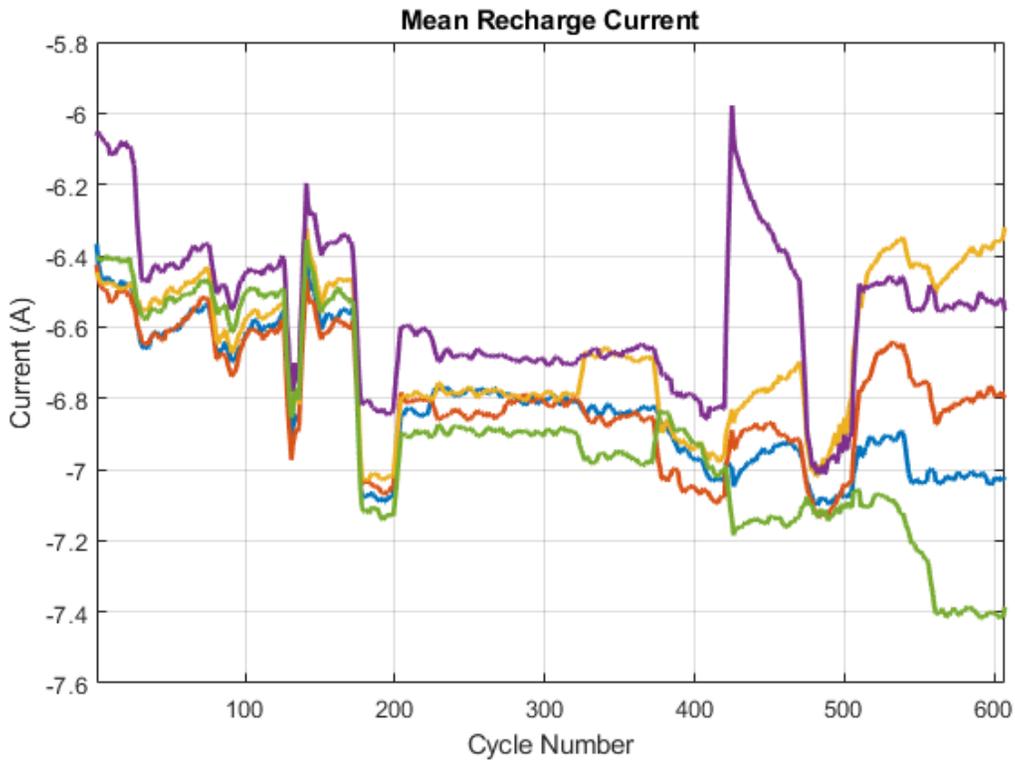
Figure 47: Test 3 Recharge current from start to 4A cutoff

The median and mean for the difference between recharge capacity and discharge capacity is negative at 1mAh and zero, respectively. The mode of the difference between recharge and discharge, which shows what individual cells are experiencing, continues this general negative trend. The previous tests have an overall negative value on the recharge capacity; this test shows a strong consistent negative trend. There are a few initial runs that have an occasional positive value. The difference between each cycle does not increase at the end as shown in test 1 and test 2.
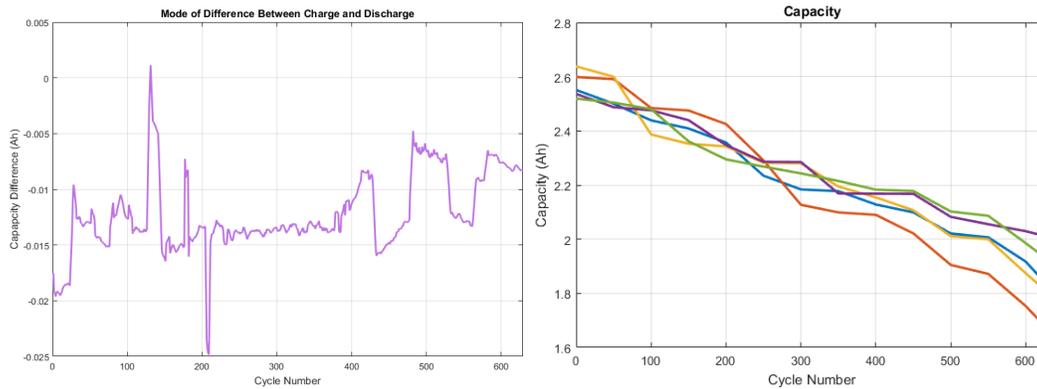
Figure 48: Test 3 A) Show the mode of the difference between recharge and charge for each cycle for the third test. B) Capacity Fade at each baseline done throughout testing

The general trend shown in this test strengthens the concept that anodic losses contribute significantly to capacity fade either due to loss of cycled material or in rare cases volume changes in LFP cells, which is backed by the literature [71] [52] [80]. The overall trend presented in this graph is that having less cells in parallel does reduce the long-term trend of continued capacity fade seen in the 30-cell setup. The trend reflects in the overall capacity fade, the first cell does not show a 20% capacity fade until cycle 450 and the total pack capacity fade does not reach 20% until 550. Although test 2 was cut short, one of the cells had experienced 19.7% capacity fade by cycle 253, significantly shorter than seen here. It suggests that highly parallel cells have detrimental long-term impact on each other.

EIS and 1 kHz

Below are Nyquist plots from the two of the cells throughout testing and then two plots of all the cells from the initial and final Nyquist plots where the initial and final focus on two different areas of the Nyquist.
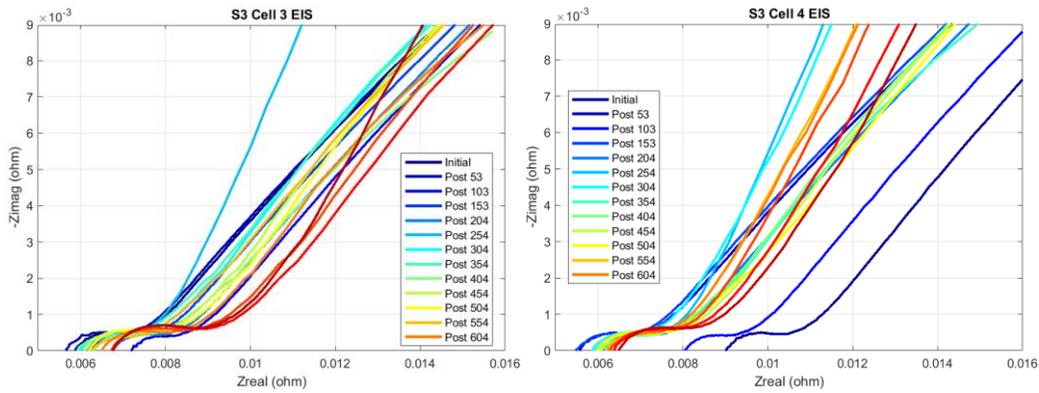
Figure 49: Test 3 A) EIS measurement of cell 3 and, B) cell 4 after each periodic baseline procedure
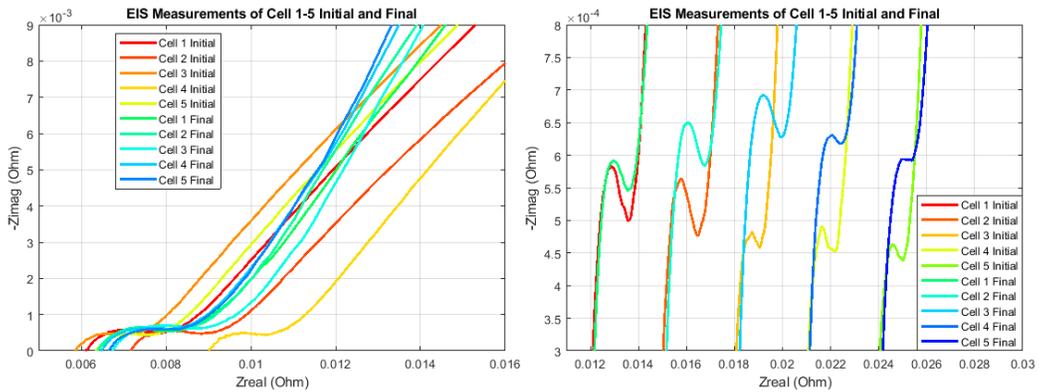
Figure 50: Test 3 Initial and final EIS measurement of all the cells A) the full EIS B) zoomed in on the mid-frequencies and shifted to same 1kHz impedance for better comparison

The above plots indicate that there is a noteworthy change in the local ω_{max}, which corresponds with the battery cells voltage responses to the current change. This shift down in frequency and increase in the time constant means that the voltage does not respond s quickly to changes in current as before. Meaning that, since power is directly related to both the current and the voltage, the power may take longer to come to a more gradual change point because the slow voltage change is still substantial in comparison to LFPs voltage discharge curve.

113

The Warburg tail of an ideal capacitor is at 90° to the semi-circles, the Warburg tail of a battery is generally at 45° to the semi-circles, and an ideal inductor's Warburg would come straight off the semi-circle 0° between their planes. Therefore, the angle increase seen in figure 11 A between the semi-circle and the Warburg tail point to an increase in the capacitive aspects of the battery charge transfer mechanisms. In the circuit element model the increase in angle results in a decrease in α so that α is closer to one, indicating that the CPE behavior is increasingly similar to the behavior of a capacitor. Physically this increase in capacitance points to an increase in the thickness of the diffusion layer or a decrease in the diffusion constant. Since non-catastrophic changes in thickness of the diffusion layer are small, the majority capacitance increase comes from the decrease in the diffusion constant. This decrease in the diffusion constant, which leads to an increased charge transfer time, results from the growth of the SEI.

Correlation

There are significant economic benefits to being able to bin the cells along a metric, which will reduce the current imbalance between cells. Therefore, the correlation between key metrics and the current supplied needs to be carried out for all tests. Even a mean correlation of 0.4 that is consistent for all tests, which does not mean it is consistent for all cycles, could increase the cycle life of a pack if the cells are binned along that metric. Although the correlation seen in test two between the three metrics presented weakens the relationship between the High C DC ESR and the current, there is still reason to see the relation between High C DC ESR, 1kHZ impedance, and Low C DC ESR.
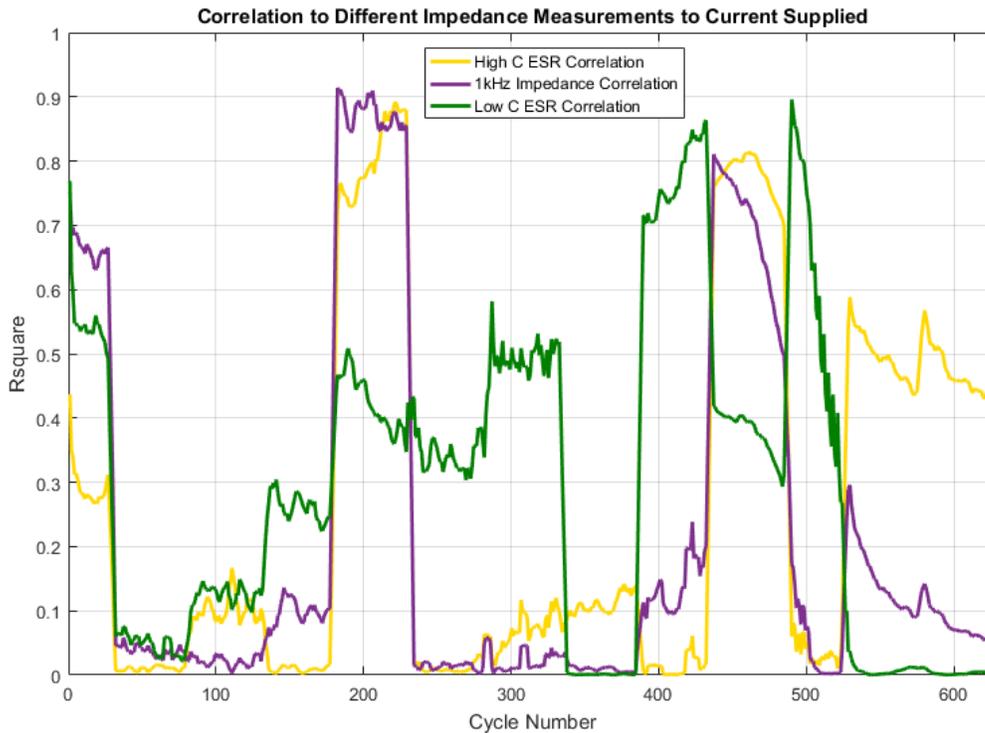
Figure 51: Test 3 correlation of the initial 1 kHz impedance, Low C DC ESR, and High C DC ESR

Test 3's current distribution has a strong correlation with the initial Low C DC ESR. High C DC ESR is weak; but, where the low seems to drop at the end cycles the high C correlation increases. The relation between the Low C DC ESR correlation and the High C DC ESR correlation suggests that some combination of key metrics might be able to give insight into the discharge characteristics of the pack. Test 3 does exhibit similarly poor correlation between 1kHz and the current for most cycles, with a few exceptions.

Potential other key merits or indicators of future cell behavior

There are several other metrics used by researchers to characterize the cell. A few of the metrics can be calculated from the in-situ metrics taken during the testing. Below are a few plots that present those metrics that could be taken for each cycle. The three metrics presented are the pulse resistance, the pulse recharge resistance, and the pulsed high C

resistance. The pulse resistance is taken from two measurements points. The first point comes from when the cell is at rest, right before the discharge is begun; the second point is taken either 5s or 10s into the discharge. The plots presented here are taken at the 10s points because that is the most common time stamp used in literature. The 5s pulse resistance was calculated and was found to be similar. For the calculations presented here the mean of the seven points leading up to the discharge were used for the first value, and seven points around the 10s mark were used for the second value. The mean was deemed to be more accurate due to the noise, given that this is 4ms of data, it is still showing the cell state at specific enough points to fit the criteria for this characterization [78],[56].
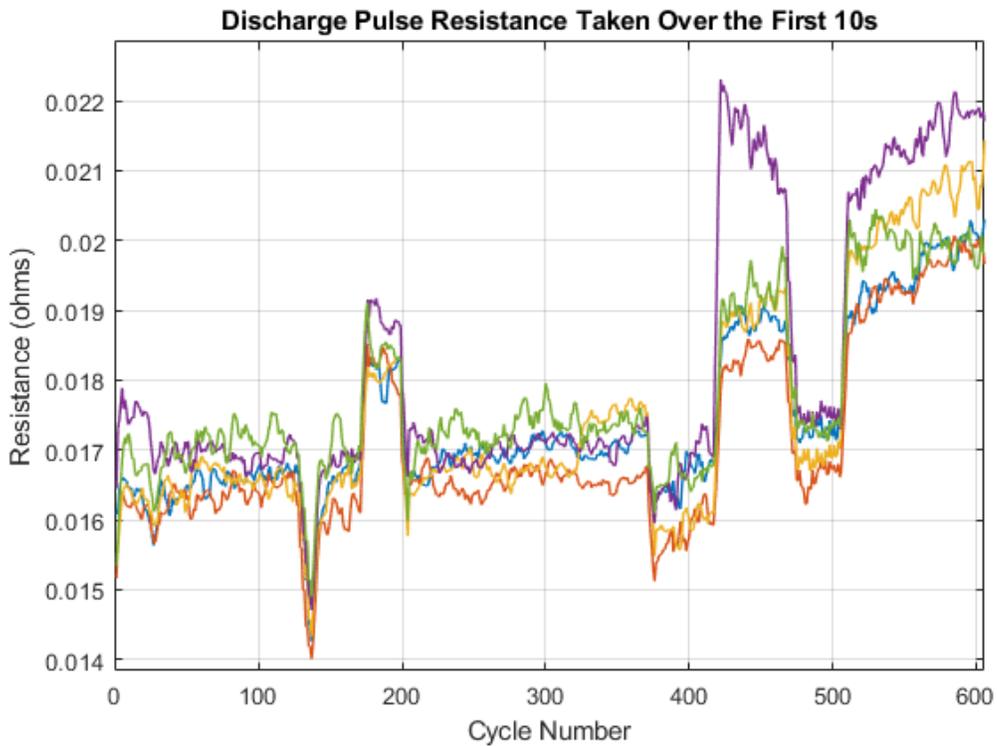
Figure 52: Test 3 The discharge pulse resistance taken from the voltage and current before the recharge

began and then the voltage and current taken 10s into the recharge

Looking at the plot of the pulse resistance the performance drop of the third cell can clearly be reflected at cycles 328 to 478. There is a peak from cycles 174 to 203. The increase in pulse resistance here happens directly after the increase in overall current provided. So that additional stress to the cells is reflected in the pulse resistance for the following tests, but then the baseline appears to recondition the cell and bring the pulse resistance back down to near initial levels.

The second metric is the inverse of the pulse resistance in that it is the same values taken for the cell recharge. Once again, the MATLAB script used to calculate these values took a few data points around the desired time stamp for more accurate measurements. In literature, it is standard for the recharge metric to be based on at 75% of the maximum recommended recharge [81]. The maximum recommended fast recharge for the A123 m1-B cell used here is 10A. Thus 7.5A on start meets the criteria. One of the challenges with the recharge measurement taken here is that the cells have not reached equilibrium by the time the recharge has started. Therefore, the cell current before a recharge is not always at zero as is generally desired and more prone to noise.
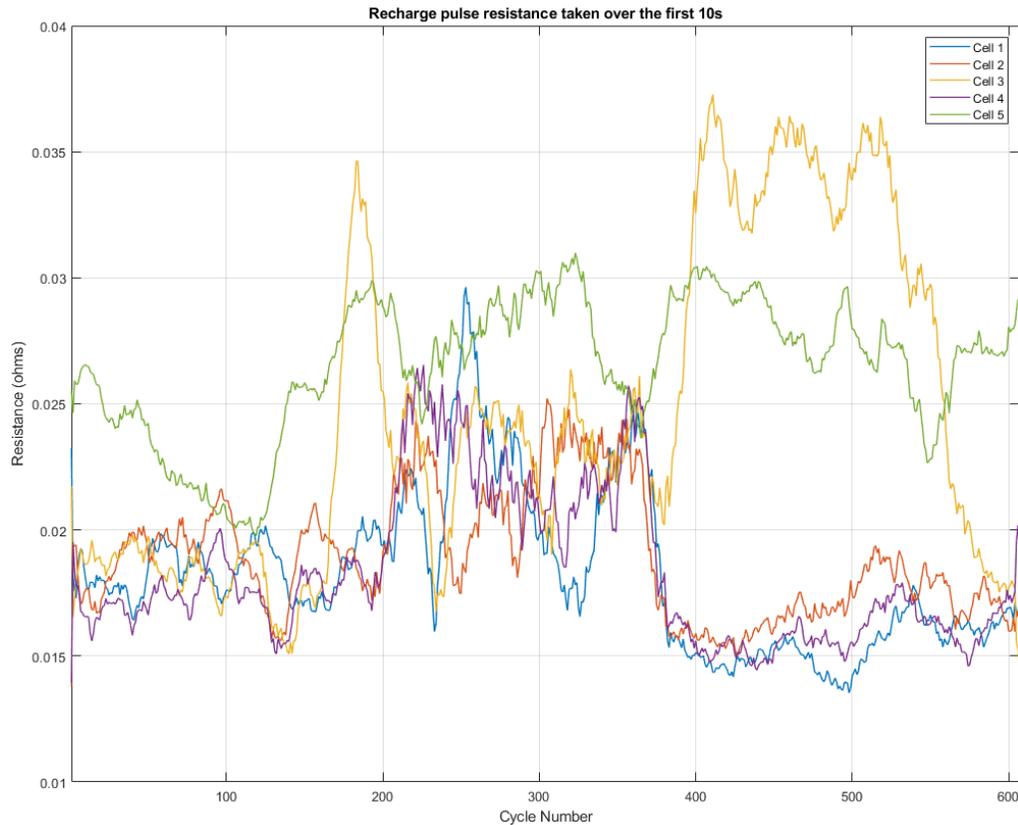
Figure 53: Test 3 The recharge pulse resistance took from the voltage and current before the recharge began and then the voltage and current taken 10s into the recharge

The recharge metric is not as clearly reflective of changes seen in the recharge current. The trends that seem to be slowly developing in cycles 1 to 202 disappear at cycles 203. Cycles 203 to 378 are significantly noisier and then for cycles 379 to 607 the clear trend of cells 1, 2, and 4 have slowly increasing resistances near starting near 15mΩ that taper out near 17mΩ whereas cells 3 and 5 have significantly higher resistance with more erratic behavior. The uniqueness of the trend at the start of the discharge suggests additional insight into the behavior of the cells in later discharges. With the uniqueness of the recharge metric and the apparent similarities between the discharge resistance and current in mind, the recharge pulse resistance along with a few other metrics was used to

118

predict the current supplied by each cell during discharge. Table 1 presents the mean

accuracy of these measurements. For the tables below, open circuit voltage is

represented by V_{OC}, Discharge Pulse Resistance by r_{pd}, recharge pulse resistance by r_{pr},

and max angular frequency by W_{max}.

Table 1: Metric combinations used to attempt prediction of the current sharing between cells

Metrics Included	Mean Correlation
1 kHz ESR, 10s High ESR, r_{pd}, V_{OC}	0.415
1 kHz ESR, 10s High ESR, r_{pd}, V_{OC}, Low C DC ESR, r_{pr}	0.418
1 kHz ESR, 10s High ESR, r_{pd}, V_{OC}, W_{max}	0.415
1 kHz ESR, 10s High ESR, r_{pd}, High C DC ESR	0.42
1 kHz ESR, 10s High ESR, V_{OC}, High C DC ESR, r_{pr}	0.413

As this table shows, the initial recharge pulse resistance is not reflective of the current

sharing throughout; it only appears in two of the top five combinations. There are a few

hopeful metric combinations seen in this table. Notably, the 1kHz ESR and 10s High ESR

are in all the metrics above 0.4, and Discharge Pulse Resistance and Open Circuit Voltage

are in all but one each. Unfortunately, when these findings were used to run similar tables

on the earlier discharges the strength of the correlation did not hold. The author continued

the further investigation into these predictive metrics in the following three tests.

The last metric presented for this test is the high C DC ESR taken over the first 10s. The

script calculated the 10s High C DC ESR metric by taking the current and voltage from the

first 10s of 1C baseline discharge and dividing it by the current and voltage from the first

10s or the cycle discharge using equation 3.
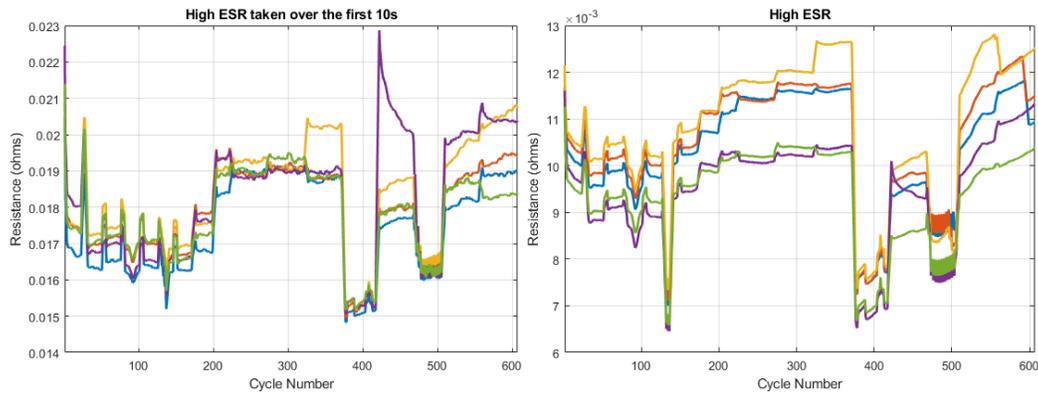
Figure 54: Test 3 A) High C DC ESR calculated from the from the first 10s of discharge B) High C DC ESR between 80% - 20% SoC

Although the significant trends are similar to the trends of the discharge pulse resistance, there are some distinct differences. One aspect is that the baseline effects of the High C DC ESR are more than it affects the pulse resistance. The first 3 cycles after the restart of cycle show a significant increase. Temperature more than pulse resistance impacts the high C DC ESR because the two thermal states of the cell are intrinsic to the High C DC ESR calculation whereas pulse resistance uses a similar thermal state with the systematic differences being in the current and voltage at the time stamps. Therefore, the post-baseline spikes show that there are some thermal based reactions taking place that do not reach equilibrium until a few cycles in even though the temperature reaches equilibrium in the first few cycles as shown by figure 2.2 for test 2. It is these differences that lend additional information to the current imbalance between cells. The initial settling is also a sign of the SEI buildup as well as other reactions that lead to cell cycle equilibrium.

Test 4 – 117 W per Cell, 5P/1S, No intermittent baselines

A second test was performed that cycled only five cells at 583W or 15C. However, this test was run without intermittent baselines--only an initial and final baseline. To investigate the impact the baselines were having, the intermitted baselines were omitted. The author used

the testbed in a 1S/5P setup; that is. one PCB was left on the copper bus bars while the other five are not electrically connected, this test used new unbinned cells. Figure 55 presents a summary of the current and temperature imbalance calculated using the average absolute deviation, for all 501 cycles.
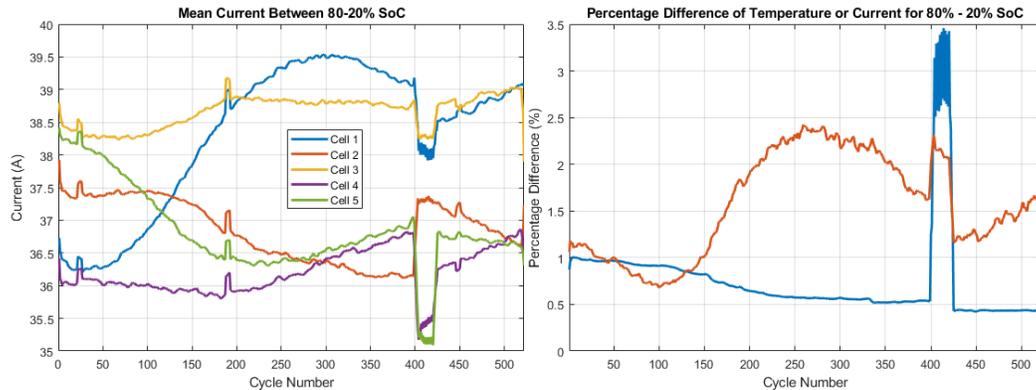
Figure 55: Test 4 A) Percent difference of the mean absolute deviation between individual cells' current and temperature B) Mean current of each cell, both A and B are based on the mean values between 80% and 20% SoC of each discharge cycle

The bump in the current and temperature difference is due to the forced air cooling accidentally being shut off, and it not being noticed for the effective length of 23 cycles. This misalignment resulted in a temperature cutoff at the end of every second cycle at the start of therefor 11 full cycles were counted by the software as 23 cycles thecycling resumed once the cells reach 25°C per the user specification. As this figure shows, there is an interesting trend in the current imbalance curve. The points of interest in this current imbalance curve are its general decrease until cycle 100 followed by a significant increase until cycle 258, with the last 71 cycles showing a slight end of life increase. Due to the small pack size, the mean current of the cells reveals the cause of the percentage current difference behavior. The almost inverse trajectories of cell 1 with cells 2 and 5, with cell 5 contributing more to the first rise and cell 2 to the rise at the end. Paired with the mean

current is a simple temperature difference that decreases then levels off. At the maximum difference this represents a less than 3°C average temperature difference. This temperature difference confirms the findings from the previous test that temperature is not a significant factor in the aging differences in the cells. Therefore, unlike what the author hypothesized before testing, the temperature is not significantly contributing to the aging. There is some initial literature that found a similar low-temperature increase in LFP cells about the current provided [82].

An in-depth look at the last three pulses in a cycle are presented, the trends are more obvious because there are only 5 cells used for this test. Figure 2A presents one full discharge from test 5 with black bars highlighting the first ~ 2.3Ah provided by the cells and the last ~2.3Ah of the discharge. Figures 2B present the end region in a single discharge which is of interest, the last two 30 second pulses measured during a single discharge make up the last 20-25% of capacity. Channel 5, represented by the green line, displays a relatively unchanging current level throughout the discharge in comparisons with the other 4 cells that show variation near the end. The last three pulses give a good overview of what is happening in this instance. The first pulse in the series shows individual currents are all at similar level and are flat for the entirety of the pulse. Whereas, the last two pulses show that for the final 20% SoC cell 4 current increase, cell 5's stays the same, and 1 through 3 decrease the current they supply. Cell 4 best displays the average current hovering around 37.5A.

End of Discharge Behavior
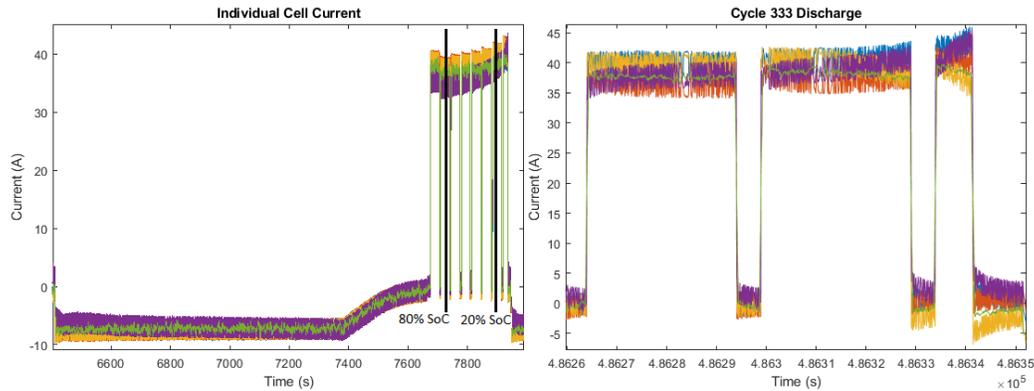
Figure 56: Test 4 A) One full recharge and discharge from the 20th cycle set B) Last three pulses of the discharge which represent roughly the last 25% SoC of the discharge from the 100th cycle

The current data are statistically insignificant at this scale. Therefore, the mean current for the last 20% SoC was calculated for every cell and cycle and is presented in Figure 3A. The current sharing for the last 25% SoC is summarized in the plot below. The average percent difference between the cells for the final 20% SoC is essentially the same, with the magnitude being slightly larger, generally 2.1A larger average. A difference of 2.1A is slight and would not be a significant safety factor at lower current level; at high power levels it pushes the cells outside of their recommended current levels; and, therefore, additional tolerances need to be factored in when sizing the battery pack. Either a cutoff that does not use the final 20% of the capacity in the battery pack or oversizing the pack so that the mean current is not more than 12C.
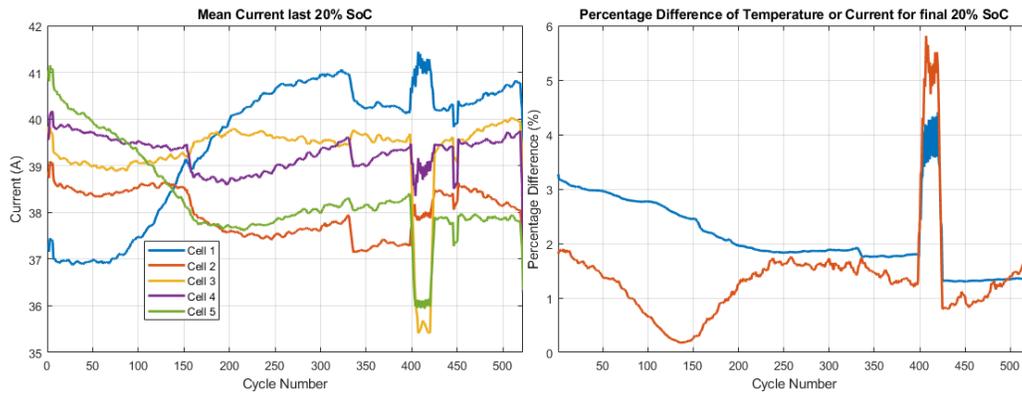
Figure 57: Test 4 A) Percent difference of the mean absolute deviation between individual cells' current and temperature B) Mean current of each cell, both A and B are based on the mean values from the final 20% SoC of each discharge cycle

Figure 3B clearly show the large difference between the cell behavior seen during the flat part of the discharge curve versus the final 20% where the voltage drops off. There is a significant change in the mean current for the final 20% SoC, especially for cells 2 and 4, between cycles 155 and 156. This drop is repeated for all but cell 3 between cycles 333 and 334. The second drop after cycle 333 occurs shortly after the mean current for cell 1 starts to decrease during the linear part of the discharge, presented in Figure 1B. These drops represent a decrease in the number of initiated pulses between cycles, shown in figure 6A and B. This loss of a ~6.9s pulse highlights the strength of using pulse power. By allowing the cells to rest for 5s and additional 6.9-7.4s, which is 924.8Wh or 395.2Ah, of discharge can be gained. For this set of cells, the overall difference between the cells is smaller during the final 20% even as the current is significantly larger, this small current difference is largely because cell 1 and 3 supply a similar amount of current. This trend can be seen in figure 5B. Furthermore, the dip in current difference plateaus for 32 cycles and does not increase until cycle 148, about 50 cycles later then the main difference increase. The temperature difference trajectory is remarkably similar to the temperature difference

of the cells between 80% to 20% SoC, only increased of two percentage points. The dramatic differences seen here are indicative of changes occurring within the cell due to aging and not the primary source of the changes.
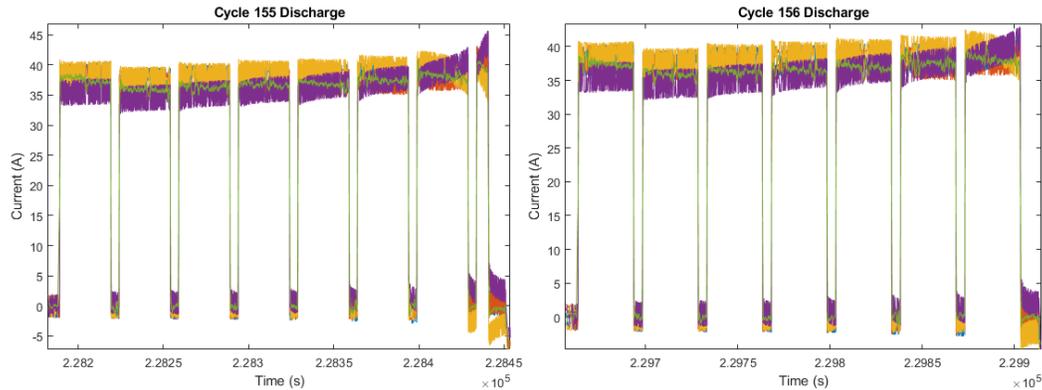
Figure 58: Test 4 Full discharge from cycle 155 and 156 showing the dropping of the last pulse between cycles. The final pulse in the 155 discharge is 7.1s

Recharge and Overall SoC Balance

As discussed in the aging mechanism section of the literature review, capacity fade rather than impedance rise is the most common form of loss of energy delivered to the load. The test presented above back these findings. Capacity fade comes from the loss of active material whether cathode material, anode material, or lithium inventory. Although the change in capacity fade is small from cycle to cycle, cell tendencies point to the likely capacity fade. The previous tests presented in this dissertation have established that a majority of the active material loss is happening at the anode. Anode side capacity fade is generally due to loss of anode material, lithium plating, or SEI formation. The more data sets and variables the better insight into the common cell behavior. Figure 5 shows the percentage of the mode of the capacity fade for Set 4.
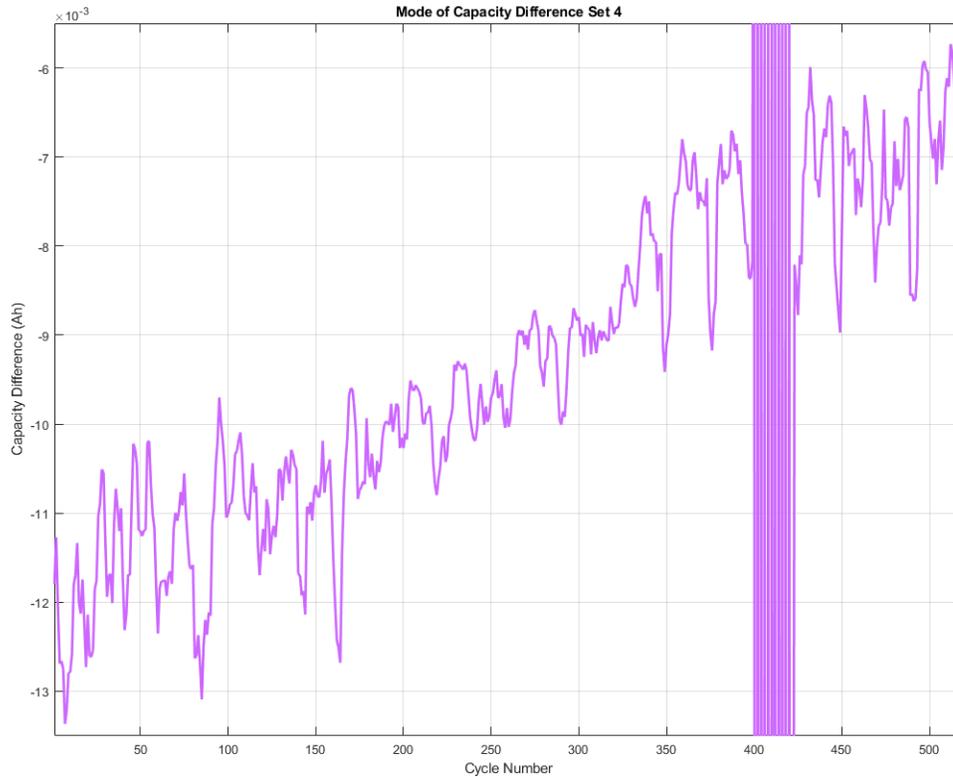
Figure 59: Test 4 the mode of the difference between recharge and charge for each cycle

The rapid variation between cycled 400-423 is due to the thermal cutoff. The cutoffs experienced during these cycles make their capacity information non-indicative of the overall trends. Thus, the script was written to not include it in the mean and median values; and, the scaling was chosen to understand the salient trends better rather than include the extremes of these cycles. The median and mean for the difference between recharge capacity and discharge capacity is at –9.6mAh and slightly negative at –11.2mAh, respectively. The mode of the difference between recharge and discharge continues the general negative trend seen throughout the testing presented in this dissertation. It is remarkably consistent for the entirety of the testing. The jump upwards at 400 can be contributed to the temperature cutoff. However, after the cells return to thermal equilibrium, they drift back to near negative 250mAhs.

126

Once again, the trends presented show anodic based capacity fade. Future research is needed to see the impact of the end of discharge on this type of aging. Other researchers have concluded that stress electrochemical cells near the limits accelerates the anodic aging [70],[83],[84]. Since the final stage is the point where the profile pushes some of the cells beyond the suggested limits, this area will have large detrimental effects on the cells anode collector.

EIS and 1 kHz
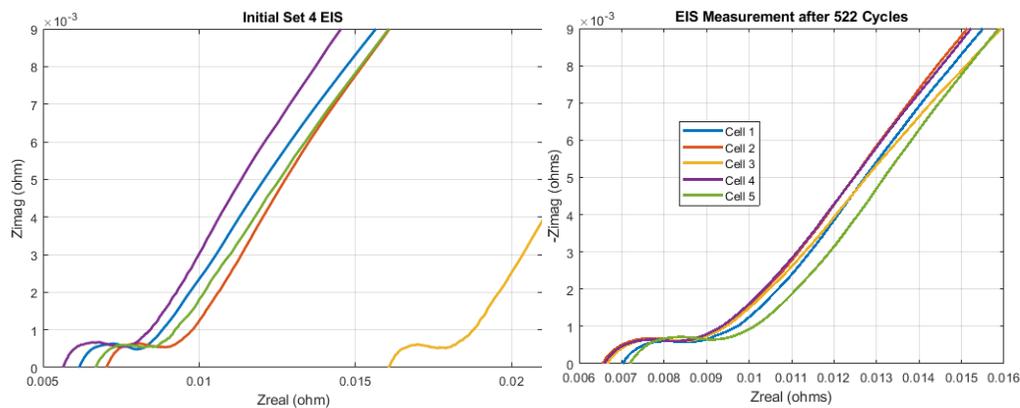
Figure 60: Test 4 EIS measurement of all the cells after cycling and after all the cycling had been completed with a full view of the zero impedance crossing and the Warburg tail

The two plots above show the randomization of the cells in that the 1kHz value, and thus the overall real part of the impedance, is widely distributed. Reviewing the datasheet and patent, it is expected that some of the cells will have a 1kHz impedance up to 18mΩ [82],[85],[86]. Then, looking back at the initial Nyquist plots from the previous test, XX cells also show an initial 1kHz above 9mΩ. The test 1 1kHz values have 3 near the 16mΩ mark. The tests run here show that the 1kHz has a bimodal distribution with 91.8% being near the nominal 7mΩ then the other 8.2% being above 11mΩ. By the end of the set of discharges, each cell's real impedance at the zero crossing aligns closely with all the other

cell's real impedance at the zero crossing. The reasons behind this bimodal distribution are unknown but do verify manufacturer variations.
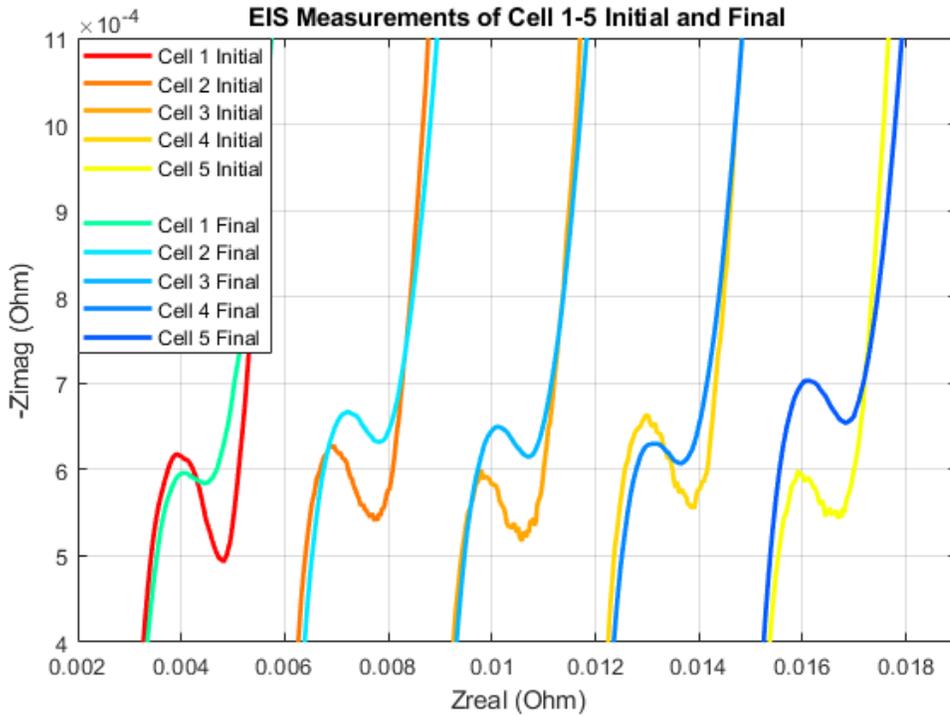
Figure 61: Test 4 EIS measurement of all the cells before cycling and after all the cycling had been completed with a focus on the mid-frequencies and shifted to same 1kHz impedance for better comparison

Cells 1 and 4 have a flattened mid-frequency region and begin with the tallest arcs before cycling. The decrease in the height of the mid-frequency semi-circle means that there is an increase in the diffusion coefficient to the point where it dominates the double-layer capacitance effects along with the charge transfer impedance. These changes have not directed relationship with the capacity fade, as is visible by reviewing the capacity plot calculated during cycling.

128
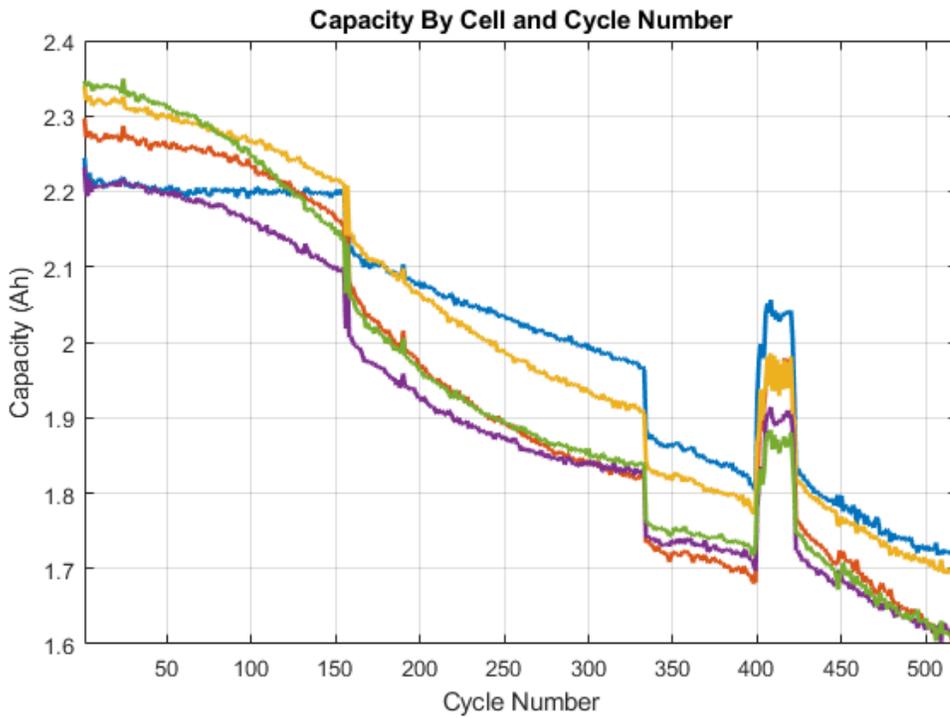
Figure 62: Test 4 Capacity fade across cycles

Correlation

Test 4 is the first test run without baselines. This allows for the investigation into the key standalone figures of merit to be more directly compared to cell behavior expected in common pack applications.
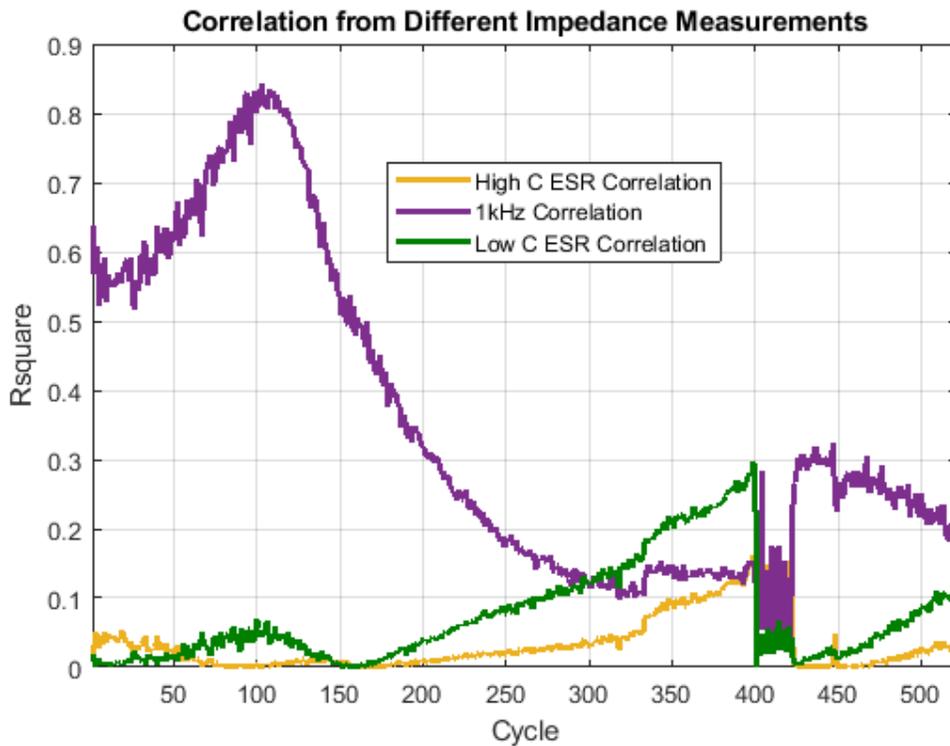
Figure 63: Test 4 Correlation of the initial 1 kHz impedance, Low C DC ESR, and High C DC ESR

This figure shows that initial 1 kHz does have a strong correlation with how the cells share current over the long term. The trend in the 1 kHz impedance points to the weakness of this single value and its strength as in a matrix of key metrics. When a matrix of metrics includes 1 kHz ESR with other initial figures-of-merit that have a stronger relation later in the cycling, the correlation can be strong throughout the cycling. The author did a similar analysis on the additional key metrics noted in test 3. In the next section the author will review the relationships that proved strongest in this test set.

Potential other key merits or indicators of future cell behavior

The mean of chosen initial conditions with the current from this continuous test show how the cells would behave if constantly cycled. Using this data alongside the mean from

the previous test with intermittent baselines shows the strength of the causality between the chosen initial conditions and current sharing.

Table 2: Test 4 Metric combinations use to attempt prediction of the current sharing between cells

Metrics Included	Mean Correlation
1 kHz ESR, 10s High ESR, r_{pd}, V_{OC}	0.582
1 kHz ESR, 10s High ESR, r_{pd}, V_{OC}, Low C DC ESR, r_{pr}	0.476
1 kHz ESR, 10s High ESR, r_{pd}, V_{OC}, W_{max}	0.612
1 kHz ESR, 10s High ESR, r_{pd}, High C DC ESR	0.530
1 kHz ESR, 10s High ESR, V_{OC}, High C DC ESR, r_{pr}	0.212

The results from test 4 show that the recharge pulse is not a generally useful metric. Adding it and the Low C DC ESR lowers the correlation than when all the same metrics are used except Low C DC ESR and pulse recharge. In the one metric where pulse recharge resistance and High C DC ESR are added the correlation is low enough as to be near noise in a system of this size. The drop between key metrics correlation with the current discrepancies could be because the discharge pulse resistance has a very strong correlation with the current and, therefore, dropping it from the calculation results in very weak correlation overall. Looking at the correlation between the discharge and the Pulse Recharge the correlation is 0.316. Therefore, for the last key metric, the loss of the pulse discharge resistance is more significant than the addition of the pulse recharge resistance. While this strengthens the hypothesis presented in test 3, it will be beneficial to continue this analysis to test 5 and test 6. Particularly, test 6, where 30 cells make for a more statistically significant evaluation of the correlation coefficients between the current and the metrics, will be more useful to the overall idea which this dissertation is evaluating here.

Test 5 – 117 W per Cell, 5P/1S, No Intermittent Baselines

A second test cycled five cells at 583W or 15C. This test similarly to test four ran without intermittent baselines--only an initial and final baseline. To further investigate the impact the baselines were having; the intermitted baselines were omitted. The author used the testbed in a 1S/5P setup; that is one PCB was left on the copper bus bars while the other five are not electrically connected, this test used new unbinned cells. The data gathered from test 5 supports the findings from the four tests presented above. The insights gained from test 5 are similar to the insights gained from test 4. Therefore, the author is not presenting the full analysis, but the plots are made available to the reader in appendix A.

Individual and Combined Correlation Coefficients

The area where adequate statistical representation is most critical is the ongoing review of starting metrics. It is essential to know how causative and predictive they are of the current difference see throughout testing. To have a high level of confidence in suggested metrics to investigate in future work a full review of each test is necessary. Thus, the correlation plot and table are presented in the main body of the dissertation.
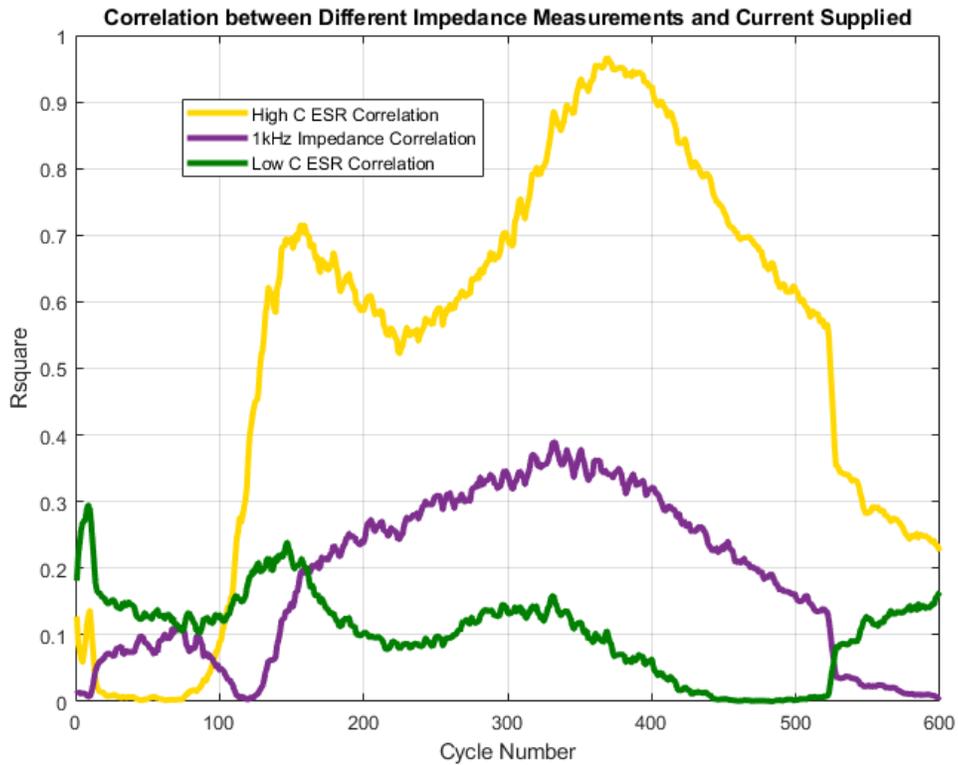
Figure 64: Test 5 Correlation of the initial 1 kHz impedance, Low C DC ESR, and High C DC ESR

The author presents the table of critical metrics for review by the reader. For a more thorough investigation of the usefulness of combined metrics.

Table 3: Test 5 Metric combinations use to attempt prediction of the current sharing between cells

Metrics Included	Mean Correlation
1 kHz ESR, 10s High ESR, r_{pd}, V_{OC}	0.078
1 kHz ESR, 10s High ESR, r_{pd}, V_{OC}, Low C DC ESR, r_{pr}	0.139
1 kHz ESR, 10s High ESR, r_{pd}, V_{OC}, W_{max}	0.12
1 kHz ESR, 10s High ESR, r_{pd}, High C DC ESR	0.426
1 kHz ESR, 10s High ESR, V_{OC}, High C DC ESR, r_{pr}	0.098

Looking over this table, the reader can see that the VoC was not contributing to the overall current supplied by the cell in this test. The only strong correlation for this test is the set with High C DC ESR. This suggests that only the High C DC ESR is correlated, and the other variables do not further contribute to the correlation in this instance. High C DC ESR as a standalone trait has not consistently been a useful metric for predicting the current supplied by each cell throughout testing. Given the trend of the High C DC ESR in this test, and test one paired with the less definite trends of test two and test three there might be a relation between the High C DC ESR and the how the cells age. Therefore, correlation at later stages has the potential to provide additional insight into increased cycle life. This requires binning according to different metrics and then studying the aging rates sharing and therefore cannot be investigated by, but the analysis done on these tests do uncover an advantageous new area of research to allow for the commercial deployment of parallel arrays.

Test 6 – 117 W per Cell, 30P/1S, no Intermittent Baselines

A second test was performed that cycled 30 cells at 3500W, which is 117W per cell or approximately 15C. The test presented in the section below was run without intermittent baselines only an initial and final baseline. Leaving out the intermitted baselines was done to investigate what impact the baselines were having. The author used the testbed in a 1S/30P setup, that is six PCBs on the copper bus bars, this test used new unbinned cells. Figure 1 presents the mean current for all the cells, and a summary of the current and temperature imbalance for the final 20% SoC calculated using the average absolute deviation, for all 501 cycles.

134
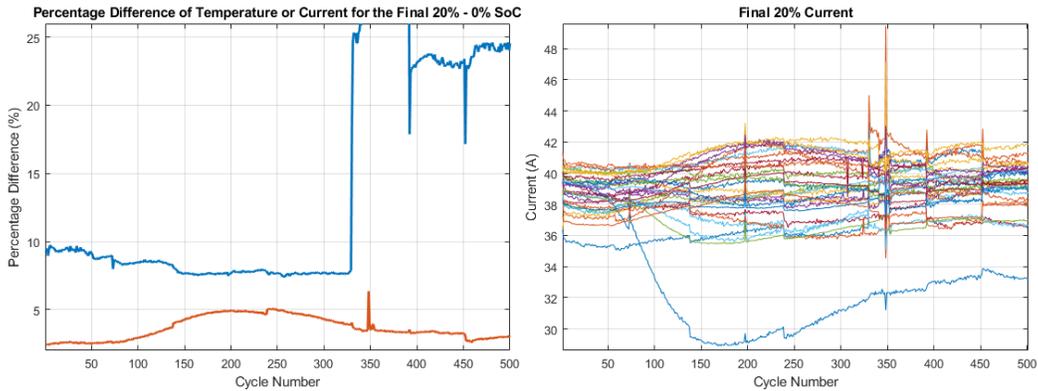
Figure 65: Test 6 A) Percent difference of the mean absolute deviation between individual cells' current and temperature B) Mean current of each cell, both A and B are based on the mean values for the final 20% SoC of each discharge cycle.

At cycle 346 the temperature logging stopped, and program recorded a temperature an incorrect value until the author observed the problerm at cycle 391 and stopped the cycling was stopped then restarted the tested under close supervision to ensure that the program was once again measuring the actual temperatures of the cells. It is unclear why this occurred. Due to the lack of temperature measurements for this region, the analysis does not take it into account when covering the percentage difference. Fortunately, there were no such errors in the current measurements, which test one and two established as the real metric of interest. Other than cell 15, the lower blue line, which quickly drops in the amount of current it is supplying there are only minor changes in the mean current during the final 20% SoC.

135
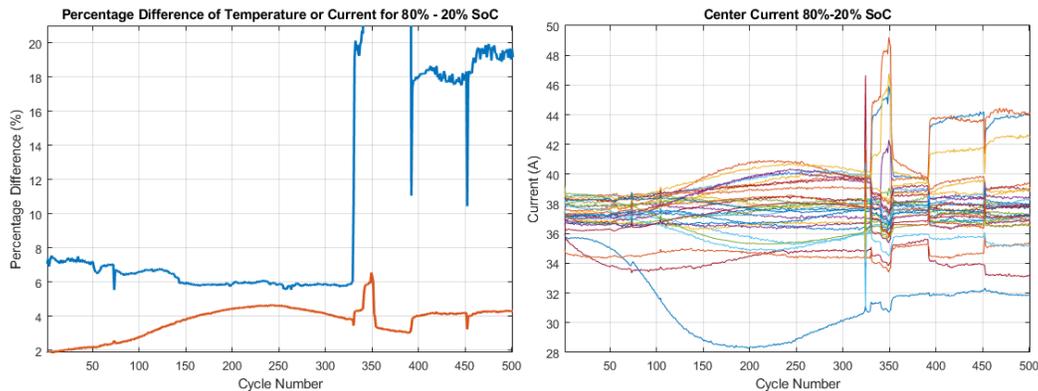
Figure 66: Test 6 A) Percent difference of the mean absolute deviation between individual cells' current and temperature B) Mean current of each cell, both A and B are based on the mean values between 80% and 20% SoC of each discharge cycle

Looking at the linear portion of the discharge there is a spike at cycle 324, and then the substantial mean current spread from cycle 326- 350. Their current spread decreased only to pick back up at 392 after the cycling resumed. Since the only actions taken was stopping and restarting the test, it is unclear what caused these changes. Between the two percentage differences, there is a 2.4% increase in the temperature difference. There is little difference between the current difference except for a 2.1% increase for the final 110 cycles. The cells had reached a cycle capacity fade of 20% at cycle 239, though the C/2 discharge at the end of cycling suggests a C/2 capacity fade of 20% closer to cycle 356. The drop at cycle 451 is due to this being the initial stopping point, but the author cycled the cells for a further 50 cycles to ensure reaching 20% capacity fade. Since the most optimistic calculations put the C/2 capacity fade at 20% at cycle 431 cycle, 451 was an acceptable stopping point. Given the significant difference between the mean current trends for the final 20% SoC and 80% - 20% SoC, the mean current for the full discharge is presented.
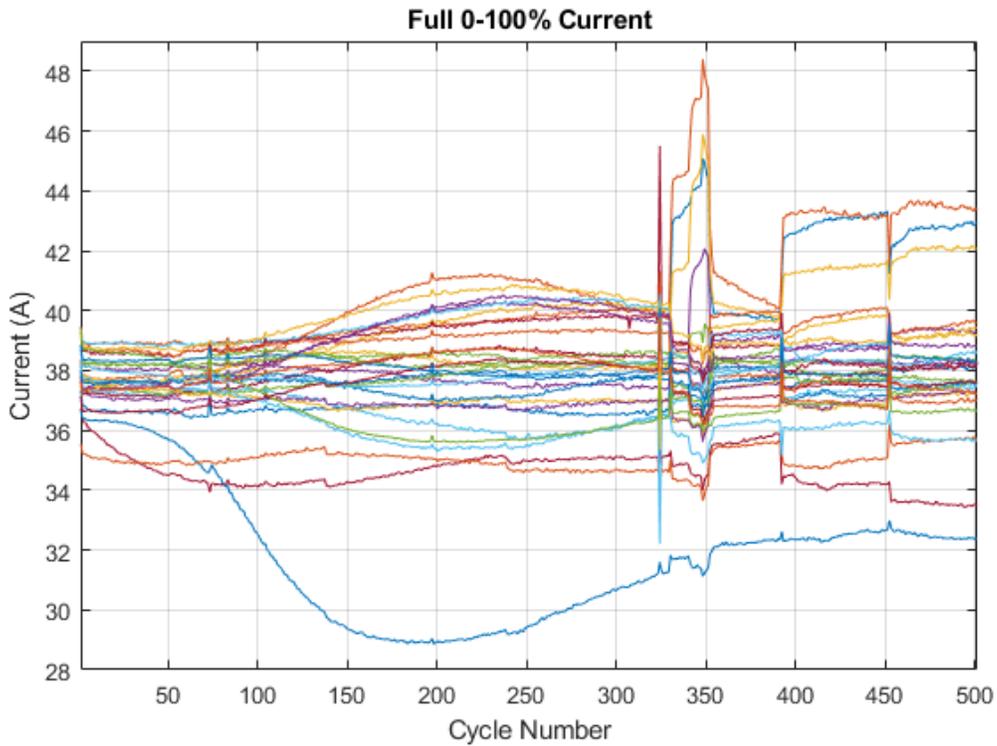
Figure 67: Test 6 Mean current of each cell based on the mean values for the full discharge cycle.

The trends seen in the mean current taken across the full discharge are similar to the behavior of the mid-section of the discharge. The shifts in these trends suggest that there are a few cells that have an above average capacity but high pulse resistance or low Wmax. The combination of these traits would lead cells with those traits take more time to meet the current demands, but as the other cells get to the end of their available charge, the cells with remaining capacity would meet the load demand. These traits are similar to the traits in the bottom orange and red cells. Both 14 and 16 have a full standard deviation more capacity; cell 14 has a standard deviation higher pulse resistance while cell 16 has 0.8 standard deviations higher pulse resistance. The one trait where these cells do not follow the expected trend is Wmax where both cells have a 0.75 standard deviation higher

ω$_{max}$. The author further explores the implications of these findings in the key metrics section.

Overall SoC Balance and Capacity Fade

The obvious points of interest in the mean current plots gives the reader insightful points of interest to look for in the mode of the capacity difference.
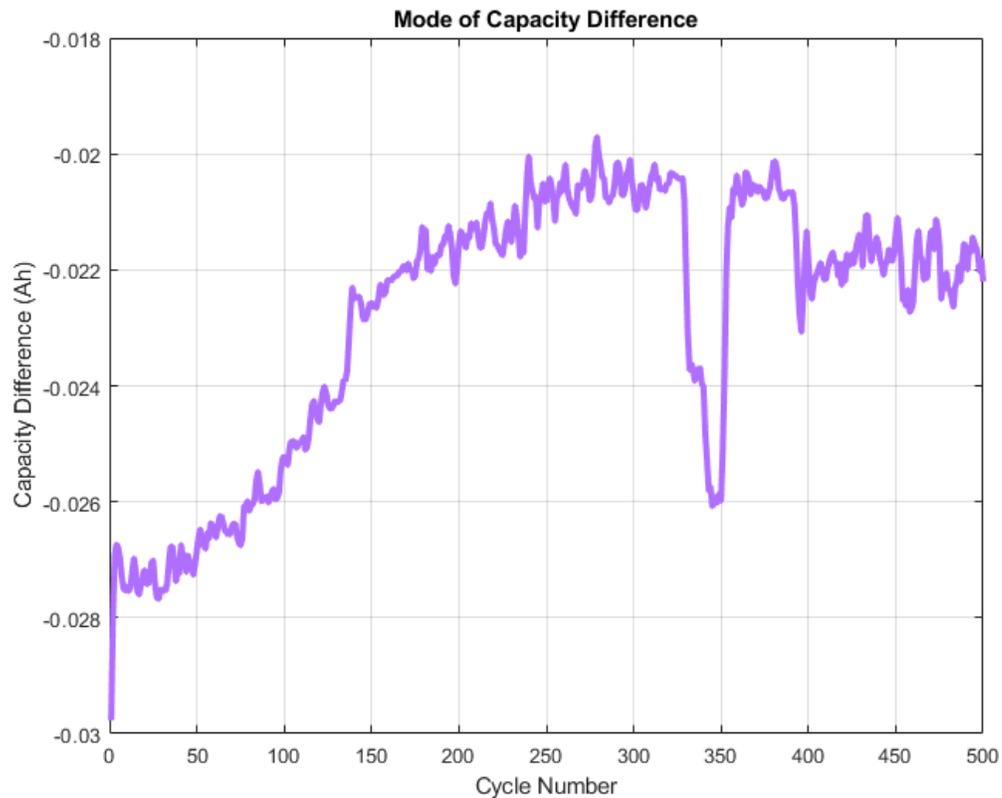
Figure 68: Test 6 mode of the difference between recharge and charge for each cycle

Looking at the mode of the capacity fade some of the trends seen in the mean current are exposed. Although these plots do not yet explain why the cells began to diverge at cycle 330 the drop in the capacity difference shows that the cells received a significant amount less recharge current during these cycles. A general trend of negative capacity use to capacity return points to aging on the anode the spike down seen at cycle 330 followed by

a spike back up to the trend at 351 points to a temporary period where the cells were supplying significant amount more power to the load then it was receiving on recharge. One these behaviors fully deplete the capacity of the cells the cycling returns to normal. The Mean and median of the Capacity Difference were both -1.8mAh. Therefore, the overall trend continues to be anodic. All these test points to well-documented aging mechanisms based on elevated temperatures and currents. What is unique about the parallel behavior of an array of cells is the uneven nature of the stress based on specific components of the battery chemical structure that limit the usability of the battery pack to each cell's worst attribute with the weakest cell's worst attribute playing a dominant role.
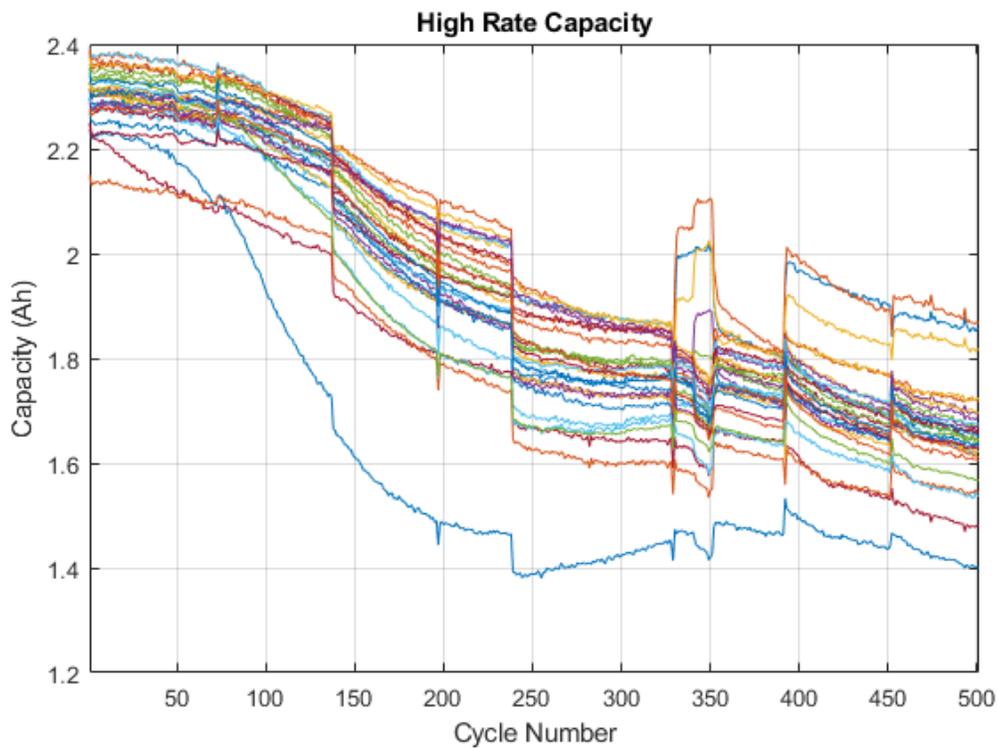
Figure 69: Test 6 Capacity fade across cycles

The capacity supplied by each cell generally reflects the current seen in the mean current for the full discharge. The negative slope of the capacity supplied makes it difficult to see

a slight trend in each cell, as is visible in the mean current plot. There is a slower capacity fade at the beginning of the cycling, but it is relatively linear after the first time the discharge decrease by one pulse at cycle 138. There is not as sharp of a peak at cycles 348-349. The is because these test runs were noticeably shorter.

EIS and 1 kHz

The investigation into the major trend changes that happen in a 30-cell array with no baseline shows only the major changes and trends that happen to the cells as they age. Although the set by set changes that occur within the cells due to events during a small number of cycles cannot be investigated it highlights major shifts that are have a higher probability of occurring in a majority of situations.
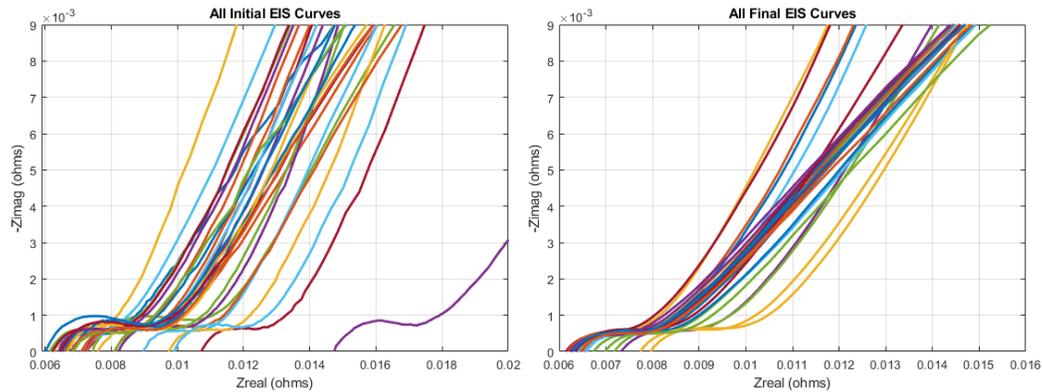
Figure 70: Test 6 EIS measurement of all cells from initial EIS and after the cycling has been completed
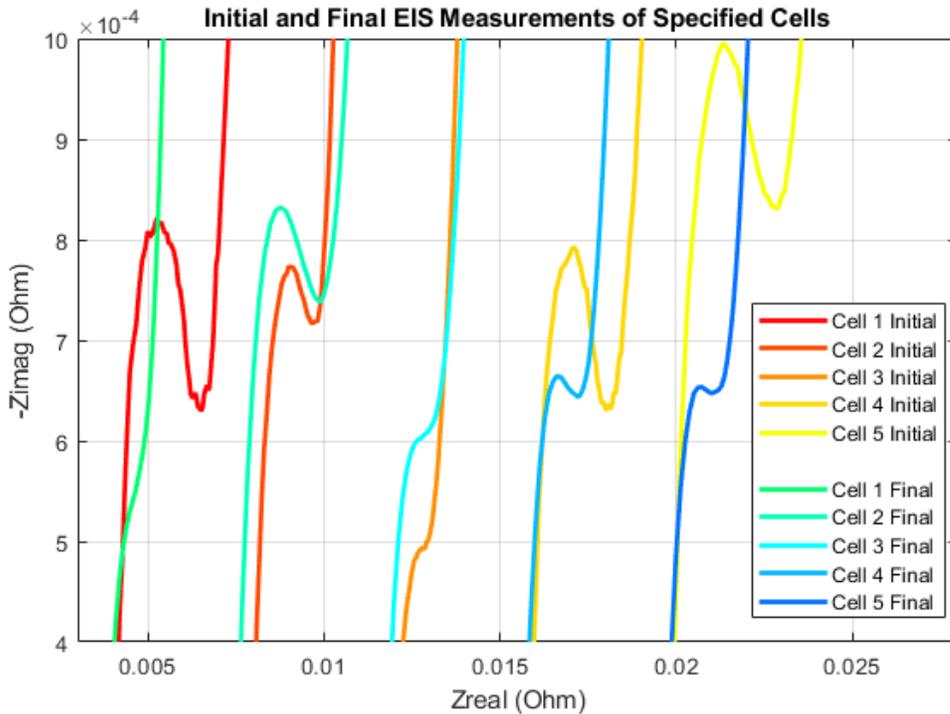
Figure 71: Test 6 EIS measurement of all cells before cycling and at the end focused in on the mid-frequencies and shifted to same 1kHz impedance for better comparison

There are a few outlying Nyquist plots with five being above 8mΩ and with two of those being above 10mOHMS. There is a distinct difference in the angle with 20 of the cells having an angle of around 35° and 10 of the cells having an angle of around 25°. The steeper angle indicates a more capacitive behavior and lower diffusion resistance. Given that these cells all started at a Warburg angle around 30° some of the cells diffusion layers increased and some decreased.

The changes in the mid-frequency are similar to changes measured in the cells in test. The most notable aspect is both Cell 1 and cell 2, figure 404 presents only cell 1, have similar starting semi-circles and ending semicircles. Cell 3 has a very similar ending semi-circle, but the starting semi-circle is similar to 9. It is likely that the spikes seen between cycles 329-350 are related to the structural differences reflected in these semi-circles.

Furthermore, the stress put on the cells during these cycles would have led to a reduction in the double layer capacitance and charge transfer resistance and for the diffusion impedance to dominate the reaction. While cell 1's C/2 capacity fade is within the standard range cell 2's capacity fade is 1.4 standard deviations above average capacity fade while cell 3 is 0.96 standard deviation above. However, before the spike cell, one was experiencing the 3rd least difference between recharge capacity and discharge capacity whereas after it is experiencing the 4th largest difference. Therefore, the author concludes that also experienced a significant reduction in capacity fade due to the event. Since 1C capacity was taken only at the beginning and end the low capacity fade cell one experienced at the beginning of cycling makes the overall capacity fade of cell 1 be on par with the pack average.

Correlation

Having thoroughly investigated the predictive abilities of the chosen figures of merit for 5P/1S arrays it is vital to investigate them for the highly parallel behavior seen in the 30p/1S array with no baseline. Comparing the correlative behavior of the two sets allows the whether these sorting metrics are scalable.
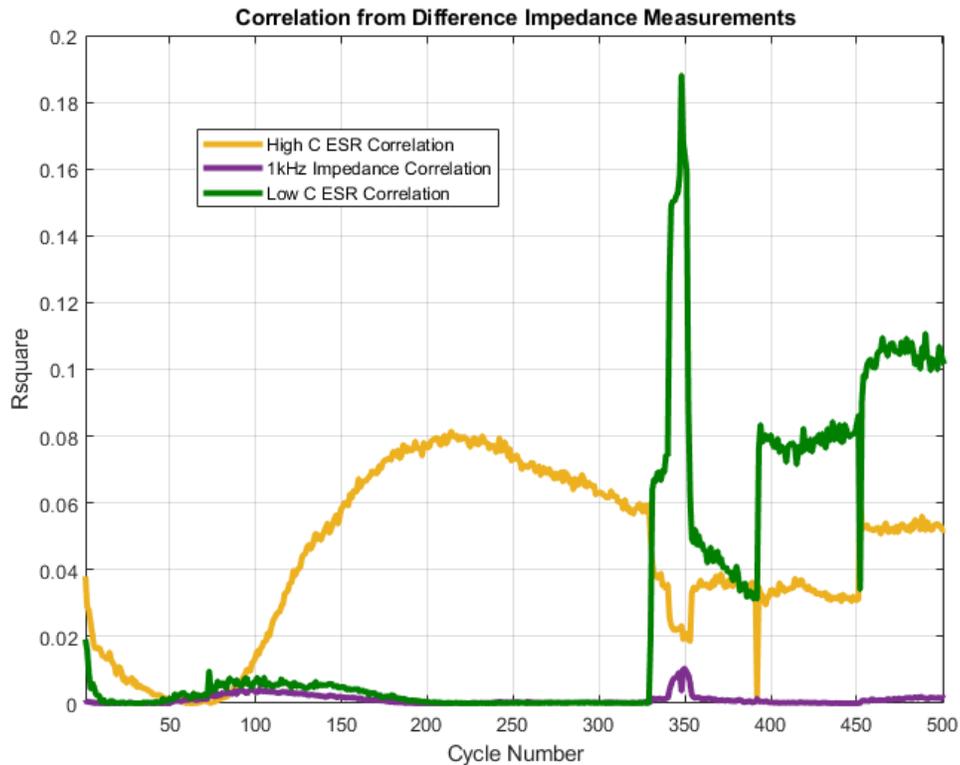
Figure 72: Test 6 Correlation of the initial 1 kHz impedance, Low C DC ESR, and High C DC ESR

Even though 1kHz impedance appears to be essential for a combined key metric, as a standalone metric, it has no value at the current rates used here. The Low C DC ESR only seems to have a higher than the negligible value at the current spike and then after the cells have reached 20% capacity fade. This trend is dissimilar from what the author presented in other tests. The dissimilarity along with the fact that the R^2 value is 0.1 means that though noteworthy it does not change previous conclusion about the value of the Low C DC ESR metric. It is valuable that High C DC ESR has the strongest correlation during the most regular portions of the discharge. At a max correlation of 0.8, it has no value as a standalone metric.

Potential other key merits or indicators of future cell behavior

With the correlation from individual metric providing little insight into the overall discharge behavior of the cells it is even more valuable to look at the combination of metrics. Perhaps the combined insight of Low C DC ESR into the current spike paired with the High C DC ESR insight into the initial cycles a predictive metric and be discovered.

Table 4:Test 6 Metric combinations use to attempt prediction of the current sharing between cells

Metrics Included	Mean Correlation
1 kHz ESR, 10s High ESR, r_{pd}, V_{OC}	0.049
1 kHz ESR, 10s High ESR, r_{pd}, V_{OC}, Low C DC ESR, r_{pr}	0.189
1 kHz ESR, 10s High ESR, r_{pd}, V_{OC}, W_{max}	0.150
1 kHz ESR, 10s High ESR, r_{pd}, High C DC ESR	0.189
1 kHz ESR, 10s High ESR, V_{OC}, High C DC ESR, r_{pr}	0.065

Overall this combined metrics did not provide the level of insight, based on their correlation, needed to suggest with high confidence a binning metric for future test. The correlation metrics used do not perform well with broader set of batteries. There are potentially different ways that researchers could calculate the key metrics, which might result in higher correlation but is unlikely to cause dramatic increases. With a maximum correlation of 0.365 out of all the metrics investigated-specifically 1 kHz ESR, 5s and 10s discharge pulse resistance 5, ω_{max} and 5s recharge pulse resistance-more than just a reformulation is needed. The correlation with all the above metrics except the recharge pulse resistance is 0.350. Suggesting that the recharge pulse resistance is not significantly affecting the current distribution. The author concludes that there are significant challenges to find a metric that would be relatively simple to implement and would successfully predict the current sharing among parallel cells.

The analysis done here does show that initial C/2 capacity, recharge pulse resistance, and r_{ss} are not helpful metrics for LFP batteries. Furthermore, Low C DC ESR and ω_{max} show weak potential. It does suggest that future researchers should look at other metrics in any further investigation of electrochemical cell binning metrics.

Chapter 6: Conclusions and Future Work

6.1 Conclusions

Six different parallel arrays, split between 1S/5P and 1S/30P configurations of ANR26650M1B cells, underwent testing under two different high power pulsed test profiles. The tests finished when the array averaged a 20% capacity fade or until cell failure. These sets of experiments investigated the effects of manufacturer variations on the behavior of parallel arrays of cells. The test measured the results of several different series parallel combinations at different per cell powers.

Table 5: Tests, P/S1wsw configurations, and W per cell

Test #	Configuration	W per Cell
1	1S/30P	46
2	1S/30P	117
3,4,5	1S/5P	117
6	1S/30P	117

Highly parallel battery arrays reduce the cycle life of the cells and increase the probability of catastrophic cell failure. As the number of cells in a parallel array increases, the cycle life decreases significantly, the probability of individual cell failure increases, and the number of unwanted side reactions increases as well. These unwanted reactions are mainly due to cell variations, but the extensive circuitry required for highly parallel array also contributes to the increased probability of array failure. Each additional cell increases the likelihood that one of the cells is multiple standard deviations away from the rest of the array in any one major figure of merit (e.g., resistance, initial capacity, time to failure). Some resulting potential problems with individual cells include:

Cell fails before the array reaches the desired end-of-life figure.

Cell's high impedance becomes an additional source of heat for the nearby cells.

Cell is weak and undersupplies current, requiring other cells in the array to compensate adding a further source of stress for the array.

For the initial test cycles, the cell that compensates for a weakly performing cell within a pulse system tends to be the cell with low pulse resistance. In turn, as the compensating cell experiences accelerated fade in capacity, it can become a low performing cell itself. The multiple sources of parasitic reactions lead to a relatively small current percentage deviation from the array mean despite some sizable differences measured cell to cell. As tested, these relative differences resulted in a 29% to 72% reduction in array cycle life. The test with the smallest reduction had 30 cells in parallel which discharged at a mean of 46W per cell. The test with the highest reduction had 30 cells discharged in parallel at a mean of 117W per cell. In this test a cell failed and vented electrolyte prior to a measured end of cycle life for the array. A different test in a similar configuration still saw a 68% reduction in cycle life. When five cells discharged in paralle at 117W per cell, tests showed a 54% reduction in the cycle life.

An alternative method of measuring array longevity is by measuring the total amp hours supplied. This method accounts for all the energy discharged in cycles of differing sizes of discharge (30%, 50%, 70%, 90%) [87]. When compared to the previous cycle life calculation, this method shows an even higher decrease in its relative figure of merit (total Ah supplied). This is due to the test's power levels magnifying the negative impact of using the full SoC window. Thus, for the user to reliably obtain the desired energy from the pack without significantly decreasing the cycle life and increasing the failure rate, the battery packs will need to be able to provide 100% of the load energy using only 70% - 80% of the cell's maximum energy.

LFP cells have a high power density in comparison to other Li-ion cells but have mid-range energy-density. The power to energy density ratio of LFP's gives them an economic advantage in power heavy loads over other Li-ion packs because the determining factor in a Li-ion pack size is power capability. Impact on cell longevity is minimized if cells are discharged no more than 80%. This enables a more accurate cost comparison between LFP packs and other Li-ion packs since 20% of the capacity is effectively unusable. Accounting for this constraint puts LFP cells more on par with other Li-ion battery packs regarding cost, though they are still considerably safer than all but LTO cells.

The low initial impedance and low impedance growth of LFP result in good high power performance, but the literature, including this dissertation, has shown this also means that they are sensitive to small changes in the circuitry around them. In these tests, the sensitivity of LFP's to circuitry impedance was an unexpected insight.

Even though the LFP cells are robust with regards to their safety boundaries and failure mechanisms, there are still some unknown aging mechanisms concerning the battery chemistry cause unexpected acceleration of aging. Unfortunately, the gaps in the literature regarding LFP aging mechanisms and the dynamics of parallel cells combine to make it difficult to predict long-term array behavior and cycle life.

Future Work

While the author initially hypothesized accelerated aging, the magnitude of the acceleration was greater than expected, which makes highly parallel arrays economically inviable. The two main results from this research is that simply designed highly parallel arrays suffer from severe aging, and that there is an unquantified relationship between common initial cell metrics and the current supplied by individual cells in a parallel array.

The demonstrated effects on aging could be mitigated by pack manufacturers reducing the total number of cells in a pack, reducing the connecting resistance between cells, and by having a battery management system for each of the smaller packs.

The unquantified relationship between metrics and behavior is a potential avenue for future research. In many areas of hard science, part of the challenge is finding a process pathway that enables specific system characteristics to enact changes in the surrounding environment. Often finding this pathway is key to making further breakthroughs. There are still many aspects of the nature of the cell's chemical reactions that are poorly understood. The investigation presented here narrowed down the number of probable impactful pathways for LFP cells, but it did not fully uncover, to a high degree of confidence, what was the proportional relationship of each cell metric to current sharing. While this research proved that two common metrics have no measurable impact on current, not enough is known about the remaining metrics to sort cells into sets that would reduce the current range and its corresponding undesirable effects.

It is also not understood what may make a specific combination of cells increase the aging reaction in the cells. It is not even clear if the poor performance of an array is due to the combination of how all the cells interact or if one or two cell's characteristics have an outsized influence on the others. This research has shown that it is not as simple as weak and strong cells but rather a complicated mix of the electrochemical behavior leading to sub-optimal discharge behavior. It could be that if an array pairs a cell with high capacity and resistance with a cell of mid-level initial capacity and low ESR that the pair has more detrimental effects than if both cells have similarly poor figures of merit. Knowing the impact of substantial differences in individual metrics could sufficiently increase the economic usability of the array of cells to make them optimal for specific use cases. Much more

research is needed, and more should be known about cell behavior before highly parallel cells become economical.

Therefore, the next step in this area of research lies in gaining a more in-depth understanding of the stochastic versus the deterministic nature of cell behavior in concert with the non-destructive metrics. There are already three available tests presented here that characterize cells where each test produces one to four single value metrics. In the literature, other teams have used these metrics to build cell models that aid how to select cells for different tasks. However, these models break down when it comes to how the cells behave in parallel, especially when they are highly paralleled [88].

It is not vital to have a complete model for each possible combination of a parallel array, just a better understanding of how cells generally interact when in parallel when there is no a master battery management system to balance the cells. Although a correlation of 0.7 is usually a lower bound for threshold of causation in hard science, a lower correlation still has the potential to be useful in this context [89] [90] [52] [91]. For economic purposes it is not necessary to have an optimal array. Since relatively small mitigation of the current range reaps long-term benefits, it is only necessary to mitigate, not eliminate, the current differences to see a sizable improvement in the life cycle of the cells. Thus, it is essential to know what level of correlation pairs with a consistent decrease in current mitigation and cycle life increase. Work done at the Naval Research Laboratory has shown that binning according to ESR, capacity, and EIS reduces this initial current imbalance, which results in a small increase in the life cycle of the pack. However, the increase was minimal in comparison to the number of unusable cells. [Huhman, 2017] What are the vital measurements that can be used to bin the cells at the beginning of the cycling effectively? What measurements and combination of measurements would better predict the discharge behavior and lead to smaller current differences? These are the first questions to be

answered in future research. From there further investigation can be done as to how to economically obtain these measurements and package the cells accordingly.

If it is known what characteristics most significantly increase the current inequality, then users can avoid mismatched arrays which will significantly increase the economic efficiency of parallel arrays. Thus, future work should investigate the metrics correlation which effectively mitigates aging. However, at the present level of understanding and insight, it is not advisable to build packs with more than six cells in parallel.

Appendix A: Extra Test 5 Plots
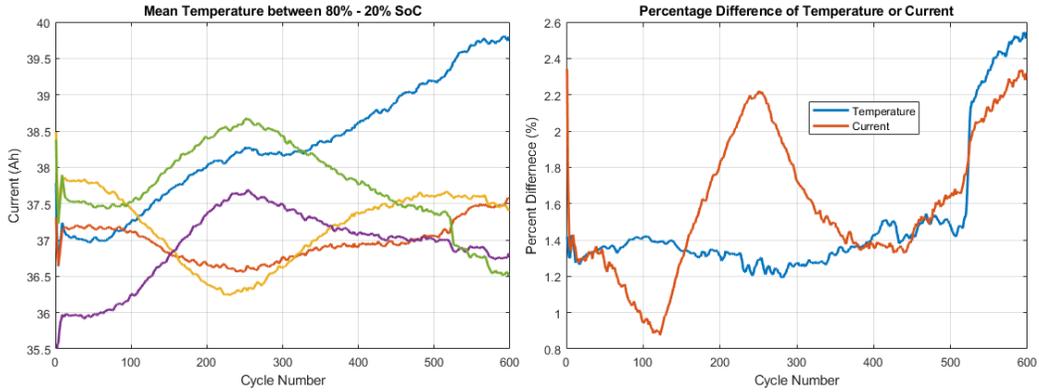
Figure 73: Test 5 A) Percent difference of the mean absolute deviation between individual cells' current and temperature B) Mean current of each cell, both A and B are based on the mean values between 80% and 20% SoC of each discharge cycle
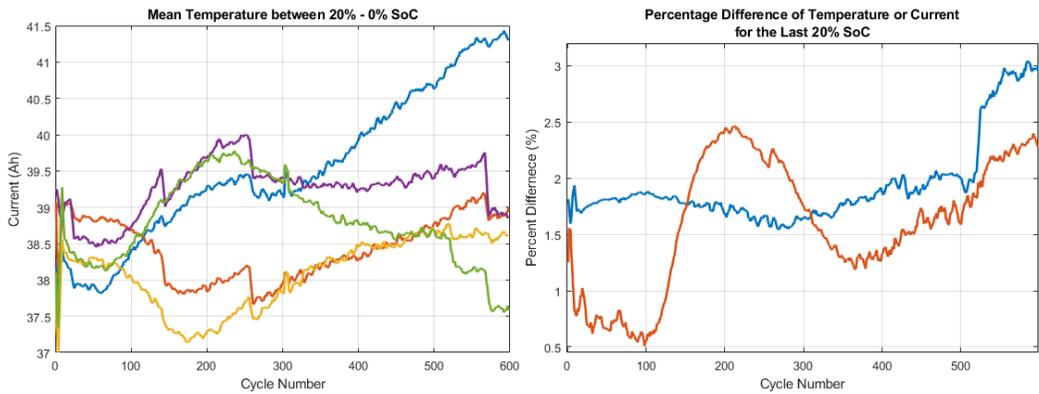
Figure 74: Test 5 A) Percent difference of the mean absolute deviation between individual cells' current and temperature B) Mean current of each cell, both A and B are based on the mean values during the final 20% SoC of each discharge cycle
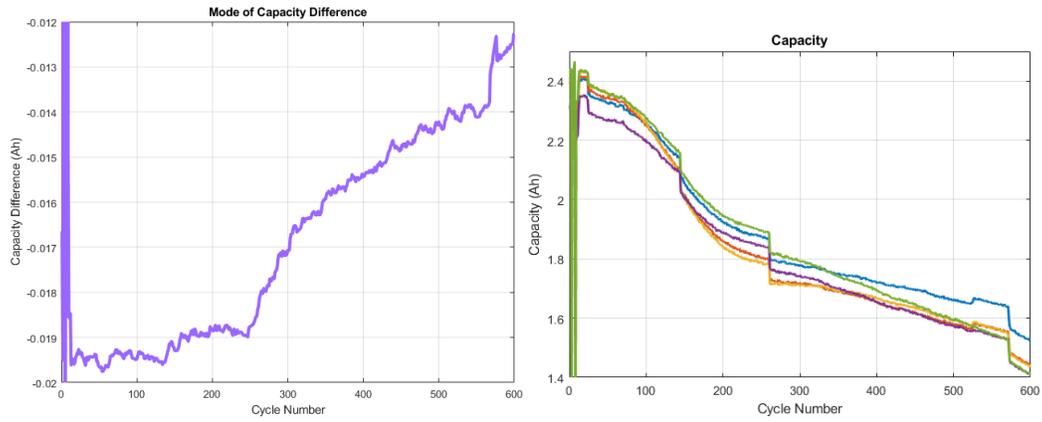
Figure 75: Test 5 A) The mode of the difference between recharge and charge for each cycle B) Capacity fade

across cycles
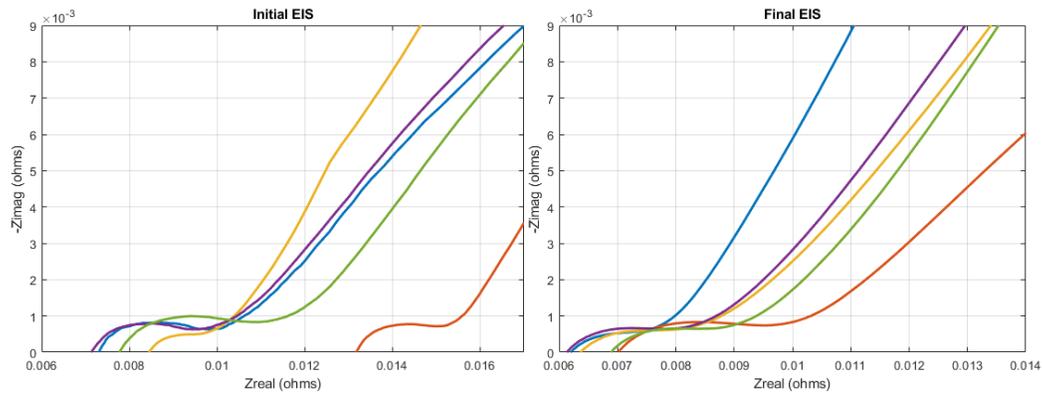
Figure 76: Test 5 EIS measurement of all cells from test 5 A) initial B) Final
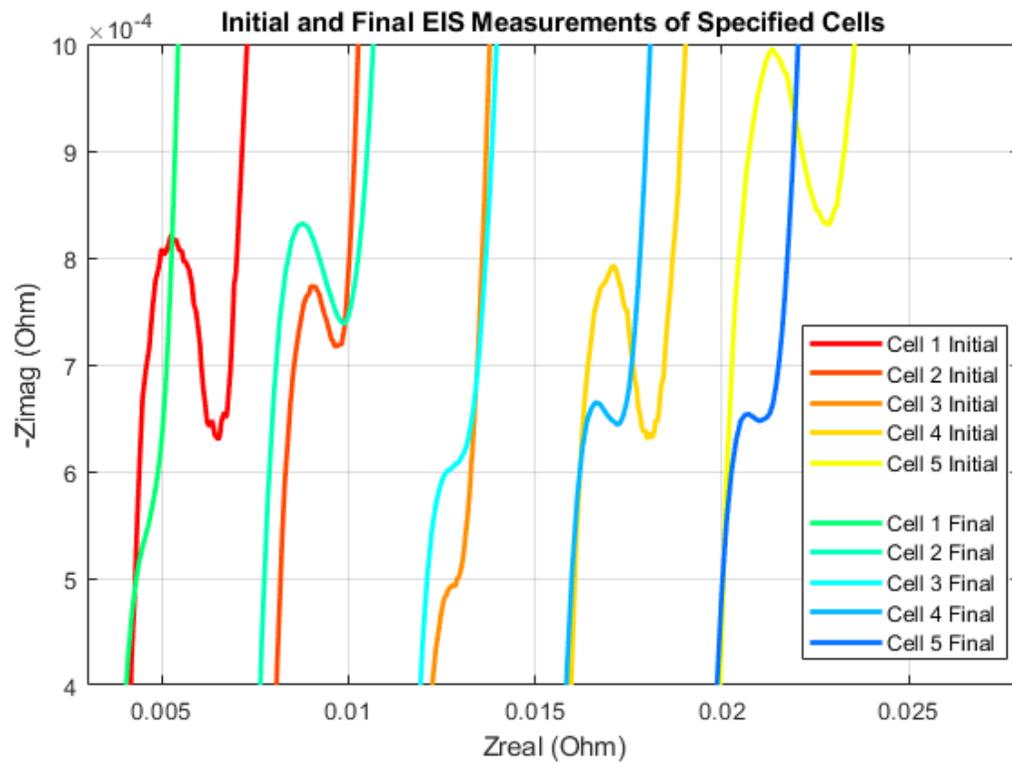
Figure 77: Test 5 EIS measurement of all the cells before cycling and at the end of test 5 focused in on the

mid-frequencies

References

[1]   F. Baronti, R. D. Rienzo, N. Papazafiropulos, R. Roncella, and R. Saletti, "Investigation of series-parallel connections of multi-module batteries for electrified vehicles," in *2014 IEEE International Electric Vehicle Conference (IEVC)*, 2014, pp. 1–7.

[2]   D. H. Doughty and E. P. Roth, "A General Discussion of Li Ion Battery Safety," *Interface Mag.*, vol. 21, no. 2, pp. 37–44, Jan. 2012.

[3]   X. Gong, R. Xiong, and C. C. Mi, "Study of the Characteristics of Battery Packs in Electric Vehicles With Parallel-Connected Lithium-Ion Battery Cells," *IEEE Trans. Ind. Appl.*, vol. 51, no. 2, pp. 1872–1879, Mar. 2015.

[4]   *IEEE Standards Dictionary: Glossary of Terms & Definitions (CDROM).* .

[5]   J. Brandstetter *et al.*, "Successful Practices for Battery Powered Medical Devices," *Med. Devices*, p. 37.

[6]   "Constant-Voltage Constant-Current Devices | DigiKey." [Online]. Available: https://www.digikey.com/en/articles/techzone/2012/nov/constant-voltageconstant-current-devices-optimize-li-ion-battery-charging-for-energy-harvesting. [Accessed: 23-Apr-2018].

[7]   M. Wakihara and O. Yamamoto, *Lithium Ion Batteries: Fundamentals and Performance*. John Wiley & Sons, 2008.

[8]   D. N. Wong, "THE CHARACTERIZATION OF SECONDARY LITHIUM-ION BATTERY DEGRADATION WHEN OPERATING COMPLEX, ULTRA-HIGH POWER PULSED LOADS," Thesis, 2016.

[9]   P. Verma, P. Maire, and P. Novák, "A review of the features and analyses of the solid electrolyte interphase in Li-ion batteries," *Electrochimica Acta*, vol. 55, no. 22, pp. 6332–6341, Sep. 2010.

[10]   J. O. Besenhard, M. Winter, J. Yang, and W. Biberacher, "Filming mechanism of lithium-carbon anodes in organic and inorganic electrolytes," *J. Power Sources*, vol. 54, no. 2, pp. 228–231, Apr. 1995.

[11]   D. A. Wetz, B. Shrestha, S. T. Donahue, D. N. Wong, M. J. Martin, and J. Heinzel, "Capacity Fade of 26650 Lithium-Ion Phosphate Batteries Considered for Use Within a Pulsed-Power System #x2019;s Prime Power Supply," *IEEE Trans. Plasma Sci.*, vol. 43, no. 5, pp. 1448–1455, May 2015.

[12]   J. Vetter *et al.*, "Ageing mechanisms in lithium-ion batteries," *J. Power Sources*, vol. 147, no. 1, pp. 269–281, Sep. 2005.

[13]   S. Grolleau *et al.*, "Calendar aging of commercial graphite/LiFePO4 cell – Predicting capacity fade under time dependent storage conditions," *J. Power Sources*, vol. 255, pp. 450–458, Jun. 2014.

[14]   M. Dubarry and B. Y. Liaw, "Identify capacity fading mechanism in a commercial LiFePO4 cell," *J. Power Sources*, vol. 194, no. 1, pp. 541–549, Oct. 2009.

[15]   D. Dees, E. Gunen, D. Abraham, A. Jansen, and J. Prakash, "Electrochemical Modeling of Lithium-Ion Positive Electrodes during Hybrid Pulse Power Characterization Tests," *J. Electrochem. Soc.*, vol. 155, no. 8, pp. A603–A613, Aug. 2008.

[16]   M. Schimpe, M. E. von Kuepach, M. Naumann, H. C. Hesse, K. Smith, and A. Jossen, "Comprehensive Modeling of Temperature-Dependent Degradation Mechanisms in Lithium Iron Phosphate Batteries," *J. Electrochem. Soc.*, vol. 165, no. 2, pp. A181–A193, Jan. 2018.

[17]   H. Z. Z. Beh, G. A. Covic, and J. T. Boys, "Effects of pulse and DC charging on lithium iron phosphate (LiFePO4) batteries," in *2013 IEEE Energy Conversion Congress and Exposition*, 2013, pp. 315–320.

[18]   H. Popp, J. Attia, F. Delcorso, and A. Trifonova, "Lifetime analysis of four different lithium ion batteries for (plug – in) electric vehicle," p. 9, 2014.

[19]   G. L. Soloveichik, "Battery Technologies for Large-Scale Stationary Energy Storage," *Annu. Rev. Chem. Biomol. Eng.*, vol. 2, no. 1, pp. 503–527, Jun. 2011.

[20]   H. Kim and K. G. Shin, "On Dynamic Reconfiguration of a Large-Scale Battery System," in *2009 15th IEEE Real-Time and Embedded Technology and Applications Symposium*, 2009, pp. 87–96.

[21]   M. T. Lawder *et al.*, "Battery Energy Storage System (BESS) and Battery Management System (BMS) for Grid-Scale Applications," *Proc. IEEE*, vol. 102, no. 6, pp. 1014–1030, Jun. 2014.

[22]   Z. Yang *et al.*, "Electrochemical Energy Storage for Green Grid," *Chem. Rev.*, vol. 111, no. 5, pp. 3577–3613, May 2011.

[23]   K.-S. Park *et al.*, "Enhanced Charge-Transfer Kinetics by Anion Surface Modification of LiFePO $_4$," *Chem. Mater.*, vol. 24, no. 16, pp. 3212–3218, Aug. 2012.

[24]   B. Dunn, H. Kamath, and J.-M. Tarascon, "Electrical Energy Storage for the Grid: A Battery of Choices," *Science*, vol. 334, no. 6058, pp. 928–935, Nov. 2011.

[25]   M. Dubarry and B. Y. Liaw, "Development of a universal modeling tool for rechargeable lithium batteries," *J. Power Sources*, vol. 174, no. 2, pp. 856–860, Dec. 2007.

[26]   J. Herbst, J. Beno, A. Ouroua, S. Pish, J. Hahne, and R. Hebner, "High slew rate power supplies for support of large pulsed loads," in *2015 IEEE Electric Ship Technologies Symposium (ESTS)*, 2015, pp. 446–452.

[27]   R. M. LaFollette and D. N. Bennion, "Design Fundamentalsof High Power Density, Pulsed Discharge, Lead Acid Batteries," p. 9.

[28]   A. Kuperman and I. Aharon, "Battery–ultracapacitor hybrids for pulsed current loads: A review," *Renew. Sustain. Energy Rev.*, vol. 15, no. 2, pp. 981–992, Feb. 2011.

[29]   T. Bruen, J. Marco, and M. Gama, "Current Variation in Parallelized Energy Storage Systems," in *2014 IEEE Vehicle Power and Propulsion Conference (VPPC)*, 2014, pp. 1–6.

[30]   R. Gogoana, M. B. Pinson, M. Z. Bazant, and S. E. Sarma, "Internal resistance matching for parallel-connected lithium-ion cells and impacts on battery pack cycle life," *J. Power Sources*, vol. 252, pp. 8–13, Apr. 2014.

[31]   J. D. Welsh, "A Comparison of Active and Passive Cell Balancing Techniques for Series/Parallel Battery Packs," The Ohio State University, 2009.

[32]   W. Shi, X. Hu, C. Jin, J. Jiang, Y. Zhang, and T. Yip, "Effects of imbalanced currents on large-format LiFePO4/graphite batteries systems connected in parallel," *J. Power Sources*, vol. 313, pp. 198–204, May 2016.

[33]   G. J. Offer, V. Yufit, D. A. Howey, B. Wu, and N. P. Brandon, "Module design and fault diagnosis in electric vehicle batteries," *J. Power Sources*, vol. 206, pp. 383–392, May 2012.

[34]   S. Miyatake, Y. Susuki, T. Hikihara, S. Itoh, and K. Tanaka, "Discharge characteristics of multicell lithium-ion battery with nonuniform cells," *J. Power Sources*, vol. 241, pp. 736–743, Nov. 2013.

[35]   T. Grün, K. Stella, and O. Wollersheim, "Influence of circuit design on load distribution and performance of parallel-connected Lithium ion cells for photovoltaic home storage systems," *J. Energy Storage*, vol. 17, pp. 367–382, Jun. 2018.

[36]   J. Wang *et al.*, "Cycle-life model for graphite-LiFePO4 cells," *J. Power Sources*, vol. 196, no. 8, pp. 3942–3948, Apr. 2011.

[37]   "Sealed Lead Acid Batteries Information and Specification Data Sheets." [Online]. Available: http://www.power-sonic.com/sealed_batteries.php. [Accessed: 14-Jun-2018].

[38]   G. E. C. B. P. Section and D. L. Barney, *Nickel-cadmium battery application engineering handbook*. General Electric, 1971.

[39]   "Nickel-based Batteries Information – Battery University." [Online]. Available: http://batteryuniversity.com/learn/article/nickel_based_batteries. [Accessed: 30-Jun-2018].

[40]   S. K. Dhar, S. R. Ovshínsky, P. R. Gifford, D. A. Corrigan, M. A. Fetcenko, and S. Venkatesan, "Nickel/metal hydride technology for consumer and electric vehicle batteries—a review and up-date," *J. Power Sources*, vol. 65, no. 1, pp. 1–7, Mar. 1997.

[41]   D. N. Galushkin, N. N. Yazvinskaya, and N. E. Galushkin, "Investigation of the process of thermal runaway in nickel–cadmium accumulators," *J. Power Sources*, vol. 177, no. 2, pp. 610–616, Mar. 2008.

[42]   T. Ohzuku and R. J. Brodd, "An overview of positive-electrode materials for advanced lithium-ion batteries," *J. Power Sources*, vol. 174, no. 2, pp. 449–456, Dec. 2007.

[43]   N. Nitta, F. Wu, J. T. Lee, and G. Yushin, "Li-ion battery materials: present and future," *Mater. Today*, vol. 18, no. 5, pp. 252–264, Jun. 2015.

[44]   X. Liu, C. Chen, Y. Zhao, and B. Jia, "A Review on the Synthesis of Manganese Oxide Nanomaterials and Their Applications on Lithium-Ion Batteries," *J. Nanomater.*, vol. 2013, Jan. 2013.

[45]   K. Kang, Y. S. Meng, J. Bréger, C. P. Grey, and G. Ceder, "Electrodes with High Power and High Capacity for Rechargeable Lithium Batteries," *Science*, vol. 311, no. 5763, pp. 977–980, 2006.

[46]   N. Omar *et al.*, "Lithium iron phosphate based battery – Assessment of the aging parameters and development of cycle life model," *Appl. Energy*, vol. 113, pp. 1575–1585, Jan. 2014.

[47]   M. Broussely *et al.*, "Main aging mechanisms in Li ion batteries," *J. Power Sources*, vol. 146, no. 1, pp. 90–96, Aug. 2005.

[48]   M. Wohlfahrt-Mehrens, C. Vogler, and J. Garche, "Aging mechanisms of lithium cathode materials," *J. Power Sources*, vol. 127, no. 1, pp. 58–64, Mar. 2004.

[49]   A. Eddahech, O. Briat, and J.-M. Vinassa, "Performance comparison of four lithium–ion battery technologies under calendar aging," *Energy*, vol. 84, pp. 542–550, May 2015.

[50]   J. Groot, M. Swierczynski, A. I. Stan, and S. K. Kær, "On the complex ageing characteristics of high-power LiFePO4/graphite battery cells cycled with high charge and discharge currents," *J. Power Sources*, vol. 286, pp. 475–487, Jul. 2015.

[51]   H.-F. Jin, Z. Liu, Y.-M. Teng, J. Gao, and Y. Zhao, "A comparison study of capacity degradation mechanism of LiFePO4-based lithium ion cells," *J. Power Sources*, vol. 189, no. 1, pp. 445–448, Apr. 2009.

[52]   B. Huhman, "A Single-Frequency Impedance Diagnostic for State of Health Determination in Li-ion 4P1S Battery Packs." Virginia Polytechnic Institute and State University, 03-Nov-2017.

[53]   M. Ouyang *et al.*, "Low temperature aging mechanism identification and lithium deposition in a large format lithium iron phosphate battery for different charge profiles," *J. Power Sources*, vol. 286, pp. 309–320, Jul. 2015.

[54]   D. Jeong and J. Lee, "Electrode design optimization of lithium secondary batteries to enhance adhesion and deformation capabilities," *Energy*, vol. 75, pp. 525–533, Oct. 2014.

[55]   W. Waag, S. Käbitz, and D. U. Sauer, "Experimental investigation of the lithium-ion battery impedance characteristic at various conditions and aging states and its influence on the application," *Appl. Energy*, vol. 102, pp. 885–897, Feb. 2013.

[56]   Y. Zhang, C.-Y. Wang, and X. Tang, "Cycling degradation of an automotive LiFePO4 lithium-ion battery," *J. Power Sources*, vol. 196, no. 3, pp. 1513–1520, Feb. 2011.

[57]   M. Lu, H. Cheng, and Y. Yang, "A comparison of solid electrolyte interphase (SEI) on the artificial graphite anode of the aged and cycled commercial lithium ion cells," *Electrochimica Acta*, vol. 53, no. 9, pp. 3539–3546, Mar. 2008.

[58]   C. Reece, "An Introduction to Electrochemical Impedance Spectroscopy," p. 11.

[59]   "Electrochemical Energy Systems," *MIT OpenCourseWare*. [Online]. Available: https://ocw.mit.edu/courses/chemical-engineering/10-626-electrochemical-energy-systems-spring-2014/. [Accessed: 30-Jun-2018].

[60]   A. Seaman, T.-S. Dao, and J. McPhee, "A survey of mathematics-based equivalent-circuit and electrochemical battery models for hybrid and electric vehicle simulation," *J. Power Sources*, vol. 256, pp. 410–423, Jun. 2014.

[61]   D. D. Macdonald, "Reflections on the history of electrochemical impedance spectroscopy," *Electrochimica Acta*, vol. 51, no. 8, pp. 1376–1388, Jan. 2006.

[62]   R. Mingant *et al.*, "EIS Measurements for Determining the SoC and SoH of Li-Ion Batteries," *ECS Trans.*, vol. 33, no. 39, pp. 41–53, Apr. 2011.

[63]   K. Zhong, Y. Cui, X.-D. Xia, J.-J. Xue, P. Liu, and Y.-X. Tong, "Study on the stability of the LiFePO4 Li-ion battery via an electrochemical method," *J. Power Sources*, vol. 250, pp. 296–305, Mar. 2014.

[64]   H.-G. Schweiger *et al.*, "Comparison of Several Methods for Determining the Internal Resistance of Lithium Ion Cells," *Sensors*, vol. 10, no. 6, pp. 5604–5625, Jun. 2010.

[65]   B. McKissock, P. Loyselle, and E. Vogel, "Guidelines on Lithium-ion Battery Use in Space Applications," p. 54.

[66]   A. Mamun, A. Sivasubramaniam, and H. K. Fathy, "Collective learning of lithium-ion aging model parameters for battery health-conscious demand response in datacenters," *Energy*.

[67]   P. Ramadass, B. Haran, R. White, and B. N. Popov, "Mathematical modeling of the capacity fade of Li-ion cells," *J. Power Sources*, vol. 123, no. 2, pp. 230–240, Sep. 2003.

[68]   D. Andre, M. Meiler, K. Steiner, C. Wimmer, T. Soczka-Guth, and D. U. Sauer, "Characterization of high-power lithium-ion batteries by electrochemical impedance spectroscopy. I. Experimental investigation," *J. Power Sources*, vol. 196, no. 12, pp. 5334–5341, Jun. 2011.

[69]   "Premature Voltage Cut-off - Battery University." [Online]. Available: http://batteryuniversity.com/learn/article/premature_voltage_cut_off. [Accessed: 22-Jun-2018].

[70]   V. Agubra and J. Fergus, "Lithium Ion Battery Anode Aging Mechanisms," *Materials*, vol. 6, no. 4, pp. 1310–1325, Mar. 2013.

[71]   "Testing Lithium-based Batteries." [Online]. Available: http://batteryuniversity.com/learn/article/testing_lithium_based_batteries. [Accessed: 23-Jun-2018].

[72]   M. Klett *et al.*, "Non-uniform aging of cycled commercial LiFePO4//graphite cylindrical cells revealed by post-mortem analysis," *J. Power Sources*, vol. 257, pp. 126–137, Jul. 2014.

[73]   D. I. Stroe, M. Swierczynski, A. I. Stroe, V. Knap, R. Teodorescu, and S. J. Andreasen, "Evaluation of different methods for measuring the impedance of Lithium-ion batteries during ageing," in *2015 Tenth International Conference on Ecological Vehicles and Renewable Energies (EVER)*, 2015, pp. 1–8.

[74]   M. Hellqvist Kjell, S. Malmgren, K. Ciosek, M. Behm, K. Edström, and G. Lindbergh, "Comparing aging of graphite/LiFePO4 cells at 22 °C and 55 °C – Electrochemical and photoelectron spectroscopy studies," *J. Power Sources*, vol. 243, pp. 290–298, Dec. 2013.

[75]   M. Giegerich *et al.*, "Electrothermal modeling and characterization of high capacity lithium-ion battery systems for mobile and stationary applications," in *IECON 2013 - 39th Annual Conference of the IEEE Industrial Electronics Society*, 2013, pp. 6721–6727.

[76]   A. Millner, "Modeling Lithium Ion battery degradation in electric vehicles," in *2010 IEEE Conference on Innovative Technologies for an Efficient and Reliable Electricity Supply*, 2010, pp. 349–356.

[77]   C. Vartanian and N. Bentley, "A123 systems' advanced battery energy storage for renewable integration," in *2011 IEEE/PES Power Systems Conference and Exposition*, 2011, pp. 1–6.

[78]   K. Smith and C.-Y. Wang, "Power and thermal characterization of a lithium-ion battery pack for hybrid-electric vehicles," *J. Power Sources*, vol. 160, no. 1, pp. 662–673, Sep. 2006.

[79]   B. Scrosati and J. Garche, "Lithium batteries: Status, prospects and future," *J. Power Sources*, vol. 195, no. 9, pp. 2419–2430, May 2010.

[80]   M. Naumann, M. Schimpe, P. Keil, H. C. Hesse, and A. Jossen, "Analysis and modeling of calendar aging of a commercial LiFePO4/graphite cell," *J. Energy Storage*, vol. 17, pp. 153–169, Jun. 2018.

[81]   S. Beninati, L. Damen, and M. Mastragostino, "Fast sol–gel synthesis of LiFePO4/C for high power lithium-ion batteries for hybrid electric vehicle application," *J. Power Sources*, vol. 194, no. 2, pp. 1094–1098, Dec. 2009.

[82]   "ANR26650m1-BDataSheet." A123 Systems, 2012.

[83]   P. Liu *et al.*, "Aging Mechanisms of LiFePO4 Batteries Deduced by Electrochemical and Structural Analyses," *J. Electrochem. Soc.*, vol. 157, no. 4, pp. A499–A507, Apr. 2010.

[84]   S. S. Choi and H. S. Lim, "Factors that affect cycle-life and possible degradation mechanisms of a Li-ion cell based on LiCoO2," *J. Power Sources*, vol. 111, no. 1, pp. 130–136, Sep. 2002.

[85]   A. Gozdz, A. Chu, R. Fulop, G. Riley, and R. Lin, "US8617745.pdf," US 8617745 B2, 31-Dec-2013.

[86]   A. Systems, "A123-Pack-Design-Guide-for-Cylindrical-Cells(1).pdf." A123 Systems, Feb-2013.

[87]   S. B. Peterson, J. Apt, and J. F. Whitacre, "Lithium-ion battery cell degradation resulting from realistic vehicle and vehicle-to-grid utilization," *J. Power Sources*, vol. 195, no. 8, pp. 2385–2392, Apr. 2010.

[88]   Y. Tripathy, A. McGordon, J. Marco, and M. Gama-Valdez, "State-of-Charge estimation algorithms and their implications on cells in parallel," in *2014 IEEE International Electric Vehicle Conference (IEVC)*, 2014, pp. 1–6.

[89]   M. Mukaka, "A guide to appropriate use of Correlation coefficient in medical research," *Malawi Med. J. J. Med. Assoc. Malawi*, vol. 24, no. 3, pp. 69–71, Sep. 2012.

[90]   R. Taylor, "Interpretation of the Correlation Coefficient: A Basic Review, Interpretation of the Correlation Coefficient: A Basic Review," *J. Diagn. Med. Sonogr.*, vol. 6, no. 1, pp. 35–39, Jan. 1990.

[91]   J. R. Benjamin and C. A. Cornell, *Probability, Statistics, and Decision for Civil Engineers*. Courier Corporation, 2014.